Interpatient registration and analysis in clinical neuroimaging

Cynthia Jongen

Colophon

This book was typeset by the author using Microsoft® Office Word 2003

ISBN: 90-393-4160-5

Printed by Febodruk BV, Enschede, The Netherlands

INTERPATIENT REGISTRATION AND ANALYSIS IN CLINICAL NEUROIMAGING

INTERPATIËNT REGISTRATIE EN ANALYSE
VAN KLINISCHE HERSENBEELDEN
(MET EEN SAMENVATTING IN HET NEDERLANDS)

PROEFSCHRIFT

TER VERKRIJGING VAN DE GRAAD VAN DOCTOR AAN DE UNIVERSITEIT UTRECHT OP GEZAG VAN DE RECTOR MAGNIFICUS, PROF. DR. W.H. GISPEN, INGEVOLGE HET BESLUIT VAN HET COLLEGE VOOR PROMOTIES IN HET OPENBAAR TE VERDEDIGEN OP DONDERDAG 16 MAART 2006 DES MIDDAGS TE 2.30 UUR

DOOR

CYNTHIA JONGEN

GEBOREN OP 11 FEBRUARI 1977 TE GOUDA

Promotor: Prof. Dr. Ir. M.A. Viergever
University Medical Center Utrecht

Copromotor: Dr. J.P.W. Pluim
University Medical Center Utrecht

The research described in this thesis was carried out at the Image Sciences Institute, University Medical Center Utrecht (Utrecht, The Netherlands), under auspices of ImagO, the graduate school for Biomedical Image Sciences. The project was financially supported by SCVR.

Financial support for the printing of this thesis was kindly provided by the Dutch Diabetes Research Foundation and ImagO.

Voor Jiri en Tim

Contents

Colophon 2
Contents 7
List of abbreviations 9
1 Introduction 11
1.1 Brain atlases and reference images 12
1.2 Construction of atlases that encode anatomical variation 14
1.3 Brain lesion distribution 15
1.4 Image registration and segmentation 17
1.5 Brain infarcts 22
1.6 Internal carotid artery stenosis 24
1.7 Diabetes Mellitus type 2 25
1.8 White Matter Lesions 27
1.9 Outline of thesis 28
2 Construction and evaluation of an average CT brain image for intersubject registration 31
2.1 Introduction 32
2.2 Material and Methods 34
2.3 Evaluation 38
2.4 Conclusion 46
3 Analysis of cerebral infarction pattern in CT images of patients with Internal Carotid Artery stenosis 47
3.1 Introduction 48
3.2 Materials and Methods 49
3.3 Results 54
3.4 Discussion 56
4 Brain tissue and white matter lesion volume analysis in diabetes mellitus type 2 59
4.1 Introduction 60
4.2 Subjects and methods 61
4.3 Results 63
4.4 Discussion 67
5 Construction and evaluation of a reference image of the lateral ventricles for interpatient white matter lesion analysis 71
5.1 Introduction 72
5.2 Materials and methods 73
5.3 Evaluation 75
5.4 Results 77
5.5 Discussion 79

6 Periventricular white matter lesions in diabetes mellitus type 2 83
6.1 Introduction 84
6.2 Materials and Methods 85
6.3 Results 86
6.4 Discussion 91
Color Images 93
Bibliography 97
Summary 107
Samenvatting 111
List of publications 115
Acknowledgements 117
Dankwoord 119
Curriculum Vitae 121

List of abbreviations

3D	three-dimensional
ACA	anterior cerebral artery
BMI	body mass index
CPS	control point spacing
CSF	cerebrospinal fluid
CT	computed tomography
DM2	diabetes mellitus type 2
DSA	digital subtraction angiography
DUS	duplex ultrasonography
F	female
FLAIR	fluid attenuated inversion recovery
GM	gray matter
HbA_{1c}	glycosylated hemoglobin
ICA	internal carotid artery
IQR	interquartile range
IR	inversion recovery
K	number of clusters
KNN	K-nearest neighbor
M	male
MAP	mean arterial pressure
MCA	middle cerebral artery
MR	magnetic resonance
MRI	magnetic resonance imaging
P	probability
PCA	posterior cerebral artery
PD	proton density
PET	positron emission tomography
PSV	peak systolic velocity
SD	standard deviation
SPECT	single photon emission computed tomography
T1	longitudinal relaxation time
T2	transversal relaxation time
TE	echo time
TI	inversion time
TR	repetition time
UDES	Utrecht Diabetic Encephalopathy Study
VBM	voxel-based morphometry
Voxel	volume element
WM	white matter
WML	white matter lesion

1

Introduction

Theories about the function of the brain have varied throughout history. The ancient Egyptians regarded the brain as a minor, unimportant organ. They discarded it during the embalming process, whereas other organs where ceremoniously preserved for mummification. Around 450 B.C. Alcmaeon, an early Greek physician, writer, and philosopher, was the first to state that the brain is the seat of understanding. This idea directly contradicted the accepted theory of his time, which held that the heart is the true seat of intelligence. Aristotle (384-322 B.C.) also believed that the heart is the organ of thought and sensation and that the brain is merely a radiator designed to cool the blood. About the perception of odours "*agreeable in their essential nature, e.g. those of flowers"* he wrote[†]:

"*The reason why the perception of such odours is peculiar to man is found in the characteristic state of man's brain. For his brain is naturally cold, and the blood which it contains in its vessels is thin and pure but easily cooled.*"

"*But the perception of the second class of odours above described* [i.e. those agreeable in their essential nature] *is confined to human beings, because man's brain is, in proportion to his whole bulk, larger and moister than the brain of any other animal. This is the reason of the further fact that man alone, so to speak, among animals perceives and takes pleasure in the odours of flowers and such things. For the heat and stimulation set up by these odours are commensurate with the excess of moisture and coldness in his cerebral region.*"

The Greek Galen (approximately 129-216), born in Pergamum, was a famous physician in the Roman Empire. He introduced experimentation to the medical research. Although many of his theories were correct, he believed that the brain's primary function was to distill and distribute spiritual pneuma throughout the body via hollow nerves. His ideas remained unchallenged until the 16th century when in 1543 the Flemish anatomist Andreas Vesalius (1514-1564) publishes the first complete textbook on human anatomy "De Humanis Corporis Fabrica". This work marks the start of modern medicine.

1.1 Brain atlases and reference images

The earliest known description of the brain has been found in an Egyptian papyrus dating back to approximately 1600 B.C. (the Edwin Smith surgical papyrus). Ever since, knowledge about the brain has been increasing. The book "Cerebri Anatome", published in 1664 by Thomas Willis, contained the first detailed description of the brain, nerves and vasculature (Figure 1.1).

[†] "On Sense and the Sensible" by Aristotle (350 B.C.) Translated by J. I. Beare.

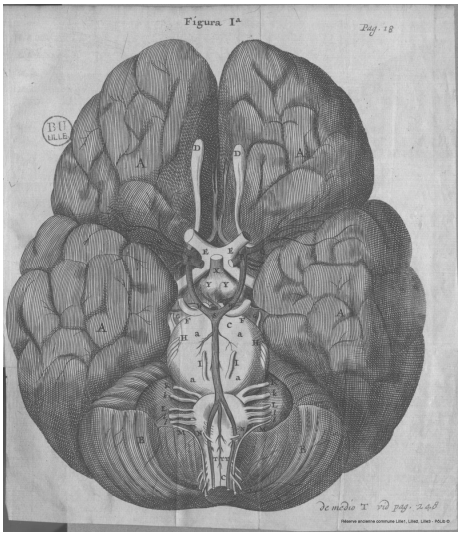

Figure 1.1 *Illustration from Cerebri Anatome by Thomas Willis (1664); drawn by Sir Christopher Wren. Image source: PôLiB, Pôle Universitaire Européen Lille-Nord pas de Calais.*

For a long time data on brain function could only be acquired by studying patients with brain damage[†]. Wilder Penfield (1891-1976) was the first to study brain function by direct stimulation of the cortical tissue during epilepsy surgery [1]. This technique enhanced our understanding of the localization of brain function enormously and resulted in the famous homunculus map of cortical motor and sensory function (Figure 1.2).

The invention of noninvasive techniques to image the living brain meant a great leap ahead in our knowledge of brain anatomy and function. Computed tomography (CT) (1971) and magnetic resonance imaging (MRI) (1973) allow 3D visualization of the brain anatomy in vivo and techniques such as positron emission tomography (PET) (1952), single photon emission computed tomography (SPECT), and functional MRI enable the measurement of brain function. Nowadays, these techniques are available in many hospitals and have made imaging of the brain and of brain function part of routine clinical practice.

[†] For a history on functional brain research: History and future directions of human brain mapping and functional neuroimaging. R.L. Savoy, 2001, Acta Psychologica 107:9-42.

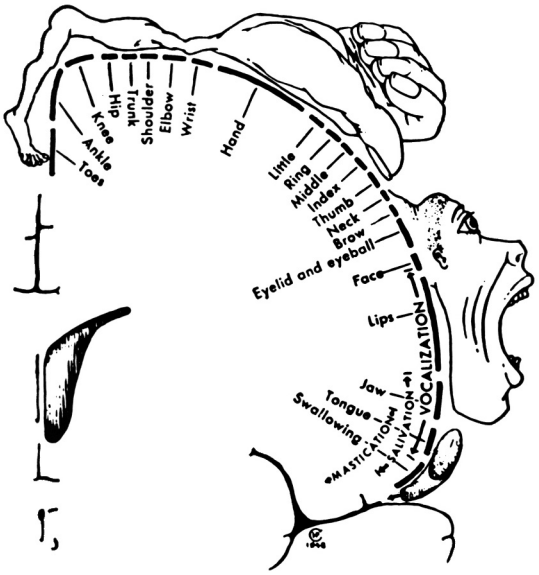

Figure 1.2 *Image of the motor homunculus [2]. The location on the cortex of the motor function of each body part is depicted by a schematic drawing of a human figure. The size of the body parts of this figure reflects the area on the motor cortex that is occupied.*

The advances of in vivo brain imaging have revolutionized the atlases of the brain. Highly detailed schematic drawings can be combined with all kinds of functional data and images of the living brain. These atlases provide great insight into brain anatomy and function. However, they are usually derived from a single subject or represent an idealized reality. Obviously, this does not represent the wide range of anatomical and functional variation that is present even in healthy people. Each individual has a unique brain, differing in size, shape, vasculature, and functional and anatomical organization from all other brains. This is a problem when combining data from different subjects. Atlases that take the anatomical and functional variations into account can aid intersubject analysis.

1.2 Construction of atlases that encode anatomical variation

Correction for differences in brain anatomy between individuals is important both for the study of brain function [3] and for the analysis of structural differences [this thesis]. One strategy is the construction of a digital reference image or atlas. This allows mapping of individual brain images to a common reference. Early digital reference

frames and atlases were based on single subject data [4-11]. These did not account for the large variation in brain anatomy and location of brain function. Therefore, digital brain atlases representing these variations have been created.

Several approaches to the construction of an atlas encoding anatomical variation exist [12,13]. For example, density-based methods [14-18] encode anatomical variation as blurring. Density-based atlases are constructed by averaging registered (i.e. matched) images of individual brains. They are often very suitable as reference for the registration of images. Another approach is the construction of label-based atlases [19-25]. These atlases are based on segmented images of different individuals and provide the probability of finding a certain type of tissue at a certain position. Label-based atlases provide exact information on anatomical variation and are particularly interesting for the comparison of a patient with the population represented by the atlas.

Each strategy has its own benefits and shortcomings and the choice for a strategy depends on the issue under investigation. In this thesis a density-based average CT brain image and a reference lateral ventricles image were constructed. These images were based on subjects that were similar to the subjects included in the studies. Therefore, they are representative of the study populations. This is important for consistent and robust mapping of new subjects to the reference images. Detailed descriptions of the construction and evaluation of these images are provided in chapters 2 and 5 of this thesis.

1.3 Brain lesion distribution

Brain lesions† are areas of damaged brain tissue. In this thesis the distribution of brain infarcts and white matter lesions is examined.

1.3.1 Brain infarct distribution

The traditional approach to studying the distribution of brain infarcts (Section 1.5) is labeling each infarct as a certain type, but the number of types or categories is limited. Usually, the categories are based on the pattern of blood supply to the brain. There are large individual differences in this pattern that cannot be derived from the images that are used to label the infarct. And what if the classification of an infarct is ambiguous? Although these issues present drawbacks to the traditional approach, it has the advantage of being quick and easy to use, of being based on the knowledge of the expert, and to pose few requirements on image quality.

† Laesie: verwonding, beschadiging, letsel, blessure, kwetsuur; Zakwoordenboek der geneeskunde, 24e druk, 1993.

1.3.2 White matter lesion distribution

The distribution of white matter lesions (Section 1.8) is studied slightly differently. White matter lesions are usually graded depending on the amount of lesion. Often lesion location is also taken into account by applying a classification as deep or periventricular. Periventricular lesions are located in the white matter surrounding the lateral ventricles, the large fluid filled cavities inside the brain. Lesions in other white matter areas are termed deep white matter lesions. Examples of various types of white matter lesions are shown in Figure 1.8. Although lesion grading allows a quick indication of lesion severity, grading methods are not very accurate and inconsistencies between different methods for white matter lesion grading have been shown [26].

1.3.3 Lesion maps

The previous shows that categorization approaches to study lesion distribution are rather coarse and might not detect subtle differences in location. Using brain lesion maps offers the important advantage of fine scale analysis of differences in lesion distribution. Lesion distribution maps are constructed by combining lesions after having transformed them to a reference image. Analysis of differences in lesion maps of two groups of patients with, for example, different risk factors provides information about the disease mechanism.

Multiple approaches to the analysis of differences between two lesion distribution maps exist. Usually, comparisons are made between corresponding voxels of the lesion maps. In this thesis, two statistical methods have been applied to analyze differences in lesion distribution.

The first approach uses a nonparametric randomization procedure [27]. This method is based on the assumption that if the groups are similar, it does not matter which subject is put into which group. Therefore, the subjects can be randomly distributed into groups and new lesion maps are constructed. If the assumption of similar groups is true, the differences between the original lesion maps will be similar to those between the newly created maps. However, if the groups are not similar, the largest differences will be found between the original lesion maps, because in the lesion maps resulting from random patient distribution the difference between the groups is evened out. Comparing the difference between the original lesion maps with the differences between the new lesion maps allows an estimation of the probability that the original patient distribution is different from the random distributions. A drawback of this method is the amount of computation required for the construction of the randomized maps.

The second approach exploits the binary nature of lesion segmentation. At each position in the image, there is either a lesion, or there is none. Thus the lesion distribution map can be seen as counts of the number of lesions for every location in the group under investigation. Fisher's exact test determines whether the proportion of lesions differs between groups by computing the probability of obtaining exactly the frequencies observed and of any configuration with a more unbalanced distribution of frequencies, given the observed number of lesions in each group. This method is easily computed and well suited for the analysis of lesion maps.

1.4 Image registration and segmentation

1.4.1 Registration

Registration is the process of estimating an optimal transformation between two images. In other words registration is translating, rotating, scaling and sometimes also warping one image to get an optimal fit with another image. In this thesis registration is used to match series of images from the same individual and, more importantly, to match images of different individuals.

1.4.1.1 Similarity measure

Central to the concept of registration is the need for a way of telling when two images are most similar. Different similarity measures exist. In this thesis normalized mutual information [28] is chosen. A detailed survey on mutual information and its applications is presented in the paper by Pluim et al. [29]. Here, the concept of mutual information will only be introduced briefly. Mutual information measures the amount of information that one image provides about the other image. The more information one image provides about the other, the better the images are aligned. Mutual information is based on the association between the gray values in both images. The association is strongest when the two images are aligned. A joint histogram shows the distribution of gray values in one image related to the gray values at the corresponding location in the other image (Figure 1.3). When the alignment of the images is optimal the spread in the joint histogram is minimal. Note that the gray values in both images need not be similar. This is a major advantage of mutual information and allows a good performance in multimodality registration problems, such as the registration of different types of MR images of the same patient.

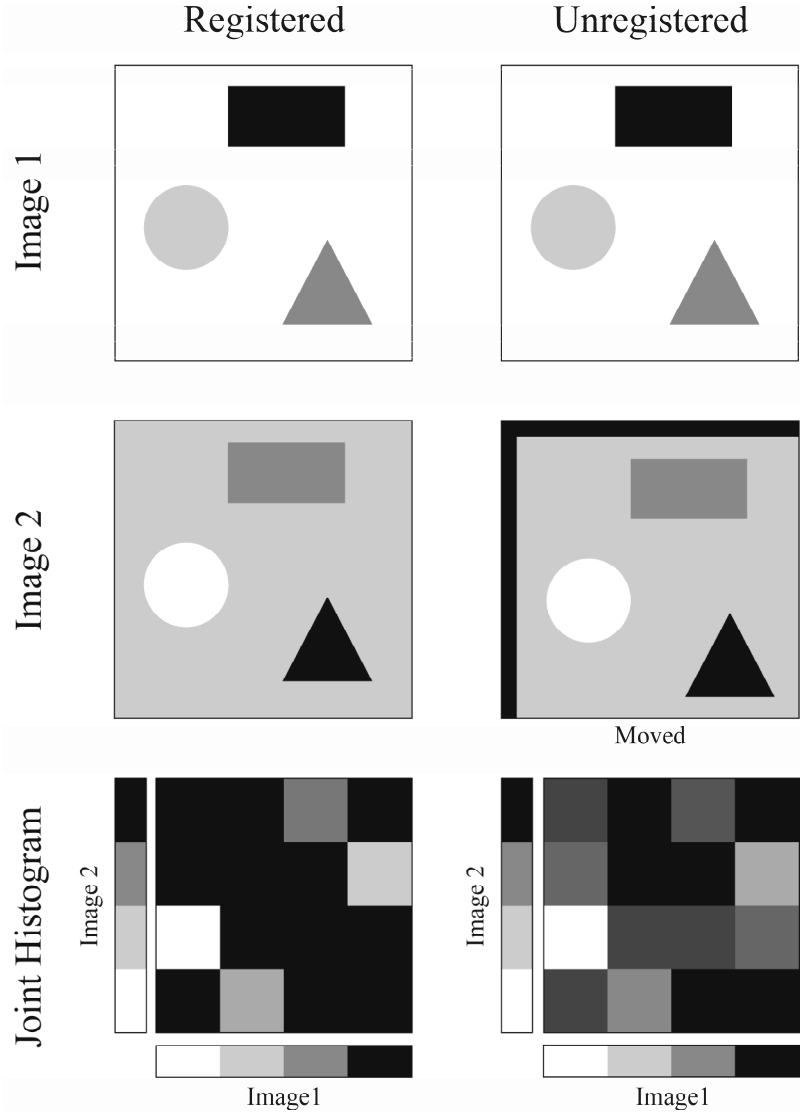

Figure 1.3 *Two images and their joint histogram.*
The upper row shows Image 1, which remains the same in both situations. The middle row shows Image 2. In the registered situation Image 2 is the same as Image 1 except that the colors have changed. In the unregistered situation Image 2 has been moved downwards and to the right. The bottom row shows the Joint Histograms for both situations. In the Joint Histogram the color of Image 1 is plotted against the color of Image 2 that occurs at the same location. The intensity in the Joint Histogram reflects the number of voxels with a certain color combination in Images 1 and 2; the higher the intensity the more frequent the combination occurs.

1.4.1.2 Transformations

In image registration a transformation is the change that is applied to one image to match it to the other image. The degree of freedom that is allowed for this change, i.e. the number of possible movements and deformations, depends on the registration task. The more freedom, the better the match, but also the more complicated and time consuming the calculations and the larger the risk of deformation errors. For instance, in this thesis only rigid transformations (translation and rotation) with scaling were allowed when images of the same person are being registered. For the registration of the lateral ventricles of different persons more complicated deformations are necessary. To correct for global differences in position and size affine transformations are used. Affine transformations include translation, rotation, scaling and skewing. The affine transformations can be used as initialization of free-form deformations or warping. In this thesis B-spline-based free-form deformation is used [30]. In short, a grid of control points is placed over the image that is to be matched with another image. The control points are moved during registration. This defines the deformation. For points in the image that are in between control points the movement of the control points is interpolated using B-splines (i.e. fitting a curve of prescribed format through the control points). The similarity of the images is determined and the control points are moved until an optimal similarity is reached.

1.4.2 Segmentation

Segmentation is the process of dividing an image into parts or segments. In this thesis three methods for image segmentation are used: manual segmentation, K-means clustering, and K-Nearest Neighbor classification. Different techniques are used to solve different segmentation tasks.

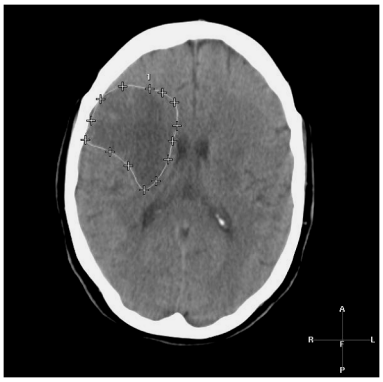

Figure 1.4 *Manual segmentation of a brain infarct on a CT image.*

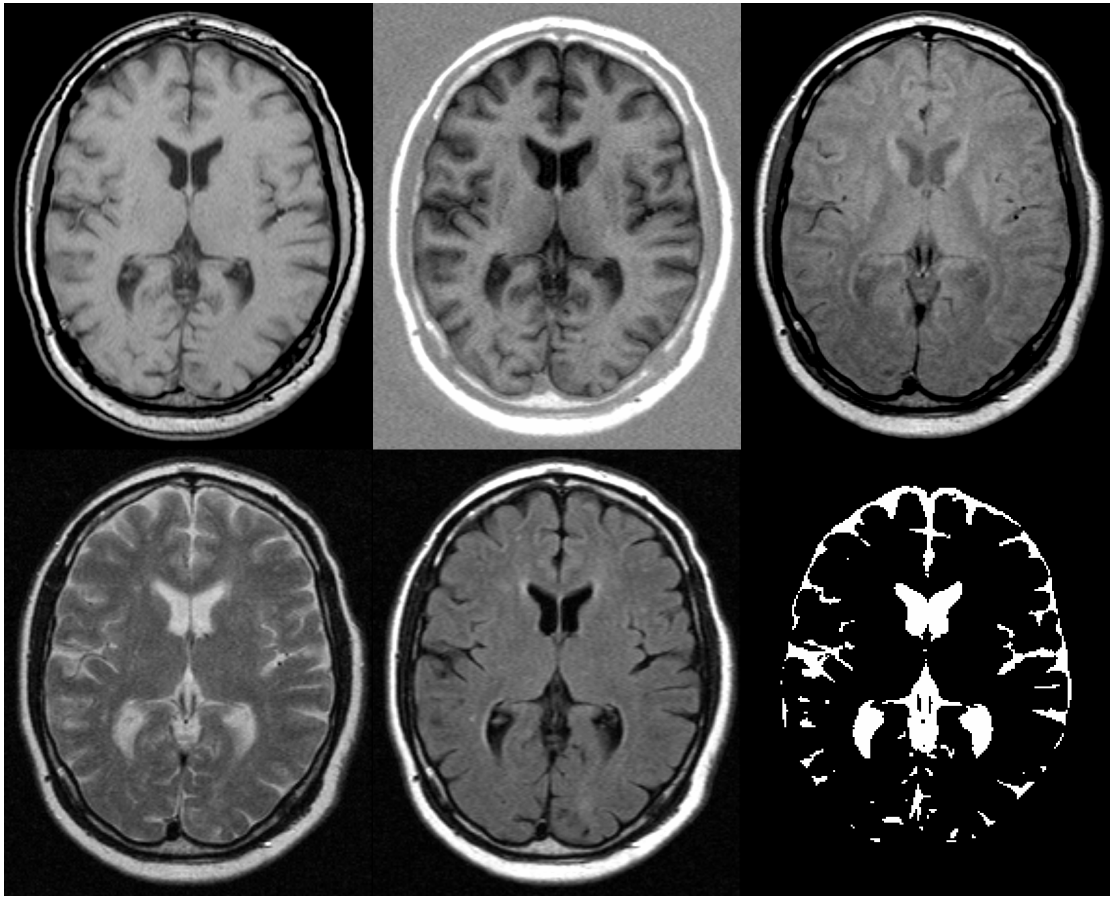

Figure 1.5 *Example of the available MR images and the CSF segmentation that results from K-means clustering.*
Top row: T1, Inversion Recovery, and Proton Density MR images.
Bottom row: T2 and FLAIR MR images and segmentation of CSF.

1.4.2.1 Manual segmentation

Manual segmentation was used to extract the brain infarcts from the CT brain images. Points around the infarct were manually selected and a curve was automatically fitted through these points (Figure 1.4). The advantage of manual segmentation is that the result is fully controlled by the expert doing the segmentation. However, manual segmentation is labor intensive and subjective when it is done by a single expert.

1.4.2.2 K-means clustering

K-means clustering is a technique that segments an image into a number of clusters by minimizing the variation of the gray values within each cluster. It does not require any user input except for the number of clusters (K) to be created. This is a major advantage over manual segmentation. However, clusters are only reliably segmented when they can be clearly distinguished from other image content. Cluster initialization is random. Therefore, it is not guaranteed that the desired clusters are found. In this thesis K-means clustering is used to extract CSF and brain tissue from series of five different types of MR images from the same subject. With the use of five different images, clusters of CSF and brain tissue can be clearly separated from other structures (Figure 1.5).

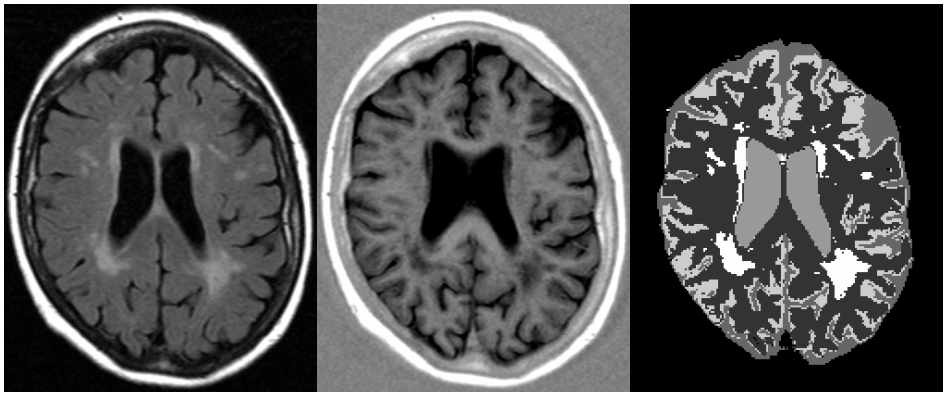

Figure 1.6 *(Color image on page 93) K-Nearest Neighbor classification in a female diabetes mellitus type 2 patient. A slice from the MR FLAIR (left) and MR Inversion Recovery (middle) scans is shown with the resulting classification (right).*
Dark gray – CSF; Light gray – Gray matter; Darkest gray – White matter; Middle gray – Lateral ventricles; White – White matter lesion.

1.4.2.3 K-Nearest Neighbor classification

K-Nearest Neighbor (KNN) classification is used for the segmentation of gray matter, white matter, CSF, lateral ventricles, and white matter lesions from MR images [31,32]. An example of a KNN classification is shown in Figure 1.6. KNN classification uses a set of manually labeled images as learning data. Features, such as intensity or location, are extracted. Classification is done by finding the K (in this thesis K=100) labeled voxels from the learning data that have features that are most similar to the features of the new voxel. The frequencies of the class labels of those K most similar voxels are calculated and used to label the new voxel. KNN classification is an automated method that uses prior knowledge. Therefore, it can be tailored to reliably perform difficult segmentation tasks such as white matter lesion segmentation.

1.5 Brain infarcts†

A brain infarct, also called an ischemic stroke, occurs when the blood supply to part of the brain is suddenly interrupted. Ischemia is the loss of oxygen and nutrients when there is inadequate blood flow. Ischemia ultimately leads to infarction, the death of brain cells. These cells are eventually replaced by a fluid-filled cavity (or infarct) in the injured brain. Ischemic stroke accounts for approximately 80 percent of all strokes. The other 20 percent of strokes are hemorrhagic strokes, which result from bleeding. An example of the appearance of an ischemic brain infarct on CT is shown in Figure 1.7.

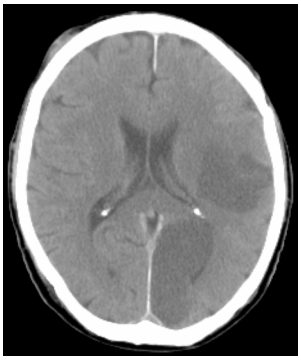

Figure 1.7 *CT image of two large ischemic brain infarcts. The infarcts show as darkened regions on CT images.*

† Based on information provided by the National Institute of Neurological Disorders and Stroke http://www.ninds.nih.gov/disorders/stroke/stroke.htm.

1.5.1 Risk factors

Some people run a higher risk of suffering a stroke than others. The most important risk factors for stroke are age, hypertension, heart disease, diabetes, and cigarette smoking. Others include heavy alcohol consumption, high blood cholesterol levels, illicit drug use, and genetic or congenital conditions, particularly vascular abnormalities.

The risk of stroke increases with age. For every decade after the age of 55, stroke risk doubles, and two-thirds of all strokes occur in people over 65 years old. People over 65 also have a seven-fold greater risk of dying when they have a stroke than the general population. Gender also plays a role: men have a higher risk of stroke. Of all risk factors that contribute to stroke, the most powerful is hypertension, or high blood pressure. People with hypertension have a risk for stroke that is four to six times higher than the risk for those without hypertension. However, the impact of hypertension on the total risk for stroke decreases with increasing age. After hypertension, the second most powerful risk factor for stroke is heart disease, especially a condition known as atrial fibrillation, which leads to an increased risk of the formation of blood clots. Diabetes is associated with a three times increase in a person's risk for stroke. Cigarette smoking almost doubles a person's risk for ischemic stroke by promoting atherosclerosis and increasing the levels of blood-clotting factors, such as fibrinogen. In addition, smoking also increases the damage that results from stroke.

1.5.2 Symptoms

The symptoms of a stroke are easy to spot. They include sudden numbness or weakness, especially on one side of the body; sudden confusion or trouble speaking or understanding speech; sudden trouble seeing in one or both eyes; sudden trouble walking, dizziness, or loss of balance or coordination; or sudden severe headache with no known cause. All of the symptoms of stroke appear suddenly, and often there is more than one symptom at the same time.

1.5.3 Consequences of stroke

Although stroke is a disease of the brain, it can affect the entire body. Some of the disabilities that can result from a stroke include paralysis, cognitive deficits, speech problems, emotional difficulties, and pain.

A common disability that results from stroke is complete paralysis on one side of the body, called hemiplegia. A related disability is one-sided weakness or hemiparesis. The paralysis or weakness may affect only the face, an arm, or a leg or may affect one entire side of the body and face. Motor deficits can result from damage to the motor cortex in the frontal lobes of the brain or from damage to the lower parts of the brain,

such as the cerebellum, which controls balance and coordination. This may cause problems with the simplest of daily activities, such as walking, dressing, eating, and using the bathroom.

Stroke may also cause problems with thinking, awareness, attention, learning, judgment, and memory. In some cases of stroke, the patient suffers a "neglect" syndrome. This means that a stroke patient has no knowledge of one side of his or her body, or one side of the visual field, and is unaware of the deficit. Stroke victims often have problems understanding or forming speech: aphasia. Aphasia usually occurs along with similar problems in reading or writing. Furthermore, a stroke can lead to emotional problems. Stroke patients may have difficulty controlling their emotions or may express inappropriate emotions in certain situations. Depression is common in stroke patients.

1.6 Internal carotid artery stenosis

The carotid arteries are located in the neck. They branch into the external and internal carotid arteries. The external carotid arteries provide blood to the tissues on the outside of the skull. The internal carotid arteries are the main suppliers of blood to the brain by providing approximately 80% of the total blood supply.

1.6.1 Internal carotid artery stenosis and brain infarcts

Stenosis[†] is a narrowing of the artery due to the build-up of plaque and blood clots along the artery wall. Plaque is a mixture of fatty substances, including cholesterol and other lipids. Atherosclerosis is the most common blood vessel disease that causes stenosis. The build-up of plaque along the inner walls of large and medium-sized arteries, causes thickening, hardening, and loss of elasticity of artery walls, and decreases blood flow.

Stenosis of the internal carotid artery (ICA) is a well-known cause of infarcts or strokes. The stenosis can be a source of emboli because small parts of the plaque dislodge. These emboli can travel along with the blood to the brain and may block an artery in the brain and thus cause an infarct. Another consequence of ICA stenosis can be a reduction of the blood flow to the brain so that some areas no longer receive adequate blood supply, resulting in infarction.

Stroke patients with severe stenosis benefit from carotid endarterectomy, a surgical procedure to reopen the vessel [33,34]. However, not all strokes in patients with a severe ICA stenosis are caused by the stenosis. It has been estimated that approximately 20%

[†] Stenose: vernauwing van een opening of kanaal, bijvoorbeeld bloedvaten; Zakwoordenboek der geneeskunde, 24e druk, 1993

of the strokes in the territory of a severe symptomatic ICA stenosis are not related to the stenosis. This percentage increases to 45% when the stenosis has not yet caused any symptoms [35].

1.6.2 Measuring stenosis

The ICA stenosis can be measured using different techniques. Digital subtraction angiography (DSA) is considered to be the gold standard. For DSA two X-ray images of the bifurcation of the carotid artery are made: the first image without and the second image with a contrast agent injected in the blood. These images are subtracted and what remains is an image of the blood in the vessels. On this subtraction image the smallest diameter of the vessel is measured. Although this method is fairly accurate, it has a risk of complications. Duplex ultrasound measurement of the blood flow velocity in the stenosis is another option. This technique is based on the Doppler effect: the shift in frequency that occurs when the source and the observer of the sound are moving with respect to each other, for example the changing pitch of the siren of an ambulance driving past. This frequency shift depends on the velocity of the movement. In duplex ultrasound this is used to measure the velocity of the blood flow. From the velocity the degree of stenosis can be derived. Duplex ultrasound is an easy, noninvasive procedure to estimate stenosis, but it is less accurate than DSA. However, a recent cost-effectiveness analysis has shown that duplex ultrasound is superior to DSA because of the risk of complications associated with DSA [36]. In this thesis the degree of ICA stenosis is derived from duplex ultrasound measurements of blood flow velocity.

1.7 Diabetes Mellitus type 2

In healthy people glucose that enters the blood after digestion of food is readily taken up by cells. This uptake is regulated by the hormone insulin. Insulin is produced by beta cells in the pancreas as a response to rising blood glucose levels after a meal. In patients with diabetes the regulation of the blood glucose level by insulin is disturbed. This leads to hyperglycemia or elevated blood glucose levels. Two major types of diabetes are distinguished. Diabetes mellitus type 1, also called insulin dependent diabetes mellitus, is characterized by defective insulin production caused by destruction of the pancreatic beta cells. Diabetes mellitus type 2 (DM2) is also called non-insulin dependent diabetes mellitus. It is characterized by insulin resistance and a subsequent impaired function of the beta cells. In insulin resistance body cells do not or insufficiently react to the insulin that is circulating in the blood.

1.7.1 Risk factors

In 2003 about 287 thousand men (34.6 per 1000) and 298 thousand women (36.3 per 1000) in The Netherlands had diabetes mellitus type 2[†]. Probably the real numbers are even higher because many people are unaware of having DM2. Although age is an important risk factor, DM2 is no longer exclusively found in adults aged 40 and over. Because obesity is an important risk factor for developing DM2, it is becoming increasingly common in adolescents and young adults. There is a strong genetic component to DM2: having first degree relatives with DM2 is a considerable risk factor and some ethnic backgrounds also carry increased risk of DM2. Furthermore, hypertension and elevated cholesterol are associated with DM2.

1.7.2 Symptoms

The onset of DM2 is usually very gradual. Therefore, it may take some time before the symptoms are recognized. The symptoms are similar to type 1 diabetes and include loss of glucose in the urine, which causes increased urine output and may lead to dehydration. This is compensated by increased thirst and water consumption. Other symptoms include fatigue and increased sensitivity to the development of infections.

1.7.3 Complications

Diabetes is a chronic disease with serious long-term complications. Diabetes leads to increased risks for cardiovascular disease, retinopathy (eye disease), neuropathy (nerve disease), and nephropathy (kidney disease). Diabetes damages the blood vessels by promoting atherosclerosis and thickening the vessel walls. This is at the base of many of the problems associated with diabetes including increased risk for stroke and heart attack. Retinopathy is one of the most prevalent complications. It is caused by damage to the small blood vessels in the retina of the eye and can ultimately lead to blindness. High blood glucose levels damage tissues and organs, causing for example neuropathy and nephropathy. Complications of diabetes also include cognitive impairment and dementia.

[†] Lisdonk EH van de, Bosch WJHM van den, Huygen FJA Ziekten in de huisartsenpraktijk. Utrecht: Bunge (2003) ISBN: 9035225848.

1.8 White Matter Lesions

White matter lesions (WMLs) show on certain MR images as bright areas in the white matter. WMLs are areas of damaged white matter tissue. WMLs are frequently seen in elderly people. A WML can be a thin line around the lateral ventricles (i.e. lining and capping), a punctate lesion, or a confluent lesion, which is usually large (Figure 1.8). WMLs are separated into periventricular, the white matter area around the lateral ventricles, and deep WMLs. Although differences between deep and periventricular WMLs exist, it is not clear where exactly to draw the line between them [37].

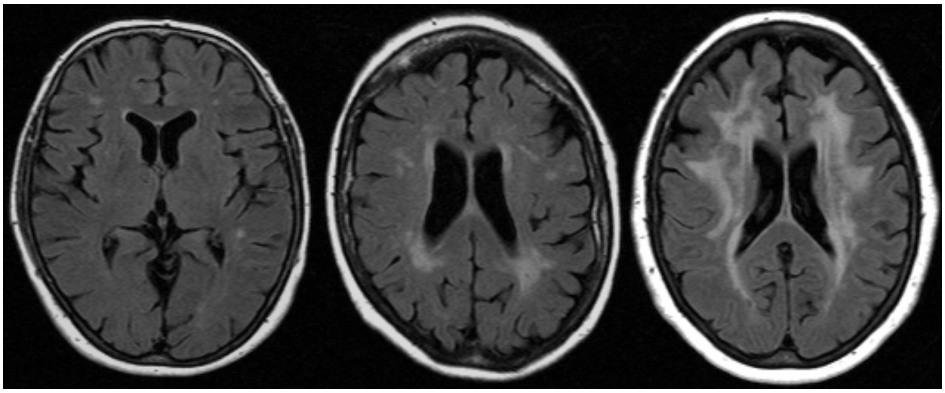

Figure 1.8 *Different degrees of white matter lesion severity.*
Left: *Punctate deep white matter lesions and capping of the lateral ventricles*
Middle: *Severe periventricular white matter lesions and some punctate deep white matter lesions*
Right: *Severe confluent white matter lesions.*

1.8.1 Risk factors

Many of the common cardiovascular risk factors also apply to WMLs. These include age, hypertension, smoking and the presence of cardiovascular disease [38,39]. Age is probably the most important risk factor for WMLs. Women appear to be more severely affected than men [40]. Hypertension has been associated with both periventricular and subcortical WMLs [41], but not consistently [42,43]. It seems that both increases and decreases in blood pressure are associated with WMLs [44], probably because hypertension leads to impaired regulation of blood flow, which may cause problems when blood pressure is suddenly reduced. Although diabetes has not been implicated in the development of WMLs consistently [45], this thesis provides further evidence of an association of diabetes with WMLs.

1.8.2 Pathophysiology

The underlying pathophysiology[†] of WMLs has not been completely elucidated. Probably, there are several different mechanisms leading to WMLs. In the case of periventricular lesions the lining of the lateral ventricles is often damaged. This leads to leakage of cerebrospinal fluid, which damages the white matter. Ischemia is another cause of WMLs [46]. Very likely the organization of the blood supply of the white matter plays an important role in the vulnerability of certain parts of the white matter to ischemia. Furthermore, arteriolosclerosis[‡] is often detected in areas with WMLs and may also lead to ischemia and impaired blood flow regulation.

1.8.3 Consequences

For quite some time WMLs were considered to be benign, because they are often seen in apparently healthy elderly. However, closer examination of elderly with WMLs has changed this opinion. Lesions in the frontal deep white matter have been associated with late-life depression [47]. Periventricular WMLs are associated with cognitive impairment and dementia [48,49]. WMLs have also been associated with impaired balance [50]. And apart from sharing common risk factors, the presence of WMLs also appears to be an independent risk factor for stroke.

1.9 Outline of thesis

The first part of this thesis deals with brain infarct patterns in patients with differing degrees of stenosis of the internal carotid artery and the second part is focused on the impact of diabetes mellitus type 2 on brain volume and on white matter lesion volume and pattern. For both topics the major research involved the construction and application of a reference image to map together the images of different subjects. For the brain infarct analysis the reference image was an average CT brain image and for the diabetes research it was a reference image of the lateral ventricles from MRI.
Construction and evaluation of the average CT brain image is described in Chapter 2.
Analysis of brain infarct patterns in patients with different degrees of internal carotid artery stenosis is performed in Chapter 3. CT brain images of individual patients are aligned with the average CT brain image. Brain infarcts are manually segmented and are combined to form infarct pattern images.
Chapter 4 concerns the comparison of the volume of gray matter, white matter, CSF, lateral ventricles, and white matter lesion in diabetes mellitus type 2 patients with controls. Volumes are automatically extracted from MR brain images.

[†] Pathophysiology: the functional changes associated with or resulting from disease or injury.
[‡] Arteriolosclerosis: changes in the vesselwall of the arterioles (small arteries) leading to thickening of the wall and narrowing of the vascular lumen.

Chapter 5 describes the construction and evaluation of a reference image of the lateral ventricles that is used for the construction of white matter lesion maps. CSF of individual patients is nonrigidly aligned with the reference lateral ventricles image. Thus, white matter lesions are also aligned.
The analysis of differences in white matter lesion distribution between diabetes mellitus type 2 patients and controls is performed in Chapter 6.

2

Construction and evaluation of an average CT brain image for intersubject registration

C. Jongen
J.P.W. Pluim
P.J. Nederkoorn
M.A. Viergever
W.J. Niessen
Computers in Biology and Medicine, 2004, 34(8):647-662

An average CT brain image is constructed to serve as reference frame for intersubject registration. A set of 96 clinical CT images is used. Registration includes translation, rotation, and anisotropic scaling. A temporary average based on a subset of 32 images is constructed. This image is used as reference for the iterative construction of the average CT image. This approach is computationally efficient and results in a consistent registration of the 96 images. Registration of new images to the average CT is more consistent than registration to a single CT image. The use of the average CT image is illustrated.

2.1 Introduction

Registration is important for intersubject comparison of brain images. Therefore, the construction of atlases and reference frames has received considerable attention [19]. Atlases and reference frames can, for example, be used for comparing anatomical structures of patients to an atlas; for comparing anatomical structures between groups of patients; for detecting and localizing pathologies; and for localizing functional data.

Early digital reference frames and atlases contained anatomical and cyto-architectural information based on images obtained from a single subject [4-11]. Obviously, the use of a single subject does not represent the wide range of anatomical variation of brain structures. Therefore, brain atlases representing these variations in anatomical structures have been created. There are three main approaches to the construction of an atlas and the coding of anatomical variation [12,13].

Density-based approaches [14-18] encode anatomical variations by the amount of blurring in a certain area in the image. This is achieved by registering and averaging the images. Thus, no user interaction is needed, which is important for the study of large numbers of images. Areas with large tissue type variability can be identified visually by the amount of blurring, but there is no data on the exact variation in tissue types. However, if the goal of the atlas is to provide a reference frame for registration of images to the same reference space, knowledge about the exact tissue distribution is not important. In that case the focus is on consistent and robust registration of images to the atlas, which can be done appropriately with a density-based atlas.

Label-based methods [19-25] provide a probability of finding a certain type of tissue at a certain position. Exact information on anatomical variance is available, but limited to the segmented tissues. Furthermore, the segmentation usually requires time-consuming user interaction. Label-based atlases are particularly interesting when information is needed on the deviation of a patient from the atlas population.

Deformation-based techniques [18,23,24,51-54] use non-linear registration algorithms to determine deformation maps. The accuracy and reliability of these methods depend on the registration algorithm used. In case abnormalities such as tumors or infarcts are present, non-linear registration can produce inaccurate results because a match is made between the abnormal tissue of the patient and the normal tissue of the atlas. Furthermore, these registration algorithms require approximately isotropic images with a high resolution. The advantage of deformation-based atlases is that they can serve both as a reference frame for non-linear registration and as a source of information on anatomical variation. In addition, the non-linear registration techniques used for this approach can also model local differences between patients.

The construction of the average CT brain image presented in this paper is part of a study that evaluates the relationship between the degree of Internal Carotid Artery (ICA) stenosis and the location of brain infarcts. For this study a large number of images need to be registered to a common reference space. Therefore, an average CT brain image is needed that can be used as a reference frame for automatic registration.

A label-based approach is not the most appropriate method to create a reference frame for registration, since our focus is not on anatomical differences between patients and the atlas population, but on the location of infarcts in different patient groups. Moreover, it requires segmentation of relevant tissues. This is unattractive for the present application that uses CT images, which have a low soft tissue contrast and thick slices. Furthermore, manual segmentation of the large number of images involved is virtually impossible. Although the use of a deformation-based technique probably leads to better local registration, it also carries the risk of local deformation and local size changes of the infarcts. Furthermore, the diagnostic CT images that are available are very anisotropic and have a low resolution in the slice direction, which hampers accurate non-linear registration.

In our case a density-based approach is best suited for the construction of an average CT brain image. An automatic registration algorithm corrects differences in pose and size between CT brain images. Thus, the available images can be handled without requiring user interaction.

The reference frame developed for stereotaxic operations by Talairach [55] is often used as a reference space for digital atlases [14-17,23,51,54,55]. However, it requires the identification of anatomical landmarks. Owing to the low soft tissue contrast of CT and the thick slices of the available images, the accurate identification of these landmarks is difficult. We use a two-step method that creates a temporary average in the first step. This average serves as reference space and as registration template for the second step, where the average CT brain image is generated. The evaluation shows that this average CT brain image is a good reference frame for intersubject registration.

2.2 Material and Methods

2.2.1 Data

Images were selected from a database of patients with a cerebrovascular accident (i.e. stroke), who were admitted to the neurology department of the University Medical Center Utrecht during the period July 1994 – April 1999. CT images with movement artefacts or abnormalities, such as operation defects, were excluded. This resulted in a database containing 400 patients. A subset of 96 randomly selected patients sufficed for the construction of the average CT brain image.
The images had a slice thickness between 4.5 and 5.0 mm and an in-plane resolution of 0.69 mm in the x-direction (left-right) and y-direction (anterior-posterior). The field of view contained at least the whole brain.

2.2.2 Method

2.2.2.1 Registration method

Both for the construction of the average CT brain image and for the registration of individual images to this reference image we used rigid registration with anisotropic scaling based on the maximization of normalized mutual information [56]. This method is intensity based and thus, did not require segmentation. Although maximization of mutual information was intended as a multi-modality registration measure, Holden et al. [57] showed that it also performed better for the registration of serial MR images of the head than several correlation-based measures. No preprocessing was done before registration. Partial volume interpolation was used with 256 bins for both the reference and the floating image. Powell optimization was used.

2.2.2.2 Construction steps

The construction of the average CT brain image was performed in two steps:
1) Construction of a temporary average image based on a subset of images.
2) Construction of a stable average image by an iterative registration procedure based on all images.

Step 1: Construction of a temporary average image

A temporary average image was created to diminish the dependence on the selection of a single image. Also, owing to optimization problems, registration between individual CT scans of different patients occasionally yields unsatisfactory results. This is prevented by using a temporary average, as will be shown in Section III. Figure 2.1 presents a flow diagram of the construction of the temporary average image.

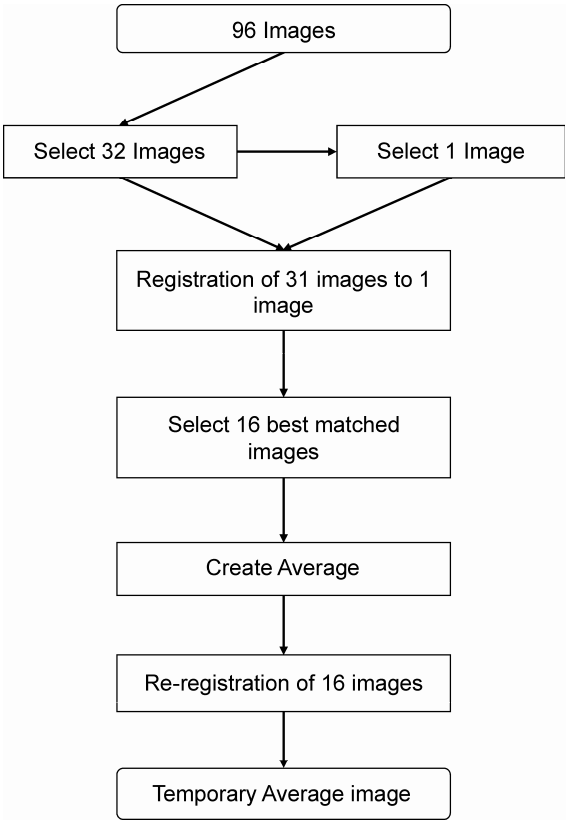

Figure 2.1 *Scheme showing the construction of the temporary average image.*

The temporary average image is constructed using 32 images, randomly selected from the 96 images. One of the 32 images was used as the reference image for registration. The only selection criterion imposed was that the number of slices of this reference image equaled the average number for the subgroup of 32 images. The reasoning for this selection criterion was that the location of the lowest slice was rather dependent on the number of slices. So, by choosing an image with an average number of slices as reference, the overlap in the field of view of the reference image and the 31 remaining images of the subgroup was optimal. Since not all intersubject registrations with single subjects result in correct registrations, the 16 images with the highest normalized mutual information measure were selected and averaged. This average was used as reference image for reregistration of the 16 selected images. The 16 registered images were averaged and formed the temporary average image. Averaging of images was performed using voxel-by-voxel averaging.

Step 2: Construction of a stable average image

The temporary average image created in the first step was used as the starting reference image for the construction of an average CT brain image. All 96 images were registered to the temporary average image. The registered images were averaged and the resulting average image served as the reference image for a new registration of the 96 images. In order to achieve a stable average image, this procedure was iterated until the average of the normalized mutual information measures of all 96 registrations did not change more than 0.5 % from one iteration to the next. Figure 2.2 illustrates this second step of constructing a stable average CT brain image.

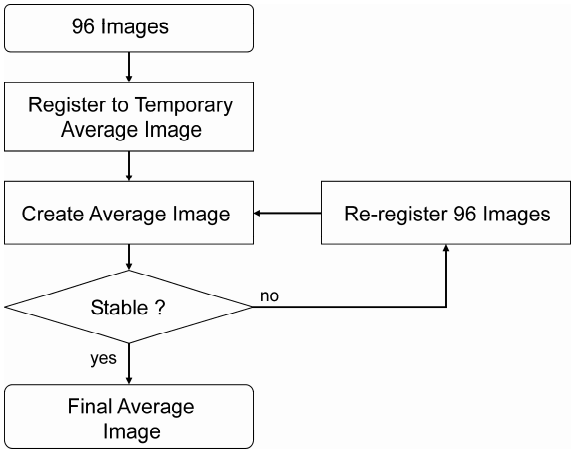

Figure 2.2 *Scheme showing the construction of the average CT brain image.*

2.2.2.3 Construction of three average CT brain images from the same set of images

A set of three average CT brain images was created based on the same set of 96 images. These average images were made with different temporary average images as starting references. The temporary average images were based on three non-overlapping subgroups of 32 images. The set of three average CT brain images can be used for evaluating the consistency of the registration to the average images (see Section III).

Table 2.1 shows that after two iterations the averaged normalized mutual information changed by less than 0.5 % for any of the three average images. Figure 2.3 shows six image slices of the three average CT brain images. The second and third average images are registered to the first to facilitate comparison. Anatomical details were well preserved in all three images.

Table 2.1 *Percentage of change in the averaged normalized mutual information between subsequent iterations of registration for the two-step method.*

Iteration	Average image A	Average image B	Average image C
1 versus 2	0.71%	0.78%	1.07%
2 versus 3	0.35%	0.31%	0.44%

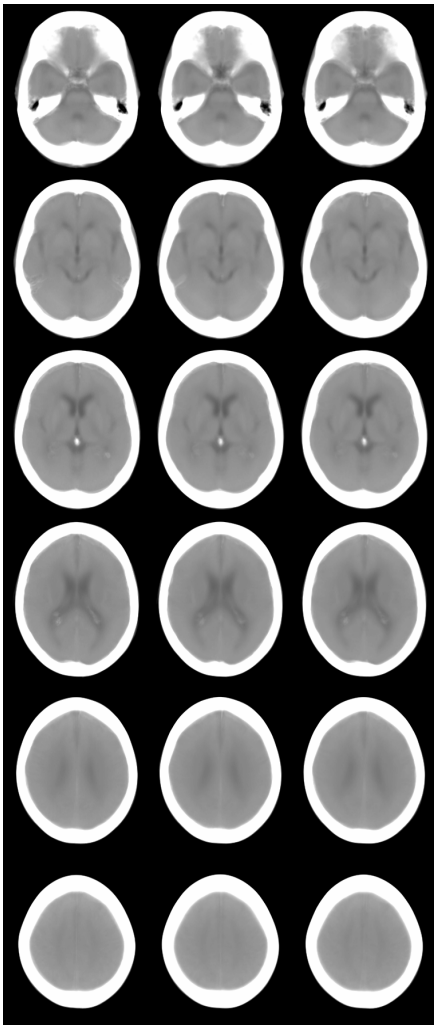

Figure 2.3 *Six slices from the three average CT brain images A, B, and C. Images B and C are registered to image A to facilitate comparison of the images*

2.3 Evaluation

The evaluation of the average brain image construction focuses on five issues:
- Consistency: have the 96 images been matched to the average image well?
- Applicability: do new images match to the average image with equal consistency?
- Robustness: is registration to an average brain image more robust than registration to a single brain image?
- Efficiency of construction: is the use of a two-step method based on a temporary average more efficient than the use of a one-step method of directly registering to a single image?
- Demonstration of use

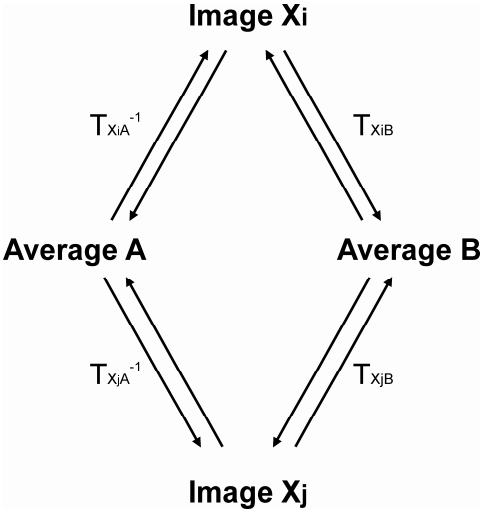

Figure 2.4 *Illustration showing that the transformation from average image A to average image B via single image Xi should be identical to the transformation from average image A to average image B via single image Xj.*

2.3.1 Consistency of registration to the average images

A gold standard for intersubject registrations is absent. However, the consistency of the method can be checked by using the transformations of the 96 images to the three average brain images. For each of the 96 images the transformation to all three average images was known. In the ideal case that all registrations are consistent, the transformations for all images from average image A - via themselves - to average image B are identical, see Figure 2.4. Therefore, the standard deviations of the rotation, translation, and scaling components of these transformations provide a measure for the

consistency of registration, whereas the means of these transformations merely reflect differences in pose and scaling between the average images.

The local consistency of registration was calculated by transforming every voxel in average image A to average image B using the 96 transformations via the individual images. The resulting spread in the voxel positions is an indication of the spatial accuracy that can be expected when registering an image with the average brain.

Results

The three average CT brain images were not aligned, since the temporary average images, obviously, differed in pose and scaling. This is reflected by the large means of the parameters for the transformations between the average images: rotations up to 3.3 degrees, translations up to 10.7 mm and scaling up to 11 percent. It is an indication of the size of the differences that have to be corrected by registration.

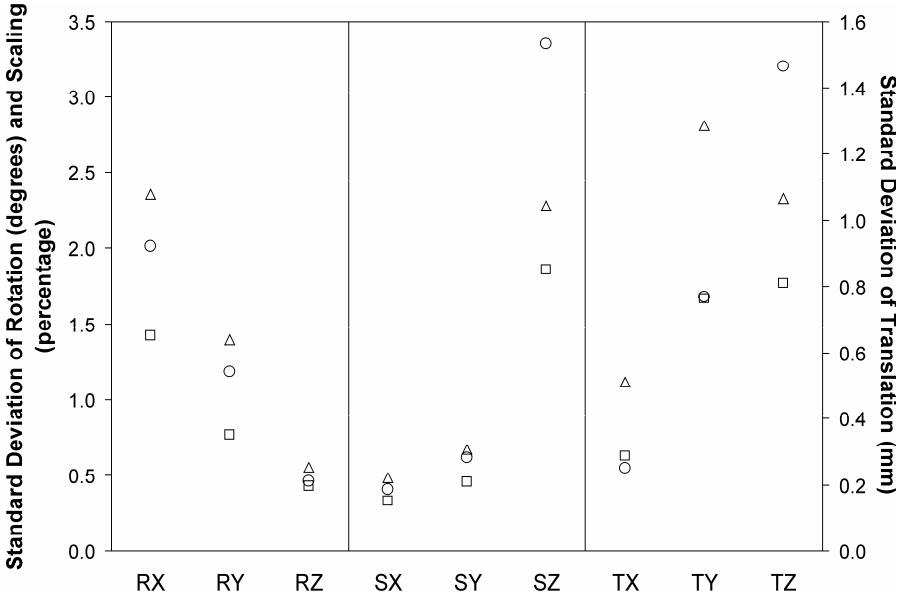

Figure 2.5 *Standard deviations of the rotation (RX, RY, RZ), scaling (SX, SY, SZ), and translation (TX, TY, TZ) parameters for the transformations of the 96 images between the three average CT brain images.*
○ *Standard deviations for transformations from average image A to average image B;*
□ *Standard deviations for transformations from average image A to average image C;*
Δ *Standard deviations for transformations from average image B to average image C.*

A measure of consistency is the standard deviation, not the mean, of the parameters for transformation of the 96 images between the average images. The standard deviations are shown in Figure 2.5. The maximum standard deviations found for all three transformations between the average images was 2.3 degrees for rotation around the x-axis, 1.47 mm for translation in the z-direction, and 3.4 percent for scaling in the z-direction. We expected that the standard deviations for rotations around the x-axis, translations in the z-direction and scaling in the z-direction would be larger because the resolution in the z-direction is poor. Furthermore, correct registration in the x-direction is slightly easier than in the y-direction, because of the brain and skull shape.

Since the standard deviations per parameter were similar for all three transformations between the averages, it is justified to use only the transformation between two average images, namely average images A and B, for the remainder of the evaluation.
The maximum standard deviations were considerably smaller than the magnitude of the transformations between the average images. This is an indication that the registration performed well. However, from these standard deviations no precise information is gathered on the displacement of voxels by the error in registration, since the errors for the single parameters may add to a large displacement or may interact to only a small displacement. Therefore, the standard deviation of the voxel positions, when the 96 transformations via the single images from average image A to average image B are applied, is shown in Figure 2.6 (see page 94). The magnitude of the standard deviation is color-coded: blue indicates a small and red indicates a large standard deviation. Segmentations of the skull and the ventricles of the average image are overlaid. The standard deviations range from 0.80 mm in the center of the image to 4.77 mm at the outer corners. The increase in standard deviation towards the corners of the image was caused by small errors in rotation and scaling. The increase does not take the shape of a sphere but of a slightly rotated ellipsoid, because of the anisotropy in the errors caused by the anisotropy in the voxel dimensions. As can be seen, the standard deviations within the brain are small compared to the voxel dimensions. This indicates that the registrations were accurate.

2.3.2 Applicability of the average images for registering new images

The second part of the evaluation was aimed at testing the applicability of the average CT brain image for registering new images. We carried out two experiments to examine this:

1) Registration of new images to the average CT brain image

   Ten new images from the database of patients with cerebral infarction were randomly selected. These were used to determine the consistency of registering new images of patients with the same disease to the average CT brain images. This was done the same way as the consistency of registration to the average CT brain image was determined above.

2) Registration of images of non-stroke patients to the average CT brain image

   We tested the applicability of the average CT brain image for registration of CT brain images of non-stroke patients. Non-stroke images were collected by taking ten recent CT images that fulfilled the following criteria:
   - The indication for the CT image was not related to stroke.
   - A radiologist had reported that the CT image showed no anatomical abnormalities.

   Furthermore, the presence of movement artifacts or abnormalities excluded the image.

Results

Figure 2.7 shows the standard deviations for the rotation, scaling and translation parameters of the transformations between average image A and average image B for the new stroke images, the non-stroke images, and the 96 images that were used to construct the averages (shown as a reference).

The standard deviations of the registration of new stroke images and non-stroke images to the average CT brain images was consistent with the registration of the 96 images used for constructing the average images. Therefore, the average CT brain image can be used to register CT brain images to the same reference space.

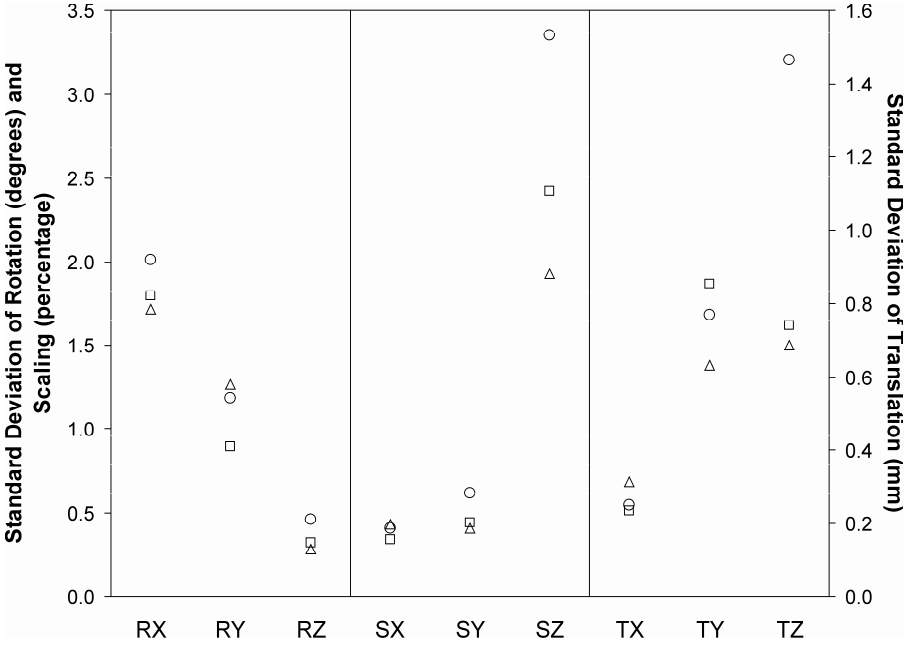

Figure 2.7 *Standard deviations of the parameters of the transformation between average images A and B.*
○ *96 images used to create the average images (as reference);*
□ *10 new images;*
Δ *10 non-stroke images.*

2.3.3 Robustness of registration to the average image

This experiment examined whether registration to an average CT brain image was more consistent than registration to a single brain image. The three single starting images used for the construction of the temporary average images served as reference images as this provided the fairest comparison. The ten new stroke images that were used in the section on applicability were registered to the single images. The consistency of these registrations was compared with the consistency of registering these images to the three average images.

Results

As can be seen in Figure 2.8, the standard deviations of the transformation parameters, using the three single images, were always larger than when using the average images. Thus, registration of images to the average CT brain images was more consistent than registration to single images.

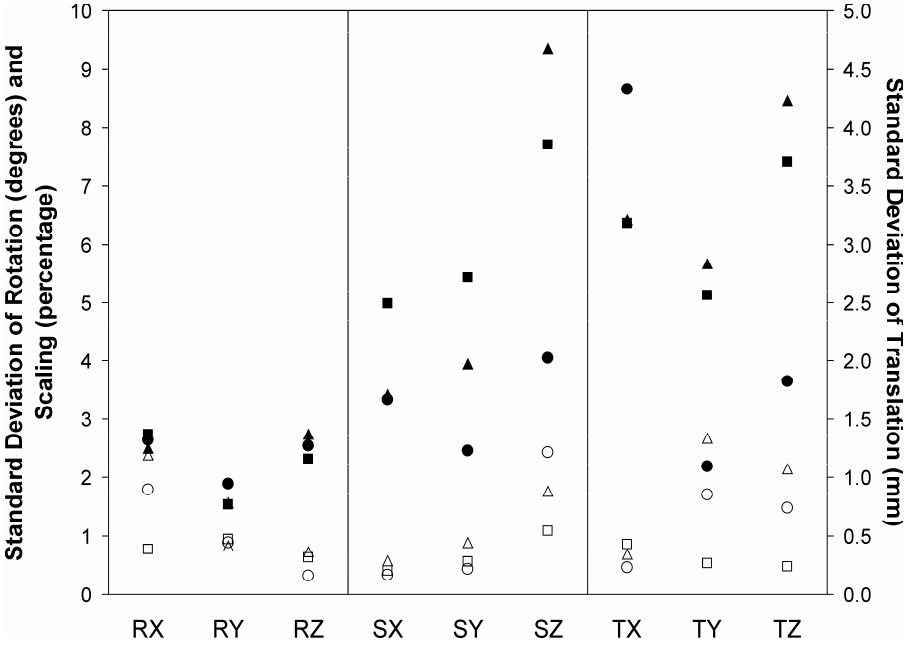

Figure 2.8 *Standard deviations of transformation parameters of the ten new images from the database to the three single images that were the starting references for the construction of the temporary average brain images shown as closed figures and the registration of the same ten images to the average images shown as open figures.*
● *and* ○ *transformation between average A and B;*
■ *and* □ *transformation between average A and C;*
▲*and* Δ *transformation between average B and C.*

2.3.4 Efficiency of the two-step construction method

The method described in this paper is based on two steps: first, the construction of a temporary average image based on a subset of all images and second, the construction of the average CT brain image using the temporary average image as the starting reference image. The efficiency of this two-step method was compared with a one-step method that used a single image as a starting reference for the registration of all 96 images and then iterated to a stable result, without the use of a temporary average image. The same two images that had been selected as the starting images for the construction of the temporary averages A and B were used as starting images to construct two average images with the one-step method.

The efficiency was measured by looking at the number of iterations and the number of function evaluations needed for convergence, which was achieved when the change in the averaged normalized mutual information from one iteration to the next was less than 0.5 %. Furthermore, the consistency of the registrations in the final iteration was evaluated.

Results

Table 2.1 shows that the two-step method converged after 2 iterations of the second step for all three average CT brain images, whereas the one-step method needed five iterations for starting image A and four iterations for starting image B to converge, as shown in Table 2.2. The number of function evaluations needed for convergence were 170 and 168 thousand for the two-step method and 328 and 287 thousand for the one-step method. Nevertheless, the consistency of the registration for the one-step and two-step methods was comparable. In conclusion, the two-step method yielded results similar to the one-step method, but was computationally more efficient.

Table 2.2 *Percentage of change in the averaged normalized mutual information between subsequent iterations of registration for the one-step method.*

Iteration	Starting image A	Starting image B
1 versus 2	11.2%	7.65%
2 versus 3	4.10%	2.64%
3 versus 4	0.82%	2.49%
4 versus 5	0.72%	0.16%
5 versus 6	0.34%	0.09%

2.3.5 Demonstration of use

The constructed average CT brain image is useful for studies comparing the location of structures in the brain for groups of patients. A reference frame is needed to map all patient images to the same reference space. This allows accurate comparison of localization patterns across groups of patients. The traditional approach to comparison of location is classification into a small number of classes. Obviously, the information provided by classification is limited by the number of categories and biased by the subjectivity associated with the choice of category boundaries and the subjectivity associated with classification if a structure is intersected by class boundaries.

The study that prompted the development of the average brain image focuses on the influence of the degree of ICA stenosis on brain infarct location. The traditional approach leads to conflicting results, depending on the boundaries of the classes on which the classification is based. This is clearly demonstrated by Hupperts et al. [58] who have used different boundaries for classification and found that risk factors for brain infarcts varied with their choice of class boundaries. No prior assumptions on the correct class boundaries have to be made when a reference frame is used to map all the patients to the same reference space.

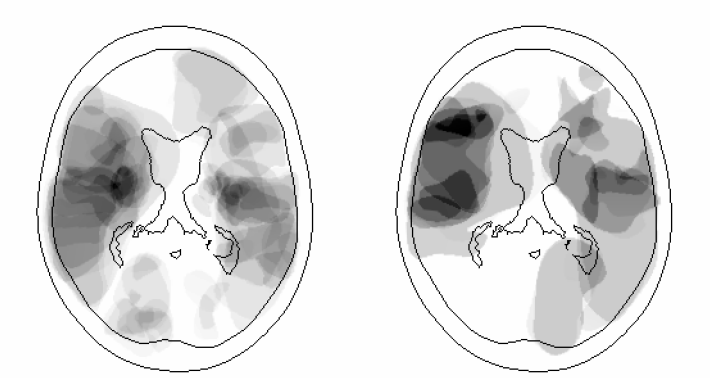

Figure 2.9 *On the left a slice showing the infarct pattern in the group of patients with 0-29% ICA stenosis and on the right the same slice showing the infarct pattern in the group of patients with ICA occlusion.*

As an illustration of the use of the average CT brain image Figure 2.9 shows one slice of the infarct pattern for patients with 0-29% ICA stenosis and for patients with ICA occlusion. These infarct patterns were made by using one of the average images described in this paper as a reference frame for registration. The patients were registered to the average CT brain image and grouped according to the severity of their ICA stenosis. The brain infarcts of all patients were segmented and also transformed to the reference space of the average brain image. For each group of patients the registered infarcts were summed to form an infarct pattern. These images allow the comparison of the location of brain infarcts in patients with different degrees of ICA stenosis.

2.4 Conclusion

An average CT brain image was constructed using a two-step method. The average CT brain image can be used as a reference frame for registering new CT brain images. The use of a two-step method approximately halved the number of function evaluations needed in the whole registration process. The construction of the average CT brain image was consistent. Registration to the average CT brain image was both robust and consistent. We demonstrated the application of the average CT brain image for the analysis of the location of brain infarcts in patients with different degrees of ICA stenosis. Thus, the described procedure offers an automated, consistent, and efficient way to construct an average CT brain image for intersubject comparisons of brain structure or lesion location.

3

Analysis of cerebral infarction pattern in CT images of patients with Internal Carotid Artery stenosis

C. Jongen
P.J. Nederkoorn
W.J. Niessen
J.P.W. Pluim
Investigative Radiology, 2004, 39(8):462-469

Rationale and Objectives – An unbiased and quantitative analysis of lesion patterns in patient groups is described and applied to the analysis of infarction patterns.
Materials and Methods – 142 CT images of patients with ischemic stroke are registered to an average CT brain image, which is used as template. Lesions are segmented manually and averaged per category of Internal Carotid Artery (ICA) stenosis. Thus, patterns of lesion distribution are formed. Differences are analyzed using non-parametric statistics. This analysis is compared with traditional classification of lesions.
Results – The non-parametric analysis showed an increased involvement of the territory of the middle cerebral artery in infarctions in patients with ICA occlusion compared to patients with mild or severe ICA stenosis. These differences did not show when classification of infarctions was used.
Conclusions – The presented method is more sensitive to differences in lesion pattern than traditional lesion classification and showed a different infarction pattern for ICA occlusion.

3.1 Introduction

Analysis of lesion locations for groups of patients is important. It can identify areas that have a high probability of being affected by disease when certain risk factors are present. The traditional approach to the analysis of lesion location is a manual classification of lesions in predefined classes of brain regions. This method is highly dependent on the number and on the definition of the classes used for the classification. The information on lesion distribution is limited to number of lesions per class. We developed a method that allows the analysis of lesion pattern differences per voxel. Segmented lesions are mapped to a common reference space and a voxel-wise analysis of differences in lesion pattern between patient groups is performed.

This method is applied to patients with a brain infarction and varying degrees of Internal Carotid Artery (ICA) stenosis. ICA stenosis is assumed to cause 20% of all strokes. Therefore, the problems associated with the use of classification to analyze infarction patterns are relevant for the current clinical practice, as is illustrated by the study of Hupperts et al. [58]. They found a correlation between lateral borderzone infarction and ipsilateral ICA occlusion when a classic definition of borderzone infarction was used, i.e. a slit-like infarction, elongated along the border of the anterior cerebral artery (ACA), middle cerebral artery (MCA) or the posterior cerebral artery (PCA). However, this correlation disappeared when the variability of the vasculature, as described by Van der Zwan et al. [59], was taken into account. Furthermore, it has been shown that severe ICA stenosis increases stroke risk and removal of the stenosis by carotid endarterectomy decreases this risk in symptomatic patients [33,60-62]. However, several hypotheses exist about the mechanisms that lead to an increased stroke risk: (i) ICA stenosis is a source of emboli; (ii) ICA stenosis causes hemodynamic impairment;

(iii) ICA stenosis is a source of emboli as well as a cause of hemodynamic impairment. Emboli are assumed to give rise to territorial infarctions, whereas compromised hemodynamics is assumed to cause infarctions at watershed areas, i.e. the borderzones between the brain areas supplied by different branches of the cerebral vasculature. Therefore, differences in infarction location provide a means to test the hypothesis of increasing involvement of watershed areas with increasing degrees of ICA stenosis. In patients with no or only mild ICA stenosis, no hemodynamic compromise is expected. We hypothesize that involvement of watershed areas will be rare in these patients. The infarctions will mainly involve the arterial territories and the lacunar and paraventricular brain areas. With increasing degrees of ICA stenosis hemodynamic impairment increases and a shift in infarction location towards a larger involvement of watershed areas is expected, especially in ICA occlusion. In that case, blood supply to the ipsilateral hemisphere depends on collateral pathways. Thus, occlusion of the ICA is likely to induce hemodynamic impairment and cause a larger involvement of watershed areas.

The method we propose uses an average CT brain image that serves as a common reference space. Brain CT images of 142 stroke patients are registered to this average CT brain image. The resulting transformations are used to map the infarct segmentations to this average CT brain image as well. Thus, all infarctions are mapped to the same reference space. The infarctions are grouped into three ICA stenosis categories: mild stenosis, severe stenosis, and occlusion and per category an infarction pattern is created. Differences in infarction pattern are analyzed using a non-parametric statistical analysis. This analysis is not biased by assumptions on the lesion distribution, but it is computationally expensive. The results are compared with analyzing differences in infarction pattern by classification of infarctions.

3.2 Materials and Methods

3.2.1 Data

Consecutive patients with a cerebral infarction who were admitted to the University Medical Center Utrecht in the period September 1994 – March 2001 were considered for selection. Inclusion criteria were the availability of both a CT scan within three months after the infarction and a duplex ultrasonography (DUS) examination of the ICA within nine months before and three months after the infarction, what resulted in a database of 506 patients. The liberal time intervals were chosen to include as many patients as possible. In practice, only two CT scans were made more than a month after the infarction and one DUS examination was done four months before the infarction, all other examinations were done within one and a half months before and three months after the infarction.

Reasons for exclusion were (number of patients in parentheses):

- no recent cerebral infarction visible on the CT scan (134)
- segmentation of infarction impossible (39)
- no primary stroke (25)
- carotid endarterectomy before the available duplex was made (25)
- operation defects (23)
- movement artifacts on CT scan (17)
- nature of cerebral lesion unclear (13)
- multiple recent cerebral infarctions (8)
- ICA dissection (3)

The main reason for infarcts not to be segmentable was that in case of CT scans made soon after the onset of stroke, the borders of the lesions were fuzzy. Although it is possible to include patients with multiple cerebral lesions we excluded them because it is dubious whether one or both infarcts should be classified or whether a separate multiple infarcts class should be made in the classic analysis of infarct location. Furthermore, when infarct volumes are compared (see section "Analysis of Data"), measurements for multiple infarcts also pose a problem: should only one infarct be measured, should the volumes be combined into a single measure or should both infarcts be included separately?

For every patient the degree of ICA stenosis was determined by a single measurement of the peak systolic velocity (PSV) in the proximal part of the ICA ipsilateral to the cerebral infarction, as measured with DUS. The PSV is considered to be the most accurate estimator of the degree of stenosis for DUS [63]. Mild ICA stenosis (0-49%) was defined as PSV values between 0 m/s and 1.9 m/s, severe ICA stenosis (50-99%) as PSV values above 1.9 m/s and ICA occlusion as a PSV of 0 m/s. A PSV value lower than 0.4 m/s with an abnormal flow spectrum was defined as a subtotal stenosis i.e. 99% stenosis and was included in the 50-99% stenosis category. In the period October 1996 to August 1997 evaluation of ultrasound PSV measures was done by digital subtraction angiography [64].

After the inclusion of 80 patients with mild ICA stenosis, further inclusion of patients in this stenosis category was stopped. This excluded 74 patients. For this group, a sample size of 80 patients was deemed sufficiently large. For three patients the registration to the average CT brain image was unsatisfactory. In total, 142 patients with cerebral infarction were used for the analysis. Table 3.1 lists some patient characteristics for each stenosis category.

Table 3.1 *Patient characteristics.*

	ICA Stenosis			
	0 - 49%	50 - 99%	Occlusion	Overall
Number of patients	80	33	29	142
Men	40	25	24	89
Women	40	8	5	53
Mean age men (years)	64.7	68.6	63.8	65.5
Mean age women (years)	65.3	65.0	68.9	65.6
Infarction volume before registration (cm^3)	17.2	16.6	43.9	22.5
Infarction volume after registration (cm^3)	20.5	19.4	52.4	26.8

The CT images have been acquired with an in-plane resolution of 0.69 mm and continuous slices of 4.5 to 5.0 mm (Philips SR8000 scanner, collimation 5 mm, no pitch, reconstruction filter 2 (head sharp)). For all 142 patients, the cerebral infarctions were manually delineated on every slice of the CT image on an EasyVision clinical workstation (Philips Medical Systems, Best, The Netherlands) by one observer (P.J.N.). The infarctions were classified by P.J.N. into classic infarction types: cortical, subcortical, lacunar, paraventricular, and watershed infarctions. The observer was blinded for the degree of ICA stenosis, but had access to the clinical report on the symptoms of the infarction.

3.2.2 Registration

The patient images were registered to an average CT brain image. The registrations optimized three translation, three rotation and three scaling parameters, using normalized mutual information [28,56] as optimization criterion. No pre-processing was done. The construction of the average CT brain image is briefly described in the section below. For an extensive description and evaluation of this procedure, we refer the reader to [65,66]. The average CT brain image is used as a reference frame for registration rather than using a single CT brain image, because it has been shown that for interpatient registration this yields superior results with respect to registration consistency [66].

To increase the amount of data for the infarction pattern analysis, we assume that the right and left hemispheres have similar vasculature. This allows us to map infarctions in the right hemisphere to the left hemisphere. First, a patient image with an infarction in the right hemisphere is registered to the average CT brain image. Thus, the segmentation of the infarction is also registered to the average CT brain image. Then,

this segmentation is mirrored in the anterior-posterior-axis. A second transformation is needed to map the mirrored infarction correctly onto the left hemisphere of the average CT brain image. This transformation is derived from registering a mirrored average CT brain image to the original average CT brain image.

3.2.3 Construction of an average CT brain image

A detailed description of the construction of an average CT brain image is provided in chapter 2. In short, the average CT brain image has been constructed from 96 CT brain images [65,66]. These were images of stroke patients scanned with the same protocol as described above, but without a DUS examination. The construction of the average CT brain image proceeds in two steps. First, a temporary average image is created based on a subset of 32 randomly selected images of the total of 96 images. One image of the subset is randomly picked as reference image and the remaining 31 are registered to the reference image. After the registration, the 16 images with the highest normalized mutual information measure are selected and averaged. The 16 images are registered to this average to obtain a converged temporary average image. The second construction step consists of registering all 96 images and forming the average CT brain image. The 96 images are registered to the temporary average image and a new average image is made. Then, the registration of the 96 images to the new average image and the construction of new average images is iterated, until the registration has converged i.e. the average normalized mutual information changes with less than 0.5%. The average CT brain image is shown in Figure 3.1.

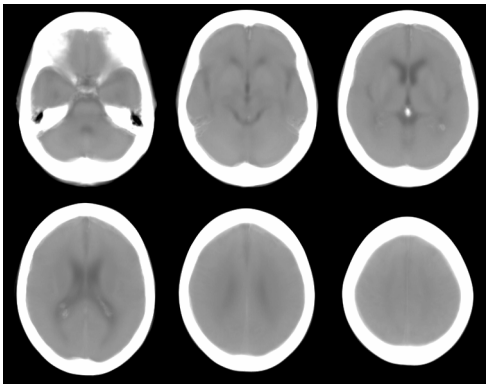

Figure 3.1 *Average CT brain image.*
The average CT brain image is used as the reference image for registration. Every third slice of the volume is shown.

3.2.4 Analysis of data

3.2.4.1 Infarction pattern analysis

The analysis of infarction pattern differences between stenosis categories is based on the non-parametric statistical method described in Holmes et al. [27]. Two stenosis categories, for example 0-49% stenosis and 50-99% stenosis, are compared. First, a probability image, or infarction pattern image, is constructed for both categories. In this infarction pattern image each voxel represents the percentage of occurrences of an infarction at that voxel position for that stenosis category. Subsequently, a statistical image is constructed by calculating for all voxel positions the absolute difference between the two infarction pattern images.

Next, we test the null hypothesis that no differences in infarction pattern between the stenosis categories exist. The idea of the method is that if the null hypothesis is true, the distribution of patients across stenosis categories is irrelevant for the resulting infarction pattern. So, every other distribution is equally valid and will result in a similar statistical image. Therefore, 999 random redistributions of the patients over the two stenosis categories are generated and the corresponding statistical images are calculated. The new statistical images resulting from the random redistributions of patients are compared with the statistical image resulting from the original distribution of patients. Since the original distribution is one of the possible distributions, it is also included in the comparison. This brings the total number of comparisons made to a thousand. The comparisons proceed as follows. For each voxel in the statistical image for the original distribution we count the times its value is exceeded or equaled by the value at that position in any of the new statistical images. This number is divided by the number of comparisons made. For each voxel this results in the chance (p) of finding a value at that position that is at least as large as the one found in the real statistical image. Small values for p indicate that differences in mean value as large as the difference found in the real situation are rare. That means that it is unlikely that the null hypothesis is true and thus, that it is likely that the infarction patterns differ.

3.2.4.2 Analysis of infarct classification

In the classic approach to lesion location analysis, Fisher's exact test is used to test for differences in distribution of ICA stenosis categories across infarction types. To allow a good comparison with our pattern analysis approach, we also did a pair-wise comparison of infarction type distribution between the stenosis categories.

The Kruskal-Wallis one-way analysis of variance by ranks is used to test for differences in distribution of PSV values across infarction types. PSV values are ranked with an increasing rank number for increasing PSV values. Occlusion of the ICA, PSV=0, is given the highest rank and subtotal stenosis is assigned a rank directly below the occlusion rank.

3.2.4.3 Analysis of infarction volume

The Kruskal-Wallis one-way analysis of variance by ranks test is used to compare ICA stenosis categories with respect to the distribution of infarction volume. Increasing ranks are assigned to increasing infarction volumes. Significant results ($p<0.05$) are further analyzed using a multiple comparison test. Significance levels are adjusted to the number of comparisons made.

The dependence between infarction volume and ICA PSV without classification into stenosis categories is examined using Spearman's Rank Correlation test. Infarction volumes are ranked as described above. PSV measures are ranked as described above.

Infarction volumes are calculated before and after registration to the average CT brain image for both analyses. The infarction volumes before registration reflect the actual infarction volumes, whereas the volumes after registration are infarction volumes normalized for differences in brain volume.

3.3 Results

Infarction patterns for 0-49% ICA stenosis, 50-99% ICA stenosis, and occlusion of the ICA are shown in Figure 3.2 (page 95). The colors reflect the proportional occurrence of infarcted tissue at a certain position. These infarction patterns show that for ICA occlusion certain brain areas are much more likely to be subject to infarction than other areas, whereas for both 0-49% and 50-99% ICA stenosis infarcted tissue is more evenly distributed.

The results of the analysis of infarction pattern differences are shown in Figure 3.3 (page 96). The colors indicate the chance that the compared infarction patterns are identical. Clearly, the 0-49% and the 50-99% ICA stenosis category are comparable (all p-values > 0.85). Patients with ICA occlusion tend to differ from both 0-49% and 50-99% stenosis categories, but the differences are small (0-49% stenosis vs. occlusion smallest $p=0.036$; 50-99% stenosis vs. occlusion smallest $p=0.055$). The smallest p-values, i.e. the largest differences, are found in the territory of the MCA, reflecting the large incidence of infarction in occluded patients in that area.

For each stenosis category the number of infarctions per infarction type is shown in Table 3.2. No significant differences were found in the distribution of infarction types across stenosis categories ($p=0.35$) or in the distribution of PSV values across infarction types ($p=0.35$). Also pair-wise comparisons of infarction types across stenosis categories did not show significant differences (0-49% vs. 50-99% $p=0.51$; 0-49% vs. occlusion $p=0.19$; 50-99% vs. occlusion $p= 0.49$).

Table 3.2 *Number of infarctions per type and percentages per stenosis category.*

	Infarction Type					
ICA Stenosis	Cortical	Subcortical	Lacunar	Paraventricular	Watershed	Total
0-49 %	38 48%	12 15%	27 34%	2 3%	1 1%	80
50-99%	14 42%	6 18%	9 27%	3 9%	1 3%	33
Occlusion	17 59%	5 17%	4 14%	1 3%	2 7%	29
Total	69 49%	23 16%	40 28%	6 4%	4 3%	142

Table 3.3 *Probabilities for several statistical analyses of stenosis degree versus infarction volume.*

	p (before registration)	p (after registration)
Kruskal-Wallis for all categories	0.005	0.009
0-49% stenosis vs. 50-99% stenosis	0.792	0.749
0-49% stenosis vs. occlusion	0.019	0.034
50-99% stenosis vs. occlusion	<0.001	<0.001
Infarction volume vs. PSV (not categorized)	0.129	0.140

Table 3.1 lists the average infarction volume per stenosis category. The Kruskal-Wallis analysis of infarction volumes across stenosis categories showed a significant difference in infarction volume distribution (Table 3.3). Further analysis revealed that the infarction volumes for the 0-49% and 50-99% stenosis categories differed significantly from the volumes for the occlusion category both before and after registration. Infarction volume and non-categorized PSV measurements were not significantly correlated (Spearman rank correlation coefficient before registration: 0.100 (p=0.88); after registration: 0.096 (p=0.87)).

3.4 Discussion

We have presented a method to compare lesion patterns between groups of patients. First, all patient images are registered to the same reference frame. After registration, differences in the distribution of lesions are analyzed using non-parametric statistics. We have applied this approach to the analysis of infarction distribution in patients with different degrees of ICA stenosis. However, this approach is also applicable to many other lesion analyses, for example white matter lesions analysis in patients with vascular diseases.

A similar approach has been taken by Adolphs et al. [67], who analyzed the role of focal brain lesion location in the visual recognition of emotion. They used a manual transfer of segmented lesions to a single reference brain and presented difference images of the compared groups. Statistical analysis of differences was done by rerandomization but only at six selected voxels. Karnath et al. [68] analyzed lesions in the thalamus and basal ganglia in patients with versus patients without spatial neglect. The lesions were manually drawn on a reference image. An image showing the difference between the two groups was calculated. No statistical analysis on the significance of these differences was performed. These methods differ from the presented method in the mapping of the segmentations to the reference space. In our method this is done using automated mutual information based image registration, whereas [67] and [68] use a manual transfer which is subject to operator bias. Furthermore, the statistical analysis of lesion patterns in the presented method is performed for the whole image instead of only for a small number of selected voxels. Our approach also resembles voxel-based morphometry (VBM) [69] in that both methods map images to a reference space and analyze differences between them. The major difference lies within the method for analysis of the data. VBM uses the general linear model for the statistical analysis. This requires that the data are normally distributed. To make sure this is the case, smoothing with a rather wide kernel is used. Since we are using binary infarction segmentations, the data are certainly not normally distributed. Therefore, we use a non-parametric statistical analysis based on randomization. Smoothing the data is not required.

To compare atlas-based analysis of lesion locations to the conventional method of assigning lesions to a class, we used a database that consisted of retrospectively collected patient data. The use of retrospective data has some shortcomings that may limit the conclusions that can be drawn. Firstly, to be included in this study, patients should have both a CT scan and a DUS examination of the ICA. This requires at least some time of survival. Thus, it is likely that our patient selection is slightly biased towards smaller, less disabling infarctions. This probably affects the group of ICA occlusion patients most, since it is likely that some of the occlusion patients have suffered a large infarct, which was immediately fatal. Furthermore, a DUS examination is not included in the standard routine for stroke patient work-up, which might result in a selection bias. Secondly, the exclusion of patients without a visible and segmentable infarction on the CT scan is a second source of bias. It will most likely exclude patients with minor strokes and only a mild ICA stenosis. Thus, the 0-49% stenosis category is

biased towards larger infarctions. Thirdly, the patients who have had a carotid endarterectomy will almost certainly have been patients with a severe ICA stenosis. This is a serious selection bias for the severe ICA stenosis category, because 25 patients were excluded and it now contains 33 patients. Lastly, patients with movement artifacts on the CT likely have suffered larger, more severe infarctions.

Areas of significant difference between ICA occlusion and both 0-49% and 50-99% ICA stenosis coincide with areas that have a high probability of infarction involvement in ICA occlusion patients. It is not possible to determine whether these differences in infarction pattern reflect differences in infarction location or in infarction volume, because a difference in volume leads to a difference in extent and thus, to a difference in location of the infarction. Barnett et al. [35] examined the causes of stroke in patients with symptomatic ICA stenosis. They estimated that approximately 35% of infarctions in patients with moderate ICA stenosis (<70%) were of lacunar or cardioembolic origin; in patients with severe ICA stenosis (70-99%), still approximately 20% of infarctions were of lacunar or cardioembolic origin. Therefore, it is likely that a substantial part of the patients with 50-99% stenosis included in our study suffer infarctions that are unrelated to their degree of ICA stenosis. This means that a large number of patients is needed to reveal any differences in infarction pattern, volume or classification between mild and severe ICA stenosis. Thus, a cause for the absence of statistically significant differences between patients with 0-49% and 50-99% ICA stenosis could be the small number of patients in the 50-99% stenosis category, although group sizes were sufficient to show differences between patients with ICA occlusion and both mild and severe ICA stenosis. A second cause for the absence of differences in infarct pattern between mild and severe ICA stenosis might be our rather liberal definition of severe ICA stenosis as 50-99% stenosis. This might have included patients with close to 50% stenosis that did not suffer from hemodynamic impairment, whereas patients with more severe stenosis did. Unfortunately, the small number of patients did not allow a finer subdivision of the categories. However, we expect the effect of the category definition to be limited since only 8 patients had PSV values between 1.9 and 2.7 m/s (50-69% ICA stenosis) and 25 patients had PSV values above 2.7 m/s (70%-99% stenosis) [64].

Application of the presented method to brain infarcts with differing degrees of ICA stenosis pointed towards differences in the territory of the MCA for 0-49% stenosis versus occlusion, and for 50-99% stenosis versus occlusion of the ICA. This was in agreement with the differences found in infarction volume. The infarction volume of patients with 0-49% and 50-99% ICA stenosis differed from the infarction volume of patients with ICA occlusion, both before and after registration to the average CT brain image. When using the traditional approach of classifying infarctions, we found no differences between ICA stenosis categories. This suggests that the presented method is more sensitive to differences in infarction pattern than the classification of infarctions. A disadvantage of the new method is that the image quality must allow segmentation and registration. A total 59 patients could not be included in the present study because the infarction could not be segmented (39), the image had severe motion artifacts (17)

or registration failed (3). A large number of these patients probably could have been used in the classification-based analysis. Thus, with low quality data classification of infarctions is preferred, because a larger amount of the data can be used. However, if image quality is good and infarctions are readily segmentable using the new method for infarction pattern analysis is preferred, because differences can be detected at a finer scale.

Thus, ICA occlusion was found to be correlated with infarctions in the territory of the MCA and with a larger infarction volume. Furthermore, this study showed that analyzing lesion patterns using a reference image and non-parametric statistics is a sensitive method for finding differences between groups of patients, provided that the image data is of good quality and lesions can be segmented. Differences are analyzed at a fine scale, allowing a precise localization. This approach is suitable for a wide range of applications involving the analysis of differences in the location of lesions or structures across patient groups.

4

Brain tissue and white matter lesion volume analysis in diabetes mellitus type 2

C. Jongen
J. van der Grond
L.J. Kappelle
G.J. Biessels
M.A. Viergever
J.P.W. Pluim
On behalf of the Utrecht Diabetic Encephalopathy Study group
Submitted

Objective – Diabetes mellitus type 2 (DM2) is associated with cognitive decline. The impact of DM2 on brain volume and white matter lesion (WML) severity is uncertain. This may be due to methodological limitations of previous neuroimaging studies. In this study we used an automated brain tissue and WML segmentation technique to assess the effects of DM2 on cerebral tissue and WML volumes.
Methods – Magnetic resonance images of ninety-nine DM2 patients and forty-six controls from a population-based sample were segmented. White matter, gray matter, lateral ventricles, cerebrospinal fluid not including lateral ventricles and WML volumes were assessed. The segmentation algorithm was a K-Nearest Neighbor classifier trained on ten manually segmented datasets. Analyses were adjusted for age, gender, level of education and intracranial volume.
Results – DM2 was significantly associated with reduced gray matter (-21.8 ml; 95% CI –34.2 to –9.4) and increased lateral ventricle (7.15 ml; 95% CI 2.28 to 12.0) and WML (1.06 ml; 95% CI .074 to 2.56) volumes. White matter volume was unaffected. The effects of DM2 were more pronounced in women.
Interpretation – Patients with DM2 have decreased gray matter and increased lateral ventricle volume. DM2 was also associated with increased WML volume.

4.1 Introduction

Diabetes mellitus type 2 (DM2) is associated with accelerated cognitive impairment and an increased incidence of dementia [70]. The structural correlates of these cognitive impairments have not yet been clearly established. Although previous neuroimaging studies have generally indicated that DM2 is associated with a moderate degree of cerebral atrophy [45,71-73], and with an increased occurrence of cerebral infarcts [74], the results of studies on white matter lesions (WMLs) are inconsistent. The impact of DM2 on brain volume has been studied semi-quantitatively using rating scales [45,71] and CSF to brain ratio's [45,72]. However, gray matter, white matter, lateral ventricle, and CSF volumes have not been assessed quantitatively. Several studies found an association between DM2 and WML severity or progression [42,72,75-80], whereas others did not [38,39,45,73,81-83]. These inconsistencies are probably due to differences in methods and study populations. Most studies applied semi-quantitative WML grading, using ordinal scales. Disagreement between the results of WML grading scales has been noted [26] and some scales are rather insensitive to the presence of mild to moderate WMLs. Furthermore, a high intersubject variability of WML severity exists even in healthy elderly [84]. Therefore, accurate quantitative measurements in a sufficiently large population-based sample are necessary. This study determined the effects of DM2 on cerebral tissue volume and WML severity. We have used an accurate magnetic resonance imaging (MRI) based automated segmentation algorithm [32] to assess cerebral tissue and WML volume in a large representative cross-sectional population-based sample of DM2 and control participants.

4.2 Subjects and methods

4.2.1 Participants

Participants were recruited as part of the Utrecht Diabetic Encephalopathy Study (UDES) on cognition in diabetes mellitus. A total of 122 DM2 patients and 61 controls were included between September 2002 and November 2004. DM2 patients were recruited through their general practitioner and had to be 55 to 80 years of age, functionally independent, and Dutch speaking. Minimal diabetes duration had to be one year. Controls were recruited among the spouses and acquaintances of the patients. Exclusion criteria were a psychiatric or neurological disorder unrelated to diabetes that could influence cognitive functioning, a history of alcohol or substance abuse, or dementia. Controls with a fasting blood glucose ≥ 7.0 mmol/l were excluded. Twice as many patients as controls were included to increase statistical power for within group analyses in the DM2 group. The study was approved by the medical ethics committee of the University Medical Center Utrecht and each participant signed an informed consent form. The present report included all DM2 patients and all controls aged 55 to 80 years with available digital MR images (48 controls and 103 DM2 patients). Image quality was too poor for processing in two controls and four DM2 patients. Data for 99 DM2 patients and 46 controls were analyzed.

In a standardized interview, participants were questioned about diabetes duration, height and weight, history of hypertension and smoking, and level of education [85]. Furthermore, all participants measured their blood pressure at home at nine different time points during the day. These values were used to calculate the mean arterial pressure. Hypertension was defined as an average systolic blood pressure ≥ 160 mm Hg and/or diastolic blood pressure ≥ 95 mm Hg and/or self reported use of blood pressure lowering drugs. Body mass index (BMI), fasting glucose, and glycosylated hemoglobin (HbA_{1c}) were determined as well.

4.2.2 MR imaging

Brain MR images were acquired on a Philips Gyroscan ACS-NT 15 whole body system operating at 1.5 Tesla (Philips Medical Systems, Best, The Netherlands). All participants were scanned using the same MRI protocol (slice thickness 4 mm, 38 contiguous slices, 230 x 230 mm field of view, 256 x 256 scan matrix). Axial T1, IR, T2, proton density (PD) and fluid attenuated inversion recovery (FLAIR) scans were made: T1: 234/2 ms (repetition time (TR)/echo time (TE)); IR: 2919/410/22 ms (TR/inversion time (TI)/TE); T2: 2200/100 ms (TR/TE); PD: 2200/11 ms (TR/TE); and FLAIR: 6000/2000/100 ms (TR/TI/TE).

4.2.3 Image processing

Pre-processing consisted of intrasubject registration of the five MR sequences and extraction of a brain mask. Registration was performed using an affine nine-parameter mutual information based algorithm [56] with the FLAIR image as reference. The brain mask was extracted by k-means clustering of the T1, IR, T2, PD and FLAIR images using eight clusters. The clusters containing cerebrospinal fluid and brain were combined and holes in the mask were filled. Appending structures, such as eyes, were removed using morphological operators. Dilation of the brain mask by three voxels ensured the inclusion of all cerebrospinal fluid. One mask had to be edited manually because appending structures were included.

Segmentation of the MR IR and FLAIR images into white matter (WM), gray matter (GM), lateral ventricle, cerebrospinal fluid not including the lateral ventricles (CSF), and WML proceeded automatically using a probabilistic K-Nearest Neighbor (KNN) based classification algorithm [32]. The algorithm was trained on manual segmentations of ten IR and FLAIR images of patients with varying degrees of WML, not included in this study. These patients were similar in age and were scanned using the same protocol as used for this study. For each participant, classification produced separate images listing WM, GM, lateral ventricle, CSF and WML probability per voxel. WM, GM, CSF and lateral ventricle volumes were calculated by summing over the probability image and multiplying with the voxel dimensions. WML volume calculation deviated slightly. A threshold at 0.5 was applied on the WML probability image and all unconnected voxels were removed. Then, WML volume was calculated by summation over the image and multiplication with the voxel dimensions. The intracranial volume was calculated as the sum of WM, GM, lateral ventricle, CSF, and WML volumes; total brain as WM plus GM volume; and total CSF as CSF plus lateral ventricle volume. Presence of cerebral infarcts was recorded and all segmentations were carefully reviewed. Twelve WML segmentations were manually edited to exclude infarcted tissue and ten were edited because of artifacts in the FLAIR image.

4.2.4 Statistical analysis

A univariate general linear model was used to analyze differences in tissue volume between DM2 and control participants adjusting for age, gender, intracranial volume, and level of education. The analyses were repeated for men and women separately, because gender affects absolute and relative cerebral tissue volumes. Furthermore, the effect of age was studied. Additionally, the effects of mean arterial pressure, hypertension, and glycosylated hemoglobin were analyzed in DM2 patients and controls separately and the effects of diabetes duration were analyzed in DM2 patients, adjusting for age, gender, intracranial volume and level of education. Kolmogorov-Smirnov tests showed that WML volumes were not normally distributed; therefore we used a natural log transformation of WML volumes in the analyses. Although lateral ventricle volume distribution was slightly non-normal non transformed volumes are

reported. Results of natural log transformation were similar results. One woman with DM2 was excluded from the statistical analyses but not from the reported tissue volumes because no data on level of education were available.

4.3 Results

Demographics and risk factors are shown in Table 4.1. Mean and standard deviation of brain tissue, CSF and WML volumes are shown in Table 4.2. For WML and lateral ventricle median and interquartile ranges are given as well. The effects of DM2 on tissue and WML volumes are shown in Table 4.3. In DM2 patients GM volume was significantly reduced and lateral ventricle volume was significantly increased. CSF volume was also increased, but not significantly, and WM volume was unaffected. WML volume was significantly increased in DM2 patients (1.06 ml; 95% CI 0.07 to 2.55 ml). The analysis was repeated for men and women separately. Strikingly, DM2 had no significant effect on tissue volume in men, whereas in women it significantly affected all cerebral volumes, except WM and WML volumes. However, the interaction between DM2 and gender was not significant ($p>0.15$ for all volumes).

Figure 4.1 shows the cumulative distribution of WML volume for male and female controls and for DM2 participants. Dichotomization of the data into very small total lesion volumes (<0.5 ml) and larger total lesion volumes indicated that relative to the control group a smaller proportion of the DM2 patients had very small lesion volumes (Pearson Chi-square with continuity correction, $p= 0.014$).

Hypertension was significantly more frequent ($p<0.001$) and mean arterial pressure was significantly higher ($p=0.011$) in diabetes subjects, but no significant effects of hypertension, analyzed using either mean arterial pressure or presence of hypertension, on cerebral volume or WML severity were observed in control or DM2 participants. Glycosylated hemoglobin was higher in DM2 patients ($p<0.001$). It was associated with a slight increase in GM volume (B = 6.48; Std. Error = 3.16; $p = 0.043$) in DM2 patients but not in controls. Diabetes duration had no significant effects. Age was significantly ($p<0.001$) associated with decreased GM and total brain volumes and increased lateral ventricle, CSF, total CSF and WML volumes. Age was the strongest predictor for WML and lateral ventricle volumes and it came second after intracranial volume for predicting GM, CSF, total brain, and total CSF volumes. No significant interactions of age and DM2 were found (all $p>0.14$). The interaction of age and gender showed a trend towards significance with men having more GM decrease ($p=0.092$) and women having more WM decrease ($p=0.079$) with age (other volumes $p>0.26$).

Table 4.1 *Demographics and risk factors (Mean (Standard Deviation)).*

		Control	DM2
N	M	20	49
	F	26	50
Age (years)	M	66.4 (6.3)	65.9 (6.0)
	F	63.8 (5.0)	65.9 (5.2)
Age range (years)	M	57.3 – 78.1	56.2 – 75.2
	F	55.2 – 73.6	56.3 – 75.4
Level of education (1-7)	M	4.5 (1.7)	4.4 (1.3)
	F	3.7 (1.1)	3.6 (1.3) (N=49)
Hypertension %	M	25	73
	F	31	68
Mean arterial pressure (mmHg)	M	98.7 (10.8)	102.2 (11.6)
	F	96.5 (10.3)	103.0 (11.5)
Glycosylated Hemoglobin (HbA_{1c})	M	5.4 (0.4)	6.7 (1.2) (N=48)
	F	5.5 (0.3)	7.0 (1.2) (N=49)
Diabetes duration (years)	M	-	7.5 (5.2) (N=48)
	F	-	9.8 (6.7)
BMI (kg/m^2)	M	28.9 (5.2)	27.9 (4.3) (N=47)
	F	25.9 (3.3)	28.2 (4.6) (N=48)

Table 4.2 *Tissue volumes in ml (Mean (Standard deviation)).*

	Control		DM2	
	Men	Women	Men	Women
White Matter	688.0 (49.3)	621.8 (46.9)	687.2 (56.5)	601.0 (56.5)
Gray Matter	401.7 (47.8)	404.4 (40.8)	388.3 (48.8)	360.1 (35.6)
Total Brain	1090 (81.0)	1026 (72.9)	1076 (91.0)	961.1 (71.0)
Lateral Ventricles	33.9 (18.7)	22.1 (8.66)	36.9 (17.4)	29.8 (13.9)
Lateral Ventricles[a]	30.1 (23.9-36.6)	20.3 (16.6-28.0)	33.8 (24.9-42.6)	26.7 (20.6-35.3)
CSF	273.3 (27.1)	222.1 (25.1)	279.7 (37.8)	229.4 (35.9)
Total CSF	307.2 (32.3)	244.2 (26.3)	316.5 (42.4)	259.2 (41.2)
White Matter Lesion	3.89 (5.76)	2.98 (4.70)	3.66 (5.37)	6.19 (14.2)
White Matter Lesion[a]	1.81 (0.47-3.48)	1.00 (0.48-3.20)	2.16 (0.91-3.86)	2.56 (0.86-4.46)
Intracranial Volume	1403 (90.7)	1275 (82.2)	1398 (104.2)	1228 (93.7)

[a] Median (Interquartile range)

Table 4.3 *Effect of DM2 on tissue volumes after adjustment for age, gender, intracranial volume, and level of education[#]. Analyses are shown for all control versus all DM2 participants and for men and women separately.*

	Dependent variable	B	95% Confidence Interval	
			Lower bound	Upper bound
All	White matter (ml)	2.80	-3.23	8.84
	Gray matter (ml)	-21.8	-34.2	-9.41
	Total brain (ml)	-19.0	-29.9	-8.10
	Lateral ventricles (ml)	7.15	2.28	12.0
	CSF without lateral ventricles (ml)	9.54	-0.413	19.5
	Total CSF (ml)	16.7	6.85	26.5
	LN White matter lesion	.448	0.039	.858
	White matter lesion[†] (ml)	1.06	0.074	2.56
Men	White matter (ml)	1.82	-7.36	11.0
	Gray matter (ml)	-14.5	-33.6	4.57
	Total brain (ml)	-12.7	-30.6	5.16
	Lateral ventricles (ml)	4.88	-3.74	13.5
	CSF without lateral ventricles (ml)	6.90	-10.2	24.0
	Total CSF (ml)	11.78	-4.92	28.5
	LN White matter lesion	0.374	-0.187	0.935
	White matter lesion[†] (ml)	0.861	-0.323	2.94
Women	White matter (ml)	7.03	-1.52	15.6
	Gray matter (ml)	-37.1	-54.1	-20.1
	Total brain (ml)	-30.1	-44.9	-15.4
	Lateral ventricles (ml)	8.99	3.18	14.8
	CSF without lateral ventricles (ml)	17.2	4.89	29.4
	Total CSF (ml)	26.1	13.6	38.7
	LN White matter lesion	0.545	-0.112	1.20
	White matter lesion[†] (ml)	1.35	-0.197	4.33

[#] Data on level of education was missing for one woman with DM2.
[†] White matter lesion volume derived from natural log transformed analysis.

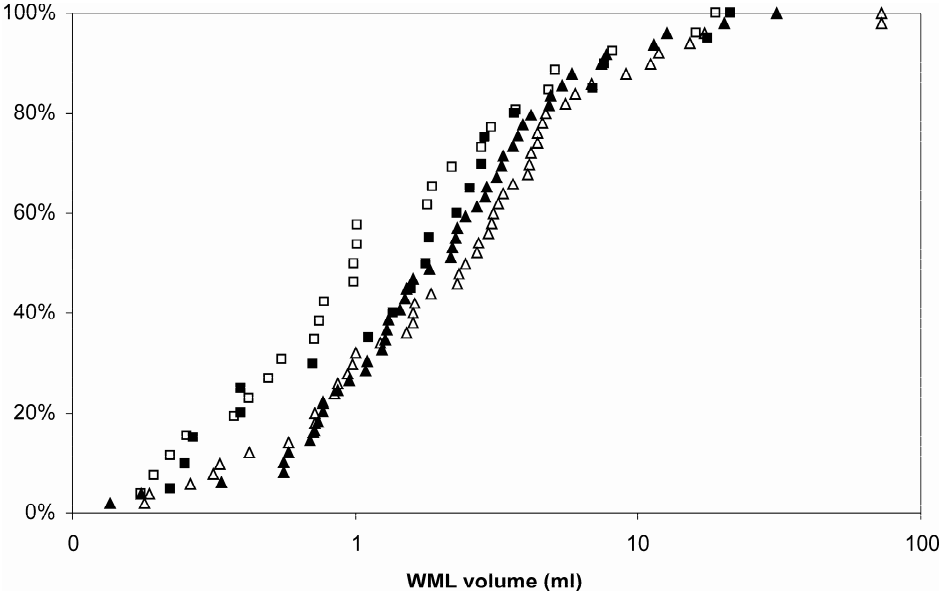

Figure 4.1 *Cumulative distribution of WML volume (control men ■, control women □, DM2 men ▲and DM2 women Δ).*

4.4 Discussion

Our MRI based segmentation paradigm showed that DM2 was significantly associated with reduced GM and increased lateral ventricle and of WML volumes, whereas WM volume was unaffected. The reduction in GM suggests cortical atrophy. The increase of ventricular volume together with the unaffected WM volume suggests limited subcortical atrophy. These findings agree with Schmidt et al. [45], who found a clear association between DM2 and cortical atrophy, measured on a rating scale, but no association with subcortical atrophy, measured as frontal ventricle-to-brain ratio.

Men and women differ in intracranial volume and in relative and absolute GM and WM volumes [86]. Gender also influences the effects of ageing [87-89]. In our study, separate analysis of women showed significant decreases in GM volume and significant increases in lateral ventricle and CSF volumes, whereas this was not found in men. However, the interaction between DM2 and gender was not statistically significant. Still, this effect of DM2 on women is remarkable, because men are generally more severely affected by age related GM decrease than women [89,90]. It could be that the effect of age masks the effect of DM2 in men. This is supported by the significant effect of age on tissue volumes and the larger age related decline in GM volume in men. WMLs might be more severe in women than in men [39,40,91,92], but have

also been reported to be similar [84]. WML volume was similar among male and female controls, whereas in DM2 patients we found significantly larger WML volumes in women than in men (p=0.022).

Our study showed that very small lesion volumes are less frequent in DM2 patients than in controls. Very small lesion volumes might reflect pencil thin lining and capping, which are sometimes considered to be a normative finding [84]. Several studies have found increased WML volumes or WML progression in DM2 patients [42,75-80], whereas others did not [38,39,45,73,81-83]. Several methodological factors are likely to be a source of these variable results. First, techniques to measure WML severity vary widely from merely denoting lesion presence or absence [79] to volumetric measurements [80,83]. The majority of studies applied ordinal grading scales. It has been shown that these scales might give inconsistent results [26] and some scales are rather insensitive to mild to moderate WMLs. Second, the examined population and the study type vary considerably. Only a small proportion of the studies had a true population-based setting, whereas the majority of studies were hospital based, involving cohorts of patients with stroke, hypertension or other forms of cardiovascular disease. Furthermore, small sample sizes may have reduced statistical power, with several studies involving less than twenty DM2 patients [42,78-80,83].

As expected, age was a very important predictor of brain volumes. Hypertension has also been marked as an important risk factor for both cerebral atrophy [93,94] and WML [41,44,95], although an association between hypertension and atrophy [96] or WML severity [42] has not been reported consistently. We did not find significant associations between hypertension and cerebral volumes. Glycosylated hemoglobin has been linked with cerebral atrophy [96] and WMLs [97] in subjects without diabetes. We could not replicate this finding. Instead we found an association between glycosylated hemoglobin and a slight increase in GM volume in DM2 patients which is difficult to understand and therefore probably due to chance. Diabetes duration had no effect.

Automated volumetric segmentation offers major advantages over manually driven methods. It enables precise volumetric measurements of cerebral tissues in large numbers of patients and controls. However, it also has some limitations. In subjects with markedly enlarged occipital horns the volume of the lateral ventricles might be slightly underestimated and the volume of the CSF might be slightly overestimated by the segmentation algorithm. Some misclassification of interhemispheric CSF as lateral ventricle might also occur. However, the involved volumes are very small compared to ventricle and CSF volumes. Both artifacts were proportionally distributed across males and females and between DM2 patients and controls. Therefore, it is unlikely that these inaccuracies have affected the analyses. WML was not separated into deep and periventricular lesions. So, it is not possible to determine whether the DM2 associated increase in WML is primarily located in the deep or in the periventricular white matter. DeCarli et al. [37] have suggested that categorical distinctions between deep and periventricular WMLs may be arbitrary because WMLs extend smoothly from the

ventricular wall. Therefore, it is hard to reliably define a meaningful boundary for WML separation.

Other studies that used automated volumetric segmentation [86-88,90] reported larger GM volumes than WM volumes, whereas we found larger WM than GM volumes both in the automated segmentations of the controls as well as in the manual gold standard segmentations. These previous studies have used either T1 and T2 [86], PD and T2 [87], T1 [88], or T1, PD, and T2 [90] MR images for segmentation. Our manual segmentation of the gray and white matter was based on MR IR images with information from T1, T2, PD and FLAIR images available to the expert. MR IR images provide the best tissue contrast for defining the GM-WM boundary. Manual segmentation of ventricle, CSF and WML was based on FLAIR images, again with the other MR images available to the expert. Thus, manual segmentation of the learning data was based on an optimal choice of MR images. Furthermore, volumes of automatically segmented cerebral tissue for control men did not differ from tissue volumes for the manual segmentations used for the gold standard (men N=8). Moreover, in a previous study we have shown that the use of IR and FLAIR images is highly preferable in brain tissue segmentation and that performance of the automated KNN classification algorithm is optimal with this image combination [32].

In summary, using an automated segmentation algorithm we acquired accurate data on white matter, gray matter, CSF, lateral ventricles, and WML volumes in a large cross-sectional population-based sample of DM2 patients and control participants. We found that DM2 is associated with decreased GM and increased lateral ventricle volume, suggesting cortical and limited subcortical atrophy. These effects were most pronounced in women. Although WML volume is very variable, even in healthy elderly, the use of an accurate segmentation algorithm and a large sample of DM2 patients, allowed us to show that DM2 patients have increased WML volumes, but the strength of the association is modest.

5

Construction and evaluation of a reference image of the lateral ventricles for interpatient white matter lesion analysis

C. Jongen
J. van der Grond
G.J. Biessels
J.P.W. Pluim

A reference image of the lateral ventricles has been constructed for the creation of white matter lesion maps. Accurate registration of the lateral ventricles is important for the creation of these maps. The reference image of the lateral ventricles is based on twenty-four subjects. The construction of the reference is described. The accuracy of registration to the reference lateral ventricles image is evaluated by measuring the overlap of registered images with the reference lateral ventricles and with the background around the reference lateral ventricles. The deformations that register the lateral ventricles are extrapolated to the white matter around the lateral ventricles. Thus the periventricular white matter and white matter lesions are registered. The accuracy of this approach is tested by calculating the difference in transformation between the voxels in the white matter and the closest voxel on the lateral ventricle boundary. The evaluations show that the constructed reference lateral ventricles image allows accurate registration of lateral ventricles and the surrounding white matter.

5.1 Introduction

Although the pathophysiology of subcortical and periventricular white matter lesions (WMLs) is different [98], the boundary between subcortical and periventricular WMLs is hard to define on magnetic resonance (MR) images [37]. The use of lesion maps allows accurate analysis of differences in WML location at the level of the lateral ventricles without the definition of a boundary. To create WML maps of the area around the lateral ventricles an accurate mapping of the lateral ventricles is necessary.
Lateral ventricle shape is highly variable between subjects. Therefore, fine-scale non rigid deformations are required to obtain an accurate registration. When gray-value images of subjects with WMLs are used for fine-scale non-rigid registration, WMLs may deform to match healthy tissue in the reference image. Excluding the WMLs from registration avoids this, but affects registration accuracy depending on the extent and location of the lesions. Therefore, we have chosen not to use gray-value images but to use binary segmentations of the lateral ventricles and cerebrospinal fluid (CSF) instead.

The CSF segmentations need to be registered, especially the lateral ventricles. The use of an average image as reference results in better registration performance than the use of an image of a single subject [66]. Therefore, a reference image based on the lateral ventricles of twenty-four subjects is constructed for the interpatient registration of CSF segmentations.

Accurate CSF segmentation can be performed automatically, whereas reliable separation of the lateral ventricles from the CSF segmentation must be done manually. Incorrect matching of sulci is very likely in interpatient registration of CSF segmentations. Therefore, we have chosen to use a reference image based on manually segmented lateral ventricles and register for each patient an automatically extracted CSF segmentation to this reference. In three subjects registration using CSF segmentations is compared with registration using manually separated lateral ventricles.

The accuracy of registering CSF segmentations to the reference lateral ventricles is evaluated by measuring the overlap of each CSF segmentation with the reference lateral ventricles and with the area around the reference. Furthermore, the accuracy of extrapolating the registration to the white matter area around the lateral ventricles is evaluated. The aim of this study is to construct a reference lateral ventricle image that allows accurate mapping of WMLs in a wide area around the lateral ventricles to create WML maps.

5.2 Materials and methods

5.2.1 MR image acquisition

Brain MR images were acquired on a Philips Gyroscan ACS-NT 15 whole body system (1.5 Tesla, Philips Medical Systems, Best, The Netherlands). The same MR protocol was used for all participants. Axial T1-weighted (T1), inversion recovery (IR), T2-weighted (T2), proton density (PD) and fluid attenuated inversion recovery (FLAIR) scans were made. Scan parameters were (repetition time (TR), echo time (TE), inversion time (TI)): T1: 234/2 ms (TR/TE); IR: 2919/410/22 ms (TR/TI/TE); T2: 2200/100 ms (TR/TE); PD: 2200/11 ms (TR/TE); and FLAIR: 6000/2000/100 ms (TR/TI/TE); slice thickness 4 mm; 38 contiguous slices; 230 x 230 mm field of view; 256 x 256 scan matrix. Twenty-four subjects (mean age 65.7, range 55 to 76 years) with peripheral arterial vascular disease were used.

5.2.2 Construction of a reference image of the lateral ventricles

A scheme of the construction of the reference lateral ventricles is shown in Figure 5.1. Lateral ventricles were segmented by thresholding the MR FLAIR scans followed by manual editing. The segmentations were interpolated to isotropic voxels using shape-based interpolation [99]. First, an estimate of the average position and size of the lateral ventricles was calculated by registering eight randomly selected ventricles with a 12-parameter affine registration [30] using normalized mutual information as registration criterion [28,56]. The ventricles were transformed to the average position, summed, and

thresholded at four. The next step was an affine registration of the eight lateral ventricles to the thresholded image. The registered images were summed and again thresholded at four. This average position image was used as reference image for the affine registration of the twenty-four lateral ventricles. After registration and summation, the resulting image was the reference for the non-rigid B-spline based registration [30] of the twenty-four affine registered lateral ventricles. A control point spacing (CPS) of 32 voxels was chosen to correct for global differences in ventricle shape only. After non-rigid registration, the ventricles were summed and thresholded at eight. The resulting binary image is the reference lateral ventricles image.

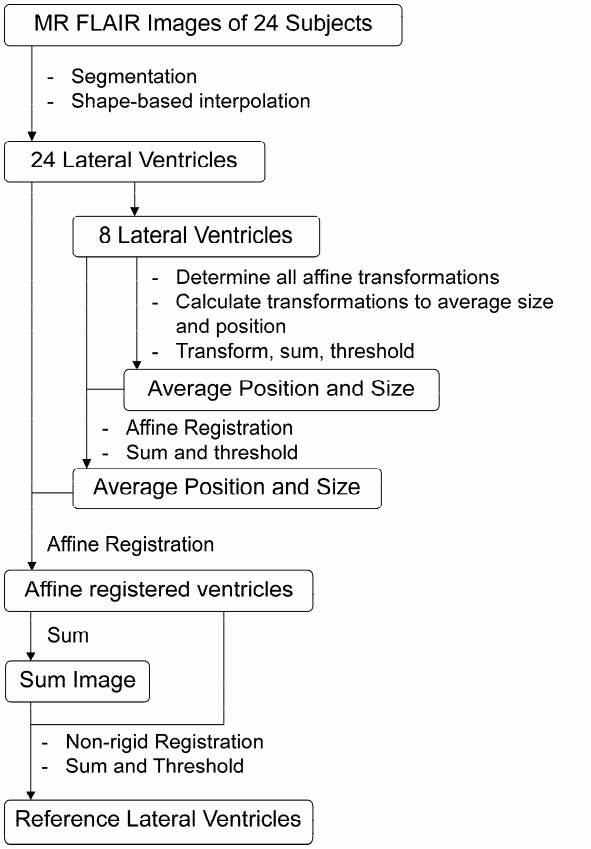

Figure 5.1 *Scheme showing the construction of the reference lateral ventricles image.*

5.2.3 Interpatient registration

For each participant a segmentation of the CSF was obtained and registered to the reference image of the lateral ventricles. Extraction of CSF consisted of three steps. First, an automatic correction of shading artifacts in the T1, T2, PD, and FLAIR images was performed. The intensity distortions were modeled with a multiplicative fourth order polynomial [100]. Second, for each patient and control the shading corrected T1, T2, and PD images and the IR images were registered to the shading corrected FLAIR image using a normalized mutual information based registration algorithm optimizing nine parameters (translation, rotation, and scaling). Third, CSF was extracted by a multi-channel k-means clustering of the five registered MR images into eight clusters. Initialization of the algorithm was done using refined initial starting points [101]. The CSF cluster was selected and the image was interpolated in the axial direction to isotropic voxels of 0.73 mm^3 using shape-based interpolation. Interpatient registration proceeded in two steps. First, CSF segmentations were registered to the reference lateral ventricle with an affine (translation, rotation, scaling, skewing) registration using normalized mutual information. Next, a free-form deformation was applied using B-spline based non-rigid registration, again with normalized mutual information as registration criterion [30]. The CPS was decreased from sixty-four to four voxels by factors of two.

5.3 Evaluation

Three aspects of this method of WML mapping need to be evaluated. These are the accuracy of registration to the reference lateral ventricles, the use of total CSF segmentations instead of segmentations of the lateral ventricles for registration with the reference lateral ventricles, and the registration accuracy in the white matter area around the lateral ventricles. This is tested by analyzing registration results for 26 control participants and 61 participants with diabetes mellitus type 2 of the Utrecht Diabetic Encephalopathy Study.

5.3.1 Registration accuracy

Validation of the registration of the lateral ventricles against a gold standard is not possible because there is no known correct solution for interpatient registration. An indication of the registration accuracy can be obtained by looking at the overlap between the registered images. In this case, registration accuracy can be measured by the overlap between the reference lateral ventricles and the registered CSF segmentations. Usually, overlap is calculated as twice the overlapping volume divided by the sum of both volumes separately. However, the CSF segmentations contain the whole CSF, whereas the reference image contains only ventricular CSF. Thus, this overlap measure will underestimate the true overlap and it will also differ between subjects depending on total CSF volume. Therefore, we have used a slightly different

approach. First, we calculated the overlap with the reference ventricles by counting the number of voxels from the CSF segmentation that overlapped with the reference ventricles and divided this by the total number of voxels in the reference ventricles. The overlap should be a hundred percent. This measure provides no information about CSF voxels that incorrectly overlap with the background. Thus, a complete overlap does not necessarily mean a good registration. To measure overlap with the background we have made four dilations around the reference lateral ventricles. From these dilations we constructed one-voxel-wide shells, ranging from directly around the reference ventricles to four voxels away. The overlap of the CSF segmentation with these shells indicates the incorrect overlap with the background. Note that some overlap with the shells will be unavoidable because CSF structures are present close to and connected to the lateral ventricles.

5.3.2 Accuracy of the use of CSF segmentations

CSF can be reliably segmented automatically. However, consistent separation of lateral ventricles from other CSF structures would require time-consuming manual segmentation. We do not expect that the presence of non-ventricle CSF makes a substantial difference to the registration results. To test this we manually segmented the lateral ventricles of three randomly selected participants. For these subjects, we compared the accuracy of registering total CSF with registering lateral ventricles only. The registration accuracy was determined as described above.

5.3.3 Accuracy of registration extrapolation

We assume that registering the lateral ventricles also registers the white matter around the lateral ventricles. If this assumption is valid, then the deformation of the white matter relative to the lateral ventricles should be approximately rigid. This means that if the boundary of the ventricle is moved during registration, the white matter should move with a similar transformation. We tested this by calculating for every voxel the difference between the transformation vector for that voxel and the closest voxel on the ventricular boundary. The length of this difference vector, the transformation difference, is an indication of the reliability of the transformation of the WML voxel. Short vector lengths indicate that the assumption of co-registration holds.

5.4 Results

Figure 5.2 shows an example of the registration of a CSF segmentation to the reference lateral ventricles image. This figure clearly illustrates that when a CPS of 32 voxels is used an almost complete overlap with the reference lateral ventricles is achieved, but that at this CPS a large overlap with the background is still present.

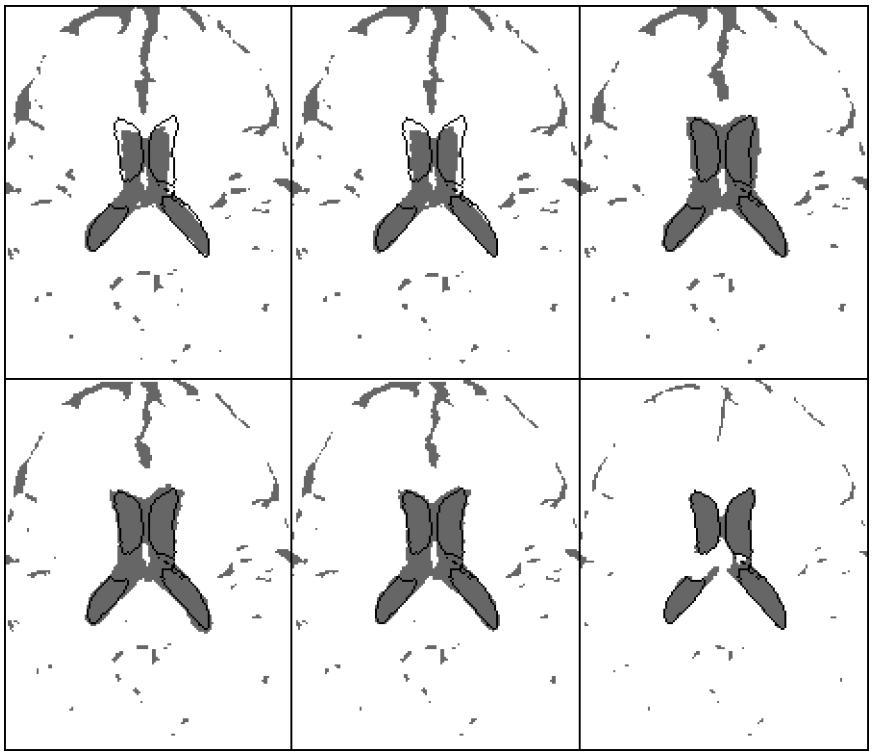

Figure 5.2 *Example of the registration of the CSF segmentation (gray) of a subject to the reference lateral ventricles image (black lines). The top row shows the registration results after affine registration and non-linear registration with a control point spacing of 64 and 32 voxels. The bottom row shows the registration results after non-linear registration with a control point spacing of 16, 8, and 4 voxels.*

Figure 5.3 shows a graph of the median overlap with the reference lateral ventricles for all participants and Figure 5.4 shows the median overlap with the shells around the reference lateral ventricles. Good registration results are reached at a CPS of four voxels as is also shown by the small overlap in the dilation shells at this CPS. When, instead of a segmentation of the whole CSF, a segmentation of only the lateral ventricles was registered to the reference lateral ventricles image, optimal performance was reached at a CPS of four voxels. Performance was similar to performance when using whole CSF segmentations.

The mean transformation difference is shown in Figure 5.5. Within an area that extends to at least ten millimeters almost everywhere around the lateral ventricles, the mean transformation difference is less than one millimeter.

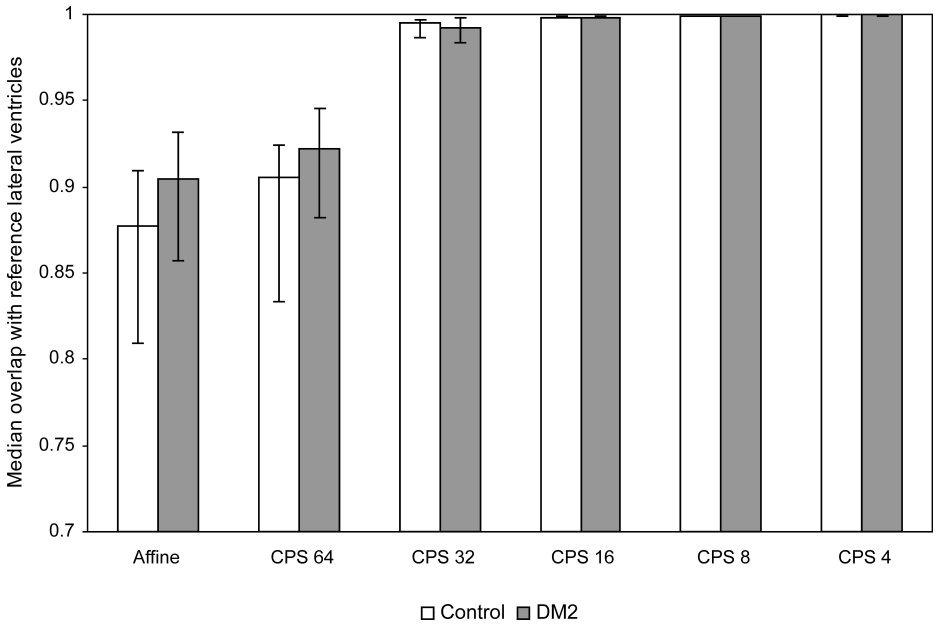

Figure 5.3 *Median of the overlap of CSF segmentations with the reference lateral ventricles (error bars indicate interquartile range).*

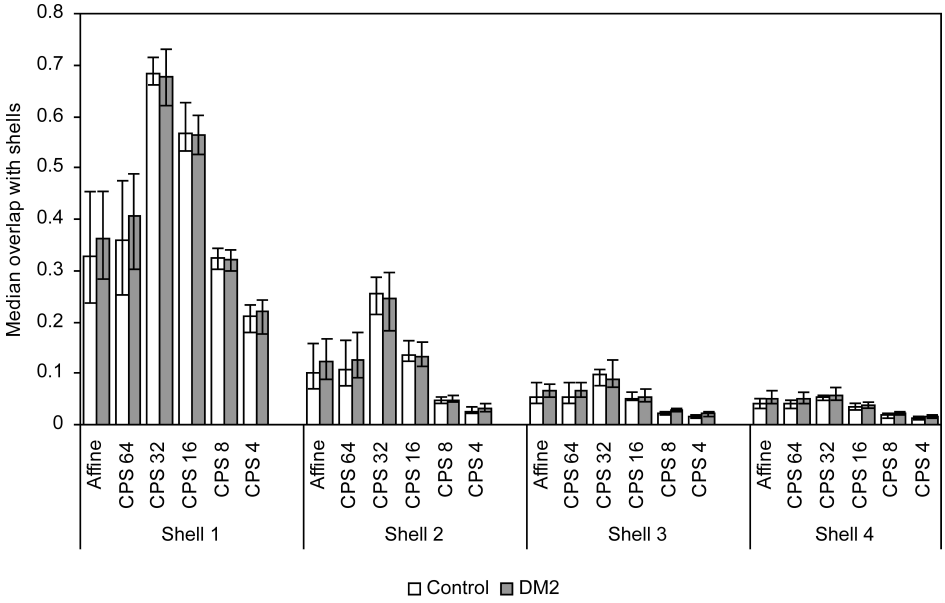

Figure 5.4 *Median overlap of the CSF segmentations with one voxel wide shells around the reference lateral ventricles (error bars indicate interquartile range).*

5.5 Discussion

A reference image of the lateral ventricles has been constructed from twenty-four subjects for the interpatient registration of WMLs at the level of the lateral ventricles. Evaluations have shown that the reference lateral ventricles image provides a good reference for registration.

Although a good overlap with the reference lateral ventricles is already achieved using a CPS of 32 voxels, the overlap with the background is considerable. Figure 5.2 illustrates that at a CPS of 32 voxels the lateral ventricles are slightly enlarged and with refinement of the CPS the lateral ventricles shrink to an almost perfect fit. There will always be some overlap with the background because some non-ventricular CSF is close to or connected to the lateral ventricles.

The mean deformation of the image, relative to the closest points on the lateral ventricles, is less than a millimeter within an area of approximately ten millimeters around the lateral ventricles. This shows that the assumption that the transformation for the ventricles can be extrapolated to transform the white matter around the lateral ventricles is valid.

At greater distances from the lateral ventricles the registration accuracy decreases. Including segmentations of other tissues in the reference image and in the segmentations of individual patients might improve registration accuracy away from the lateral ventricles. However, this also carries the risk of registration errors, particularly the incorrect matching of gyri or sulci between the reference image and the images of the individual subjects. Because the main focus was on the WMLs in the periventricular area, high registration accuracy near the lateral ventricles was required, but lower accuracy at greater distances was acceptable.

The lateral ventricles were not separated from the subarachnoidal CSF for the registration of individual subjects to the reference lateral ventricles. Evaluations showed that this did not decrease registration accuracy. Moreover, reliable and consistent separation would have required user interaction.

The constructed reference lateral ventricles image has proven to be a good reference image for interpatient registration. It has been shown that at the level of the lateral ventricles an accurate mapping of white matter and white matter lesions is achieved.

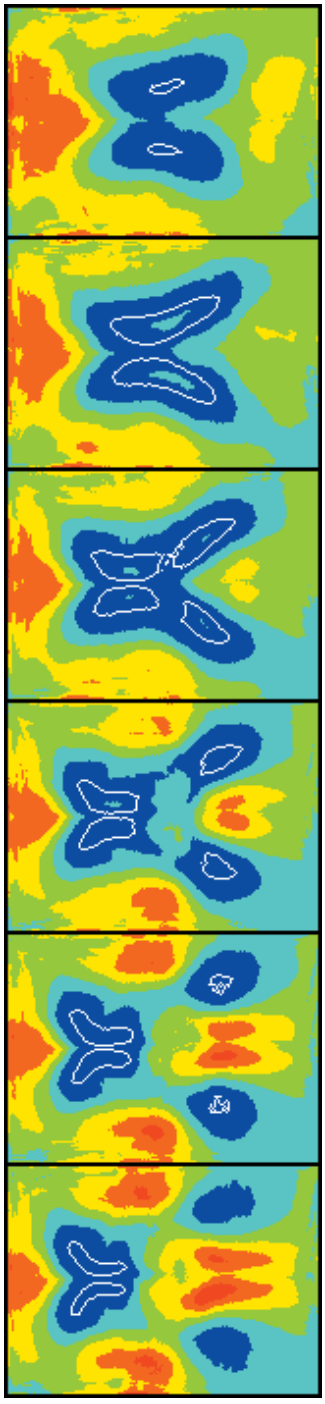

Figure 5.5 *Mean of the transformation difference for the registration of 87 participants.*

Colors: dark blue 0-0.5 mm, light blue 0.5-1 mm, green 1-1.5 mm, yellow 1.5-2 mm, orange 2-2.5 mm, red > 2.5 mm.

6

Periventricular white matter lesions in diabetes mellitus type 2

C. Jongen
J. van der Grond
G.J. Biessels
J.P.W. Pluim
Submitted

The role of diabetes mellitus type 2 (DM2) in the development of white matter lesions (WMLs) is unclear. The use of lesion maps allows precise analysis of differences in WML location. This study aims at determining differences between WML maps at the level of the lateral ventricles for 61 DM2 patients and 26 controls. WMLs were segmented using a combination of magnetic resonance inversion recovery and fluid attenuated inversion recovery images by a K-Nearest Neighbor based classification algorithm. For each subject nonrigid registration of a binary cerebrospinal fluid segmentation to a binary reference lateral ventricles image was performed. All WMLs were mapped to the same reference space by applying this deformation. The WMLs were summed to form WML maps for DM2 patients and controls. Differences between the WML maps were analyzed using Fisher's exact test. Differences in WML volume were analyzed adjusting for age, gender, intracranial volume, and level of education. Subtle increases in WML volume in DM2 patients exist (76%; 95% C.I. 16 to 205%). DM2 patients showed higher frequencies of frontal capping and WML presence along the body of the lateral ventricle. The differences in WML volume and frequency were more prominent in women.

6.1 Introduction

Diabetes mellitus type 2 (DM2) is common in the ageing population. DM2 is an important vascular risk factor and is associated with accelerated cognitive impairment and dementia [70]. White matter lesions (WMLs) are also common in the elderly and are associated with cognitive decline [49]. The association between DM2 and the development of WMLs is not completely clear. Although, there is increasing evidence for an association of DM2 with WML severity and progression [42,43,76-80], not all studies have identified DM2 as a risk factor for WMLs [38,39,45,73,81-83]. A possible cause for this inconsistency is the use of different methods for the grading of WML severity. Furthermore, few studies had a population-based design; most used cohorts of patients with for example stroke or hypertension. Furthermore, high intersubject variability of WML severity exists even in healthy elderly [84].

Periventricular WMLs and subcortical WMLs may differ with respect to pathophysiology [98] and have different correlations with cognitive function [49], emotion [102], and brain atrophy [103]. However, it is hard to reliably and consistently separate periventricular from subcortical WMLs on magnetic resonance (MR) images [37]. Studies on WMLs in DM2 have relied on semi-quantitative WML grading scales. Most studies graded lesion severity only for the whole brain. Of five studies that rated periventricular and subcortical WMLs separately, two showed a significant correlation of DM2 with periventricular WML [42,76], one found a significant effect of DM2 with subcortical WML [72], and two found no significant effects of DM2 [45,81]. WML mapping

does not rely on a categorization into periventricular and subcortical WMLs. Moreover, precise spatial localization is possible.

The aim of this study was to determine differences in WML maps of DM2 patients and control participants in the area around the lateral ventricles. To create WML maps of DM2 patients and control participants accurate mapping of the lateral ventricles is necessary. Lateral ventricle shape is highly variable between subjects. Therefore, fine-scale deformations are required. However, WMLs should not be actively deformed by the registration. This might occur when gray-value information is being used for registration. Although excluding the lesion from registration would avoid this, it might affect registration accuracy depending on the extent of the lesions. Therefore, we have chosen to register binary segmentations of the cerebrospinal fluid (CSF) to a reference lateral ventricles image that has been created as reference for interpatient registration as described in chapter 5. WMLs are registered to the reference lateral ventricles image by applying the deformation that was calculated for registering the lateral ventricles in the CSF segmentation.

6.2 Materials and Methods

6.2.1 Patients

Participants were recruited as part of the Utrecht Diabetic Encephalopathy Study (UDES). UDES is a cross-sectional, population-based study on cognition in diabetes mellitus. For the present report 26 control participants and 61 patients with DM2 were consecutively included between September 2002 and November 2004. DM2 patients were recruited through their general practitioner. Controls were recruited among the spouses and acquaintances of the patients. Participants were 55 to 80 years of age, functionally independent, and Dutch speaking. Minimal diabetes duration for DM2 participants had to be one year. Exclusion criteria were a psychiatric or neurological disorder unrelated to diabetes that could influence cognitive functioning, a history of alcohol or substance abuse, or dementia. Controls with a fasting blood glucose $\geq$ 7.0 mmol/l were excluded. The medical ethics committee of the University Medical Center Utrecht approved the study and each participant signed an informed consent form. All participants measured their blood pressure at home at nine different time points during the day. Mean arterial pressure (MAP) was calculated using these values. Hypertension was defined as an average systolic blood pressure $\geq$ 160 mm Hg and/or diastolic blood pressure $\geq$ 95 mm Hg and/or self reported use of blood pressure lowering drugs. Participants were questioned about diabetes duration, height and weight and history of hypertension and smoking, in a standardized interview. Fasting glucose, glycosylated hemoglobin (HbA_{1c}) and level of education [85] were determined.

6.2.2 MR image acquisition

Brain MR images were acquired on a Philips Gyroscan ACS-NT 15 whole body system (1.5 Tesla, Philips Medical Systems, Best, The Netherlands). The same MR protocol was used for all participants. Axial T1-weighted (T1), inversion recovery (IR), T2-weighted (T2), proton density (PD) and fluid attenuated inversion recovery (FLAIR) scans were made. Scan parameters were (repetition time (TR), echo time (TE), inversion time (TI)): T1: 234/2 ms (TR/TE); IR: 2919/410/22 ms (TR/TI/TE); T2: 2200/100 ms (TR/TE); PD: 2200/11 ms (TR/TE); and FLAIR: 6000/2000/100 ms (TR/TI/TE); slice thickness 4 mm; 38 contiguous slices; 230 x 230 mm field of view; 256 x 256 scan matrix.

6.2.3 WML segmentation and analysis

WMLs were segmented using a probabilistic classification algorithm [32]. A K-Nearest Neighbor classifier was used that was trained on ten manually segmented datasets from a similar population. The FLAIR and IR MR images were used for the classification. This resulted in a probability image per subject. These images show for every voxel the probability of belonging to the WML tissue class. The WML probability images were thresholded at 0.5 and single voxels were removed. Volumes were calculated by summation over the image and multiplication with the voxel dimensions. Volume analysis was done using a general linear model adjusting for age, gender, intracranial volume, and level of education. WML volume is not normally distributed (Kolmogorov-Smirnov test $p<0.001$). Therefore, natural log transformed WML volumes were used in the volume analysis. For the construction and analysis of the WML maps, all WMLs were transformed to the reference lateral ventricles image. A detailed description of the construction of the reference image of the lateral ventricles that is used as reference for interpatient registration is given in chapter 5. The interpatient registration and segmentation of cerebrospinal fluid (CSF) are also described in chapter 5. For each control or DM2 participant a CSF segmentation was non-linearly registered to the reference lateral ventricles image. The obtained transformation was applied to the segmented WMLs. Nearest neighbor interpolation was used. Lesion pattern images were made by summation of the spatially normalized WML images. Differences in WML maps were examined by a voxel-by-voxel application of Fisher's exact test.

6.3 Results

Demographic data for the study participants is shown in Table 6.1. Control and DM2 participants did not differ with respect to age, level of education or body mass index. In DM2 patients hypertension was more frequent ($p<0.001$) and mean arterial pressure ($p=0.001$) and glycosylated hemoglobin ($p<0.001$) were higher.

Table 6.1 *Demographic data.*

	Control participants	DM2 patients
N (M/F)	26 (12/14)	61 (30/31)
Mean age in years (SD)	65.8 (5.5)	67.8 (5.2)
Age Range in years	57.3-78.1	56.2-75.4
Level of education (SD)	4.1 (1.4)	3.8 (1.4)
Hypertension %	23	69
Mean arterial pressure in mm Hg (SD)	97.1 (9.6)	106.0 (11.5)
HbA1c (SD)	5.5 (0.3)	6.9 (1.1)
Body Mass Index in kg/m^2 (SD)	28.5 (4.7)	28.2 (4.3)

SD Standard Deviation

WML volumes are given in Table 6.2. DM2 is associated with a 76% increase in WML volume (p=0.044) (Table 6.3). The increase in WML volume in DM2 patients was not significant in men (10.6% p=0.787 men; 128.4% p=0.056 women). Glycosylated hemoglobin, body mass index, or presence of hypertension was not significantly associated with WML volume. However, higher mean arterial pressure was related to higher WML volume in control subjects, but not in DM2 patients (p=0.029 controls; p=0.536 DM2 patients). Including MAP and the interaction between DM2 and MAP in the WML analysis, still resulted in a significant association of DM2 with increased WML volume (DM2 p=0.026; MAP p=0.005; DM2 x MAP p=0.035). Further analysis showed that only in male controls the association of MAP and WML volume was significant (p=0.046).

Table 6.2 *WML volume in ml.*

	Control participants			DM2 patients		
	All	Men	Women	All	Men	Women
Mean (SD)	3.44 (5.23)	5.19 (7.04)	1.94 (2.28)	5.95 (13.0)	3.56 (4.03)	8.26 (17.6)
Median IQR	1.71 0.41-3.20	2.31 0.87-6.64	0.89 0.34-2.85	2.68 1.20-4.51	2.36 1.06-4.34	3.05 1.52-4.61
Range	0.17-21.4	0.27-21.4	0.17-8.11	0.26-72.9	0.34-20.2	0.26-72.9

SD standard deviation; IQR interquartile range

Table 6.3 *Effect of DM2 on natural log transformed WML volume after adjustment for age, gender, intracranial volume, and level of education.*

	p	B	95% Confidence Interval	
			Lower Bound	Upper Bound
All	0.044	0.566	0.015	1.116
Men	0.787	0.101	-0.656	0.859
Women	0.056	0.826	-0.022	1.673

The WML map for control and DM2 participants is shown in Figure 6.1. Frontal capping is the most common WML type in both groups. The analysis of the WML maps showed that in the area around the frontal horns significant differences in WML frequency between controls and DM2 patients exist (Figure 6.2). Significant differences also exist along the body of the lateral ventricles and along the occipital horns. Assessment of differences in WML maps for men and women separately showed that only in women the WML maps were significantly different. In women differences were found in frontal capping and in WML presence along the body of the lateral ventricle. No significant differences were present between male controls and DM2 patients.

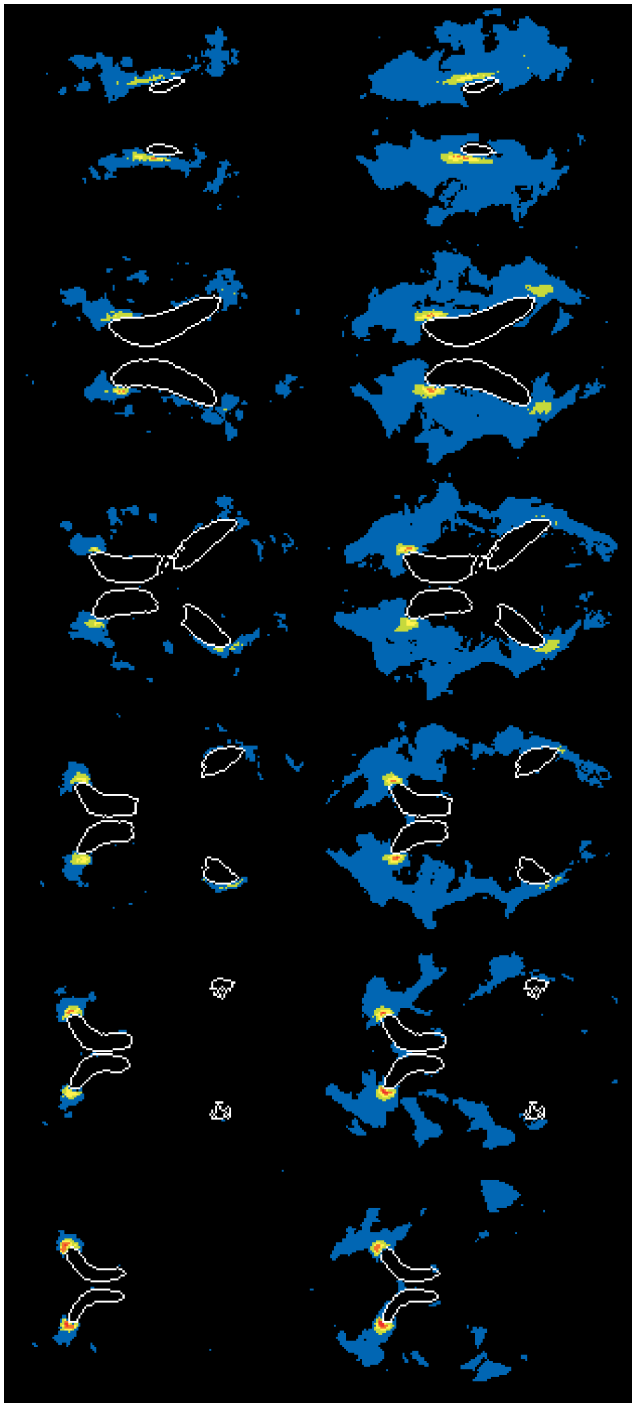

Figure 6.1 *White matter lesion pattern for controls (top row) and for DM2 patients (bottom row). Colors show percentage of subjects with white matter lesion: black 0%, dark blue 0–12.5%, green 12.5–25%, yellow 25–37.5%, orange 37.5–50%, red 50–62.5%.*

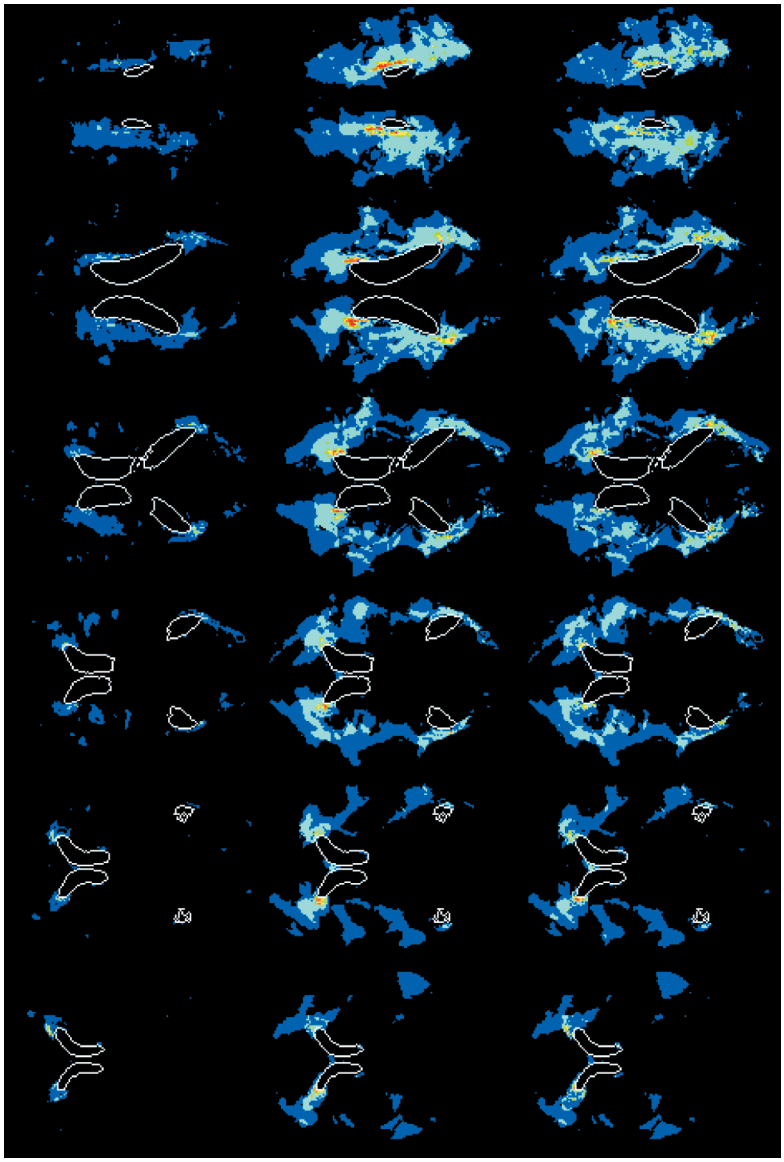

Figure 6.2 *Fisher's exact test on differences in lesion pattern between controls and patients with DM2. (Top row: All; Middle row: Men; Bottom row:women.) Colors indicate p-values: red $p \leq 0.01$; orange $0.01 < p \leq 0.05$; yellow $0.05 < p \leq 0.10$; green $0.10 < p \leq 0.20$; light blue $0.20 < p \leq 0.50$; dark blue $p > 0.50$.*

6.4 Discussion

The mapping of WMLs allowed a voxel-based analysis of the differences in WML frequency between DM2 patients and control participants in a wide area around the lateral ventricles. Frontal capping was frequent in both controls and DM2 patients, but in DM2 patients frontal and occipital capping and lining of the lateral ventricles was significantly more frequent. Separate analyses for men and women showed that women were affected most. No significant differences were present in men. These findings agree with the WML volume analyses that also found a significant increase in WML volume associated with DM2, which was most notable in women. The results for WML volume analysis in this subgroup are comparable to the results for the whole UDES study [43]. Therefore, the absence of WML volume differences for men is probably not caused by the small number of male controls. It is unlikely that effects of DM2 on WMLs in men are masked by age related differences because controls and DM2 patients were similar in age. It could be that women are more susceptible to WMLs. Several studies have shown that women have larger WML volumes [39,40,92] and a higher rate of deep WML progression [91].

The construction of WML maps allows detailed analysis of confluent WMLs and lining and capping of the lateral ventricles. However, this method is not particularly suited for the analysis of punctate WMLs for two reasons. First, punctate WMLs usually appear in the subcortical white matter and registration accuracy decreases with the distance from the lateral ventricles. Second, punctate WMLs have no preferred locations. Therefore, it is unlikely that differences in punctate WML load will lead to significant differences between lesion maps.

It is unlikely that the higher levels of glycosylated hemoglobin and the higher frequency of hypertension in DM2 patients have affected the results of the analyses of WML maps because glycosylated hemoglobin and hypertension were not associated with WML volume. Mean arterial pressure was associated with WML volume in male controls, but not in female controls or in DM2 patients. After adjustment for mean arterial pressure, WML volume was smaller (not significant) in male DM2 patients than in male controls. Because the WML maps were not corrected for mean arterial pressure, differences in the WML maps of men caused by DM2 will likely be overestimated. No differences were found in the WML maps for men, thus, it is unlikely that differences in mean arterial pressure have influenced results.

Although hypertension has been marked as a risk factor for WMLs [41,44,95], an association between hypertension and WML severity has not been reported consistently [42]. In this subgroup of UDES participants an association of WML volume with mean arterial pressure but not with presence of hypertension was found. For the whole UDES group mean arterial pressure or presence of hypertension was not significantly associated with larger WML volumes. Therefore, the current association might be a chance finding.

Recently, a WML probability map has been constructed for 477 healthy volunteers aged 60-64 years [84]. It showed that periventricular WMLs were most frequent. The WML pattern and prevalence was similar to the WML prevalence in control participants of this study. WML maps have been studied for stroke patients [104] and late-life depression [47]. These studies showed that WML load differences between controls and stroke patients varied with brain region and that age-related WML clusters in control and depressed subjects were different, illustrating the importance of examining lesion topography. These studies have used SPM99 to analyze the lesion patterns. SPM99 requires smoothing with rather large kernels to convert the binary WML segmentation to represent WML density and to render the data more normally distributed to increase the validity of the parametric statistical tests [69]. In the present study we have used Fisher's exact test, which is designed to compare categorical data, but which does not allow for adjustments for disease parameters like age and gender. However, the age of control and DM2 participants was similar and we included a separate analysis for men and women. We did not correct for multiple comparisons. However, if p-values were adjusted by dividing by the number of clusters of five or more connected voxels with $p \leq 0.05$, then three of six clusters for all participants and three of seven clusters in women were still significant. In men no clusters of significant voxels were present. All significant voxels had a sub-voxel transformation difference and within an area of approximately ten millimeters around the lateral ventricle the transformation difference was less than a millimeter. This shows that the assumption that the transformation for the ventricles can be extrapolated to transform the periventricular white matter is valid. Thus, intersubject registration of the lateral ventricles proved to be an accurate method to map WMLs at the level of the lateral ventricles to a reference image.

In summary, using WML maps we were able to show subtle changes in WML load at the level of the lateral ventricles associated with DM2. These changes mainly occurred at the frontal horns, but also along the body of the ventricles. Remarkably, no significant differences in WML maps were found for men. The reason for this is not clear. Therefore, future research directed at gender differences in the impact of DM2 on WMLs is necessary.

Color Images

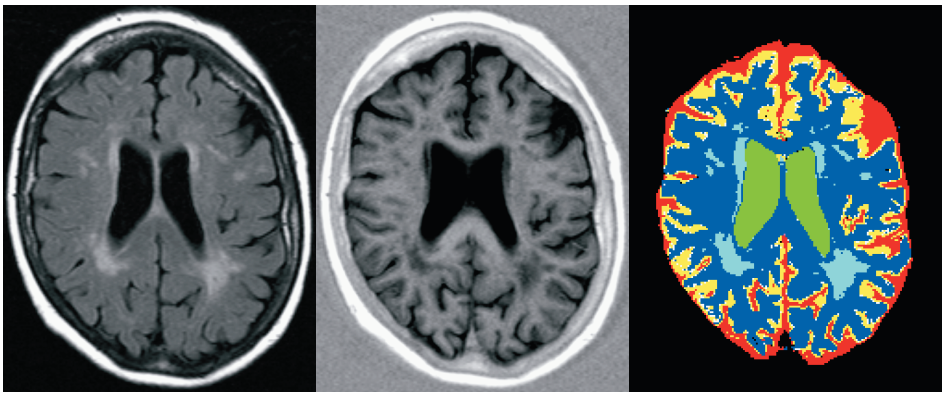

Figure 1.6 *K-Nearest Neighbor classification in a female diabetes mellitus type 2 patient. A slice from the MR FLAIR (left) and MR Inversion Recovery (middle) scans is shown with the resulting classification (right).*
Red – CSF; Yellow – Gray matter; Dark blue – White matter; Green – Lateral ventricles; Light blue – White matter lesion.

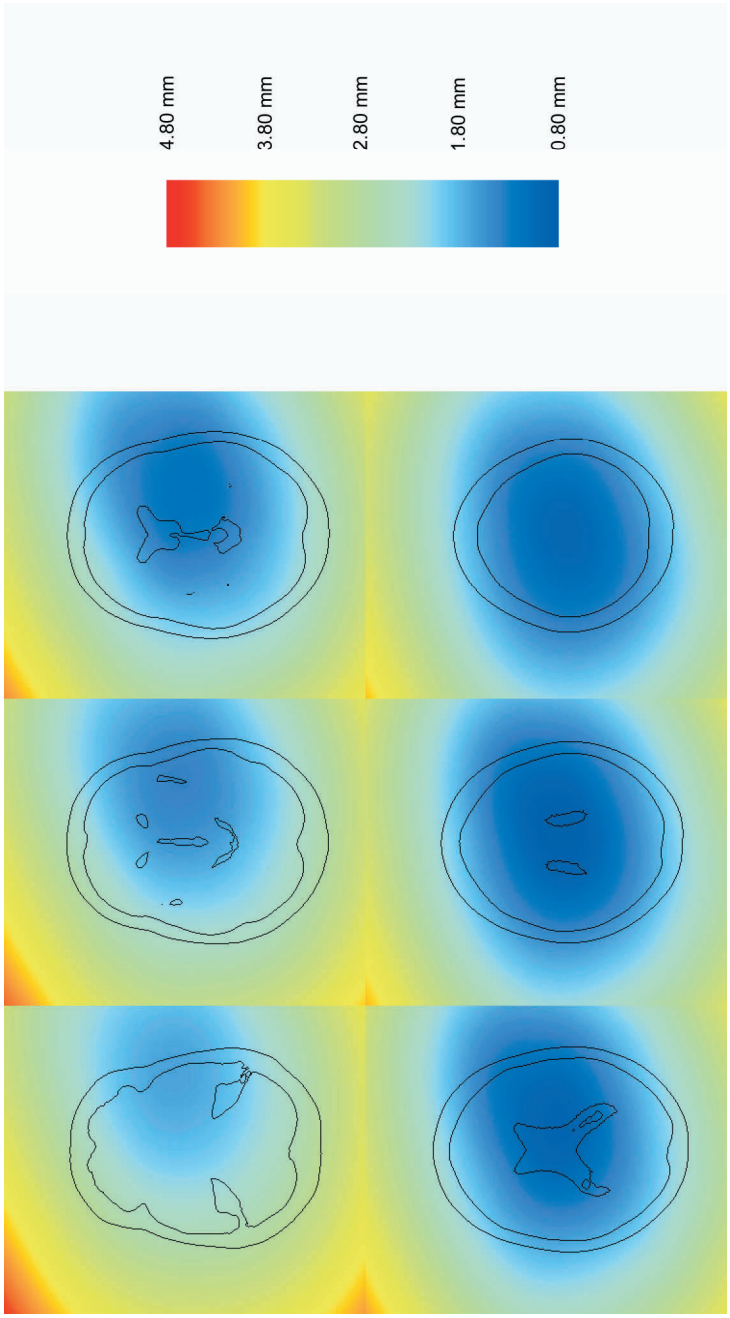

Figure 2.6 *Standard deviation of voxel positions using the 96 transformations from average image A to average image B via the individual images shown for each point as a colour image with the contours of the skull and the ventricles overlaid.*

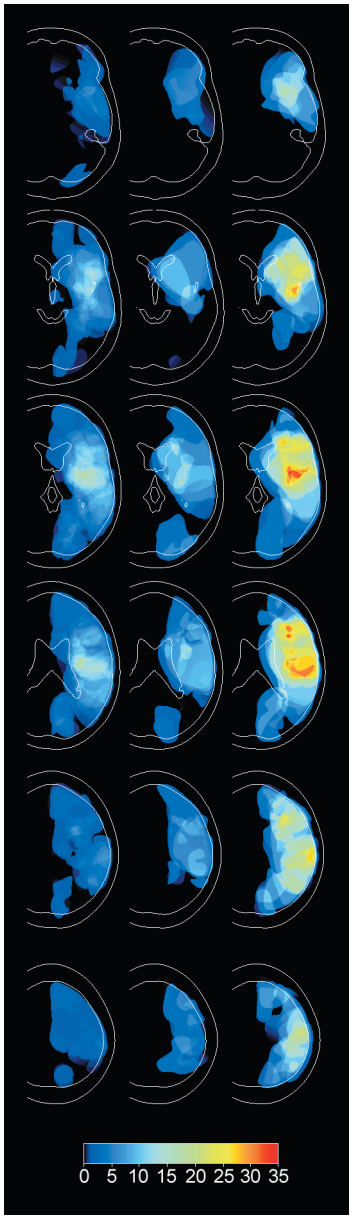

Figure 3.2 *Infarction patterns*
Infarction pattern for 0-49% ICA stenosis (left column), 50-99% ICA stenosis (middle column) and occlusion of the ICA (right column) with color scale indicating the percentage of cases with infarction at a certain location. Every third slice of the volume is shown.

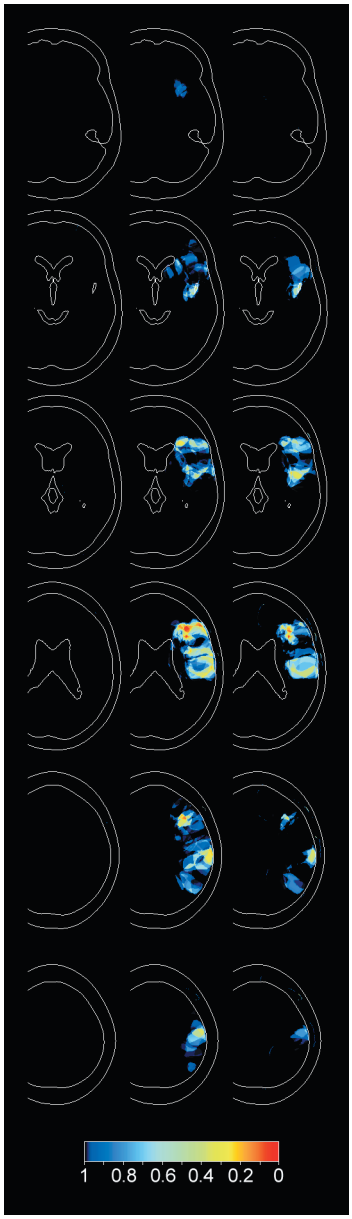

Figure 3.3 *Infarction pattern differences*
Differences in infarction pattern for 0-49% versus 50-99% ICA stenosis (left column), 0-49% ICA stenosis versus ICA occlusion (middle column), and 50-99% ICA stenosis versus ICA occlusion (right column) with color scale indicating the probability that the compared infarction patterns are identical. Every third slice of the volume is shown.

Bibliography

1. Penfield W, Jasper H. Epilepsy and the functional anatomy of the human brain. Boston: Little, Brown and Company, 1954

2. Phillips CG, Porter R. Corticospinal neurones. Their role in movement. Monographs of the physiological society. 1977; 34:1-450

3. Uylings HBM, Rajkowska G, Sanz-Arigita E, Amunts K, Zilles K. Consequences of large interindividual variability for human brain atlases: converging macroscopical imaging and microscopical neuroanatomy. Anat Embryol. 2005; In press

4. Bohm C, Greitz T, Berggren BM, Olsson L. Adjustable computerized stereotaxic brain atlas for transmission and emission tomography. AJNR American Journal of Neuroradiology. 1983; 4, 731-733.

5. Bohm C, Greitz T, Blomqvist G, Farde L, Forsgren PO, Kingsley D, Sjogren I, Wiesel F, Wik G. Applications of a computerized adjustable brain atlas in positron emission tomography. Acta Radiologica Supplement. 1986; 369:449-452

6. Bohm C, Greitz T, Eriksson L. A computerized adjustable brain atlas. European Journal of Nuclear Medicine. 1989; 15:687-689

7. Dann R, Hoford J, Kovacic S, Reivich M, Bajcsy R. Evaluation of elastic matching system for anatomic (CT, MR) and functional (PET) cerebral images. Journal of Computer Assisted Tomography. 1989; 13:603-611

8. Evans AC, Bell C, Marrett S, Thompson CJ, Hakim A. Anatomical-functional correlation using an adjustable MRI-based region of interest atlas with positron emission tomography. Journal of Cerebral Blood Flow and Metabolism. 1988; 8, 513-530.

9. Evans AC, Marrett S, Torrescorzo J, Ku S, Collins L. MRI-PET correlation in three dimensions using a volume-of-interest (VOI) atlas. Journal of Cerebral Blood Flow and Metabolism. 1991; 11:A69-A78

10. Greitz T, Bohm C, Holte S, Eriksson L. A computerized brain atlas: construction, anatomical content, and some applications. Journal of Computer Assisted Tomography. 1991; 15:26-38

11. Rizzo G, Gilardi MC, Prinster A, Grassi F, Scotti G, Cerutti S, Fazio F. An elastic computerized brain atlas for the analysis of clinical PET/SPET data. European Journal of Nuclear Medicine. 1995; 22:1313-1318

12. Toga AW, Thompson PM. Maps of the brain. Anatomical Record. 2001; 265:37-53

13. Toga AW, Thompson PM. The role of image registration in brain mapping. Image and Vision Computing. 2001; 19[1-2], 3-24.

14. Andreasen NC, Arndt S, Swayze V, Cizadlo T, Flaum M, O'Leary DS, Ehrhardt JC, Yuh WTC. Thalamic abnormalities in schizophrenia visualized through magnetic resonance image averaging. Science. 1994; 266, 294-298.

15. Evans AC, Collins DL, Milner B. An MRI-based stereotactic atlas from 250 young normal subjects. Society for Neuroscience Abstracts. 1992; 10, 408.

16. Woods RP, Dapretto M, Sicotte NL, Toga AW, Mazziotta JC. Creation and use of a Talairach-compatible atlas for accurate, automated, nonlinear intersubject registration, and analysis of functional imaging data. Human Brain Mapping. 1999; 8:73-79

17. Collins DL, Neelin P, Peters TM, Evans AC. Automatic 3D intersubject registration of MR volumetric data in standardized Talairach space. Journal of Computer Assisted Tomography. 1994; 18:192-205

18. Guimond A, Meunier J, Thirion JP. Average brain models: a convergence study. Computer Vision and Image Understanding. 2000; 77, 192-210.

19. Mazziotta JC, Toga AW, Evans A, Fox P, Lancaster J. A probabilistic atlas of the human brain: theory and rationale for its development. The International Consortium for Brain Mapping (ICBM). Neuroimage. 1995; 2:89-101

20. Collins DL, Zijdenbos AP, Kollokian V, Sled JG, Kabani NJ, Holmes CJ, Evans AC. Design and construction of a realistic digital brain phantom. IEEE transactions on medical imaging. 1998; 17[3], 463-468.

21. Dinov ID, Mega MS, Thompson PM, Lee L, Woods RP, Holmes CJ, Sumners DWL, Toga AW. Analyzing functional brain images in a probabilistic atlas: a validation of subvolume thresholding. Journal of Computer Assisted Tomography. 2000; 24[1], 128-138.

22. Thompson PM, Schwartz C, Toga AW. High-resolution random mesh algorithms for creating a probabilistic 3D surface atlas of the human brain. Neuroimage. 1996; 3:19-34

23. Thompson PM, Toga AW. Detection, visualization and animation of abnormal anatomic structure with a deformable probabilistic brain atlas based on random vector field transformations. Medical Image Analysis. 1997; 1:271-294

24. Thompson PM, MacDonald D, Mega MS, Holmes CJ, Evans AC, Toga AW. Detection and mapping of abnormal brain structure with a probabilistic atlas of cortical surfaces. Journal of Computer Assisted Tomography. 1997; 21:567-581

25. Mazziotta JC, Toga A, Evans AC, Fox P. Human brain atlas development: Probabilistic approaches. Biological Psychiatry. 1997; 42[1], 2S.

26. Mantyla R, Erkinjuntti T, Salonen O, Aronen HJ, Peltonen T, Pohjasvaara T, Standertskjold-Nordenstam CG. Variable agreement between visual rating scales for white matter hyperintensities on MRI. Comparison of 13 rating scales in a poststroke cohort. Stroke. 1997; 28:1614-1623

27. Holmes AP, Blair RC, Watson JDG, Ford I. Nonparametric analysis of statistic images from functional mapping experiments. Journal of Cerebral Blood Flow and Metabolism. 1996; 16, 7-22.

28. Studholme C, Hill DLG, Hawkes DJ. An overlap invariant entropy measure of 3D medical image alignment. Pattern Recognition. 1999; 32:71-86

29. Pluim JPW, Maintz JBA, Viergever MA. Mutual-information-based registration of medical images: A survey. IEEE transactions on medical imaging. 2003; 22:986-1004

30. Rueckert D, Sonoda LI, Hayes C, Hill DLG, Leach MO, Hawkes DJ. Nonrigid registration using free-form deformations: application to breast MR images. IEEE transactions on medical imaging. 1999; 18[8], 712-721.

31. Anbeek P. Thesis: Probabilistic segmentation of MR brain images. 2005.

32. Anbeek P, Vincken KL, van Bochove GS, van Osch MJP, van der Grond J. Probabilistic segmentation of brain tissue in MR imaging. Neuroimage. 2005; 27[4]:795-804

33. Barnett HJM, Taylor W, Eliasziw M, Fox AJ, Ferguson GG, Haynes RB, Rankin RN, Clagett GP, Hachinski VC, Sackett DL, Thorpe KE, Meldrum HE. Benefit of carotid endarterectomy in patients with symptomatic moderate or severe stenosis. New England Journal of Medicine. 1998; 339:1415-1425

34. Chaturvedi S, Bruno A, Feasby T, Holloway R, Benavente O, Cohen SN, Cote R, Hess D, Saver J, Spence JD, Stern B, Wilterdink J. Carotid endarterectomy--An evidence-based review: Report of the Therapeutics and Technology Assessment Subcommittee of the American Academy of Neurology. Neurology. 2005; 65:794-801

35. Barnett HJM, Gunton RW, Eliasziw M, Fleming L, Sharpe B, Gates P, Meldrum H. Causes and severity of ischemic stroke in patients with internal carotid artery stenosis. Journal of the American Medical Association. 2000; 283, 1429-1436.

36. Buskens E, Nederkoorn PJ, Buijs-van der Woude T, Mali WPTM, Kappelle LJ, Eikelboom BC, van der Graaf Y, Myriam Hunink MG. Imaging of Carotid Arteries in Symptomatic Patients: Cost-effectiveness of Diagnostic Strategies. Radiology. 2004; 233:101-112

37. DeCarli CM, Fletcher EP, Ramey V, Harvey DP, Jagust WJM. Anatomical mapping of white matter hyperintensities (WMH): Exploring the relationships between periventricular WMH, deep WMH, and total WMH burden. Stroke. 2005; 36:50-55

38. Jeerakathil T, Wolf PA, Beiser A, Massaro J, Seshadri S, D'Agostino RB, DeCarli C. Stroke risk profile predicts white matter hyperintensity volume: The Framingham Study. Stroke. 2004; 35:1857-1861

39. Longstreth WT, Manolio TA, Arnold A, Burke GL, Bryan N, Jungreis CA, Enright PL, O'Leary D, Fried L. Clinical correlates of white matter findings on cranial magnetic resonance imaging of 3301 elderly people. The Cardiovascular Health Study. Stroke. 1996; 27:1274-1282

40. de Leeuw FE, de Groot JC, Achten E, Oudkerk M, Ramos LM, Heijboer R, Hofman A, Jolles J, van Gijn J, Breteler MM. Prevalence of cerebral white matter lesions in elderly people: a population based magnetic resonance imaging study. The Rotterdam Scan Study. Journal of Neurology, Neurosurgery, and Psychiatry. 2001; 70:9-14

41. de Leeuw FE, de Groot JC, Oudkerk M, Witteman JC, Hofman A, van Gijn J, Breteler MM. Hypertension and cerebral white matter lesions in a prospective cohort study. Brain: a journal of neurology. 2002; 125:765-772

42. Ylikoski A, Erkinjuntti T, Raininko R, Sarna S, Sulkava R, Tilvis R. White matter hyperintensities on MRI in the neurologically nondiseased elderly. Analysis of cohorts of consecutive subjects aged 55 to 85 years living at home. Stroke. 1995; 26:1171-1177

43. Jongen C, van der Grond J, Kappelle LJ, Biessels G-J, Viergever MA, Pluim JPW. Automated analysis of brain tissue and white matter lesion volume in diabetes type 2. In preparation. 2005;

44. van Dijk EJ, Breteler MMB, Schmidt R, Berger K, Nilsson LG, Oudkerk M, Pajak A, Sans S, de Ridder M, Dufouil C, Fuhrer R, Giampaoli S, Launer LJ, Hofman A, for the CASCADE Consortium. The association between blood pressure, hypertension, and cerebral white matter lesions: Cardiovascular determinants of dementia study. Hypertension. 2004; 44:625-630

45. Schmidt R, Launer LJ, Nilsson LG, Pajak A, Sans S, Berger K, Breteler MM, de Ridder M, Dufouil C, Fuhrer R, Giampaoli S, Hofman A. Magnetic Resonance Imaging of the Brain in Diabetes: The Cardiovascular Determinants of Dementia (CASCADE) Study. Diabetes. 2004; 53:687-692

46. Pantoni L, Garcia JH. Pathogenesis of leukoaraiosis: a review. Stroke. 1997; 28:652-659

47. Taylor WD, MacFall JR, Steffens DC, Payne ME, Provenzale JM, Krishnan KR. Localization of age-associated white matter hyperintensities in late-life depression. Progress in Neuro-Psychopharmacology and Biological Psychiatry. 2003; 27:539-544

48. de Groot JC, de Leeuw FE, Oudkerk M, van Gijn J, Hofman A, Jolles J, Breteler MMB. Cerebral white matter lesions and cognitive function: The Rotterdam scan study. Annals of Neurology. 2000; 47[2]:145-151

49. de Groot JC, de Leeuw FE, Oudkerk M, van Gijn J, Hofman A, Jolles J, Breteler MM. Periventricular cerebral white matter lesions predict rate of cognitive decline. Annals of Neurology. 2002; 52:335-341

50. Starr JM, Leaper SA, Murray AD, Lemmon HA, Staff RT, Deary IJ, Whalley LJ. Brain white matter lesions detected by magnetic resosnance imaging are associated with balance and gait speed. Journal of Neurology, Neurosurgery, and Psychiatry. 2003; 74:94-98

51. Roland PE, Graufelds CJ, Wahlin J, et al. Human brain atlas: for high resolution functional and anatomical mapping. Human Brain Mapping. 1994; 1, 173-184.

52. Sandor S, Leahy R. Surface-based labeling of cortical anatomy using a deformable atlas. IEEE transactions on medical imaging. 1997; 16:41-54

53. Thompson PM, Mega MS, Woods RP, Zoumalan CI, Lindshield CJ, Blanton RE, Moussai J, Holmes CJ, Cummings JL, Toga AW. Cortical change in Alzheimer's disease detected with a disease-specific population-based brain atlas. Cerebral Cortex. 2001; 11:1-16

54. Thompson PM, Woods RP, Mega MS, Toga AW. Mathematical/computational challenges in creating deformable and probabilistic atlases of the human brain. Human Brain Mapping. 2000; 9:81-92

55. Talairach J, Tournoux P. Co-planar stereotaxic atlas of the human brain. New York: Thieme, 1988

56. Maes F, Collignon A, Vandermeulen D, Marchal G, Suetens P. Multimodality image registration by maximization of mutual information. IEEE transactions on medical imaging. 1997; 16:187-198

57. Holden M, Hill DL, Denton ER, Jarosz JM, Cox TC, Rohlfing T, Goodey J, Hawkes DJ. Voxel similarity measures for 3-D serial MR brain image registration. IEEE transactions on medical imaging. 2000; 19:94-102

58. Hupperts RMM, Lodder J, Heuts-van Raak EPM, Wilmink J, Kessels AGH. Borderzone brain infarcts on CT taking into account the variability in vascular supply areas. Cerebrovascular Diseases. 1996; 6, 294-300.

59. van der Zwan A, Hillen B, Tulleken CAF, Dujovny M, Dragovic L. Variability of the territories of the major cerebral arteries. Journal of Neurosurgery. 1992; 77, 927-940.

60. European Carotid Surgery Trialists' Collaborative Group. MRC European carotid surgery trial: interim results for symptomatic patients with severe (70-99%) or with mild (0-29%) carotid stenosis. Lancet. 1991; 337, 1235-1243.

61. North American Symptomatic Carotid Endarterectomy Trial Collaborators. Beneficial effect of carotid endarterectomy in symptomatic patients with high-grade carotid stenosis. New England Journal of Medicine. 1991; 325[7], 445-453.

62. Farrell B, Fraser A, Sandercock P, Slattery J, Warlow CP. Randomised trial of endarterectomy for recently symptomatic carotid stenosis: final results of the MRC European carotid surgery trial (ECST). Lancet. 1998; 351:1379-1387

63. Hunink MG, Polak JF, Barlan MM, O'Leary DH. Detection and quantification of carotid artery stenosis: efficacy of various Doppler velocity parameters. AJR American journal of roentgenology. 1993; 160:619-625

64. Elgersma OE, van Leersum M, Buijs PC, van Leeuwen MS, van de Schouw YT, Eikelboom BC, van der Graaf Y. Changes over time in optimal duplex threshold for the identification of patients eligible for carotid endarterectomy. Stroke. 1998; 29:2352-2356

65. Jongen C, Pluim JPW, Viergever MA, Niessen WJ. Construction of an average CT brain image for brain infarct pattern comparison. 2002; Computer Assisted Radiology and Surgery, 425-429. Springer.

66. Jongen C, Pluim JPW, Nederkoorn PJ, Viergever MA, Niessen WJ. Construction and evaluation of an average CT brain image for inter-subject registration. Computers in biology and medicine. 2004; 34[8]:647-662

67. Adolphs R, Damasio H, Tranel D, Cooper G, Damasio AR. A role for somatosensory cortices in the visual recognition of emotion as revealed by three-dimensional lesion mapping. Journal of Neuroscience. 2000; 20:2683-2690

68. Karnath H-O, Himmelbach M, Rorden C. The subcortical anatomy of human spatial neglect: putamen, caudate nucleas and pulvinar. Brain: a journal of neurology. 2002; 125:350-360

69. Ashburner J, Friston KJ. Voxel-based morphometry - the methods. Neuroimage. 2000; 11[6 Pt 1], 805-821.

70. Allen KV, Frier BM, Strachan MWJ. The relationship between type 2 diabetes and cognitive dysfunction: longitudinal studies and their methodological limitations. European Journal of Pharmacology. 2004; 490:169-175

71. Araki Y, Nomura M, Tanaka H, Yamamoto H, Yamamoto T, Tsukaguchi I, Nakamura H. MRI of the brain in diabetes mellitus. Neuroradiology. 1994; 36:101-103

72. Manschot SM, Biessels G-J, on behalf of the Utrecht DM Encephalopathy Study Group. Impaired cognition in type 2 diabetes: MRI correlates and vascular risk factors. Diabetologia. 2005; 48[Suppl. 1], A34.

73. den Heijer T, Vermeer SE, van Dijk EJ, Prins ND, Koudstaal PJ, Hofman A, Breteler MMB. Type 2 diabetes and atrophy of medial temporal lobe structures on brain MRI. Diabetologia. 2003; 46:1604-1610

74. Vermeer SE, den Heijer T, Koudstaal PJ, Oudkerk M, Hofman A, Breteler MMB. Incidence and Risk Factors of Silent Brain Infarcts in the Population-Based Rotterdam Scan Study. Stroke. 2003; 34:392-396

75. Streifler JY, Eliasziw M, Benavente OR, Alamowitch S, Fox AJ, Hachinski V, Barnett HJM. Development and progression of leukoaraiosis in patients with brain ischemia and carotid artery disease. Stroke. 2003; 34:1913-1916

76. Kertesz A, Black SE, Tokar G, Benke T, Carr T, Nicholson L. Periventricular and subcortical hyperintensities on magnetic resonance imaging. 'Rims, caps, and unidentified bright objects'. Archives of Neurology. 1988; 45:404-408

77. Schmidt R, Fazekas F, Kleinert G, Offenbacher H, Gindl K, Payer F, Freidl W, Niederkorn K, Lechner H. Magnetic resonance imaging signal hyperintensities in the deep and subcortical white matter. A comparative study between stroke patients and normal volunteers. Archives of Neurology. 1992; 49:825-827

78. Erkinjuntti T, Gao F, Lee DH, Eliasziw M, Merskey H, Hachinski VC. Lack of difference in brain hyperintensities between patients with early Alzheimer's disease and control subjects. Archives of Neurology. 1994; 51:260-268

79. Fazekas F, Niederkorn K, Schmidt R, Offenbacher H, Horner S, Bertha G, Lechner H. White matter signal abnormalities in normal individuals: correlation with carotid ultrasonography, cerebral blood flow measurements, and cerebrovascular risk factors. Stroke. 1988; 19:1285-1288

80. Taylor WD, MacFall JR, Provenzale JM, Payne ME, McQuoid DR, Steffens DC, Krishnan KR. Serial MR imaging of volumes of hyperintense white matter lesions in elderly patients: correlation with vascular risk factors. AJR American journal of roentgenology. 2003; 181:571-576

81. Fukuda H, Kitani M. Differences between treated and untreated hypertensive subjects in the extent of periventricular hyperintensities observed on brain MRI. Stroke. 1995; 26:1593-1597

82. Manolio TA, Kronmal RA, Burke GL, Poirier V, O'Leary DH, Gardin JM, Fried LP, Steinberg EP, Bryan RN. Magnetic resonance abnormalities and cardiovascular disease in older adults. The Cardiovascular Health Study. Stroke. 1994; 25:318-327

83. Schmidt R, Enzinger C, Ropele S, Schmidt H, Fazekas F. Progression of cerebral white matter lesions: 6-year results of the Austrian Stroke Prevention Study. Lancet. 2003; 361:2046-2048

84. Wen W, Sachdev P. The topography of white matter hyperintensities on brain MRI in healthy 60- to 64-year-old individuals. Neuroimage. 2004; 22:144-154

85. Hochstenbach J, Mulder T, van Limbeek J, Donders R, Schoonderwaldt H. Cognitive decline following stroke: A comprehensive study of cognitive decline following stroke. J Clin Exp Neuropsychol. 1998; 20[4]:503-517

86. Lemaitre H, Crivello F, Grassiot B, Alperovitch A, Tzourio C, Mazoyer B. Age- and sex-related effects on the neuroanatomy of healthy elderly. Neuroimage. 2005; 26:900-911

87. Blatter DD, Bigler ED, Gale SD, Johnson SC, Anderson CV, Burnett BM, Parker N, Kurth S, Horn SD. Quantitative volumetric analysis of brain MR: normative database spanning 5 decades of life. AJNR American Journal of Neuroradiology. 1995; 16:241-251

88. Good CD, Johnsrude IS, Ashburner J, Henson RNA, Friston KJ, Frackowiak RSJ. A voxel-based morphometric study of ageing in 465 normal adult human brains. Neuroimage. 2001; 14, 21-36.

89. Xu J, Kobayashi S, Yamaguchi S, Iijima Ki, Okada K, Yamashita K. Gender effects on age-related changes in brain structure. AJNR American Journal of Neuroradiology. 2000; 21:112-118

90. Taki Y, Goto R, Evans A, Zijdenbos A, Neelin P, Lerch J, Sato K, Ono S, Kinomura S, Nakagawa M. Voxel-based morphometry of human brain with age and cerebrovascular risk factors. Neurobiology of Aging. 2004; 25:455-463

91. van den Heuvel DM, Admiraal-Behloul F, ten Dam VH, Olofsen H, Bollen EL, Murray HM, Blauw GJ, Westendorp RG, de Craen AJ, van Buchem MA. Different progression rates for deep white matter hyperintensities in elderly men and women. Neurology. 2004; 63:1699-1701

92. Sawada H, Udaka F, Izumi Y, Nishinaka K, Kawakami H, Nakamura S, Kameyama M. Cerebral white matter lesions are not associated with apoE genotype but with age and female sex in Alzheimer's disease. Journal of Neurology, Neurosurgery, and Psychiatry. 2000; 68:653-656

93. den Heijer T, Skoog I, Oudkerk M, de Leeuw FE, de Groot JC, Hofman A, Breteler MMB. Association between blood pressure levels over time and brain atrophy in the elderly. Neurobiology of Aging. 2003; 24:307-313

94. Wiseman RM, Saxby BK, Burton EJ, Barber R, Ford GA, O'Brien JT. Hippocampal atrophy, whole brain volume, and white matter lesions in older hypertensive subjects. Neurology. 2004; 63:1892-1897

95. Dufouil C, Kersaint-Gilly A, Besancon V, Levy C, Auffray E, Brunnereau L, Alperovitch A, Tzourio C. Longitudinal study of blood pressure and white matter hyperintensities: the EVA MRI Cohort. Neurology. 2001; 56:921-926

96. Enzinger C, Fazekas F, Matthews PM, Ropele S, Schmidt H, Smith S, Schmidt R. Risk factors for progression of brain atrophy in aging: Six-year follow-up of normal subjects. Neurology. 2005; 64:1704-1711

97. Murray AD, Staff RT, Shenkin SD, Deary IJ, Starr JM, Whalley LJ. Brain white matter hyperintensities: Relative importance of vascular risk factors in nondemented elderly people. Radiology. 2005; 237:251-257

98. Fazekas F, Kleinert R, Offenbacher H, Schmidt R, Kleinert G, Payer F, Radner H, Lechner H. Pathologic correlates of incidental MRI white matter signal hyperintensities. Neurology. 1993; 43:1683-1689

99. Herman GT, Zheng JS, Bucholtz CA. Shape-based interpolation. IEEE Computer Graphics and Applications. 1992; 12:69-79

100. Likar B, Viergever MA, Pernus F. Retrospective correction of MR intensity inhomogeneity by information minimization. IEEE transactions on medical imaging. 2001; 20:1398-1410

101. Bradley PS, Fayyad UM. Refining initial points for K-means clustering. International Conference on Machine Learning. 1998; 91-99.

102. de Groot JC, de Leeuw FE, Oudkerk M, Hofman A, Jolles J, Breteler MM. Cerebral white matter lesions and depressive symptoms in elderly adults. Archives of general psychiatry. 2000; 57:1071-1076

103. Wen W, Sachdev PS, Chen X, Anstey K. Gray matter reduction is correlated with white matter hyperintensity volume: A voxel-based morphometric study in a large epidemiological sample. Neuroimage. 2005; In Press, Corrected Proof

104. Wen W, Sachdev PS. Extent and Distribution of White Matter Hyperintensities in Stroke Patients: The Sydney Stroke Study. Stroke. 2004; 35:2813-2819

Summary

The first part of this thesis deals with the correlation of internal carotid artery (ICA) stenosis with brain infarct maps. Patients with an infarct were grouped according to their degree of ICA stenosis. For each group a map was created showing the infarct distribution. These maps were analyzed to find brain areas involved in ICA stenosis related infarcts.
The second part of this thesis focuses on the impact of diabetes mellitus type 2 (DM2) on the brain. Volumes of gray matter tissue, white matter tissue, lateral ventricles, cerebrospinal fluid (CSF), and white matter lesion (WML) were compared between DM2 patients and controls. WML distribution maps for DM2 patients and controls were constructed and analyzed.

Internal carotid artery stenosis and brain infarcts

Stenosis or narrowing of the internal carotid artery (ICA) is a well-known cause of infarcts or strokes. Surgery on a stenosed ICA carries a high mortality risk. Therefore, it is important to determine who should be operated upon. Examination of the characteristics of ICA stenosis associated infarcts provides information that may aid the selection of patients for surgery and will add to our knowledge of infarct mechanisms. The work presented here aimed at detecting which locations in the brain are specifically involved in stenosis associated infarcts by creating maps showing infarct distribution instead of using the standard approach of infarct classification.

Construction and evaluation of an average CT brain image

To create infarct maps it is necessary to transform images of individual patients to a reference brain image. Therefore, an average brain image was constructed. The construction proceeded in two steps. First, a temporary average image was made, based on a small number of images. The temporary average image was used as reference image for the construction of the real average image. The use of a temporary average provides a better starting point than the use of a randomly selected image. Three different average images based on the same data were created. This was important for the evaluation of the registration consistency during the construction of the average brain image and of mapping new images to the average. The use of an average brain image as reference results in more consistent registration than the use of a single image.

Brain infarct patterns in ICA stenosis

ICA stenosis was categorized into mild (0-49% stenosis), severe (50-99% stenosis), or occlusion (100% stenosis). In total, 80 patients with mild stenosis, 33 with severe stenosis, and 29 with occlusion of the ICA were included. For each category infarct distribution maps were created by mapping the CT image of each patient to the average brain image and applying this transformation to the manually segmented infarcts. These maps showed a fairly even infarct distribution in mild and severe stenosis patients. In patients with ICA occlusion the middle cerebral artery territory was more frequently involved in infarcts. Differences between the infarct maps were analyzed using a non-parametric randomization based technique. Subtle differences were found between mild stenosis and occlusion maps and between severe stenosis and occlusion maps, but not between mild and severe stenosis maps. Differences were located in the territory of the middle cerebral artery. Analysis of infarct volume showed that patients with ICA occlusion had larger infarct volumes than patients with mild or severe stenosis and that volumes between mild and severe stenosis did not differ. The standard approach showed no differences between the stenosis categories. This indicates that mapping the infarct distribution allows for more sensitive comparisons.

Diabetes Mellitus type 2 and the brain

Diabetes is a disorder of blood glucose regulation. Diabetes mellitus type 2 (DM2) occurs frequently in the elderly population. DM2 is associated with cognitive decline and dementia. It has not yet been clearly established which structural changes in the brain are related to DM2. Although an association of DM2 with brain atrophy and infarcts is generally reported, the role of white matter lesions (WMLs) remains unclear. The use of rating scales instead of true volume measurements is likely at the base of this. MR images of DM2 patients and control participants were collected as part of the Utrecht Diabetic Encephalopathy Study (UDES) on cognition in diabetes mellitus. The research presented in this thesis aimed at determining brain volume changes and the presence and location of WMLs in DM2 patients.

Brain tissue and WML volume in DM2

Gray matter tissue, white matter tissue, lateral ventricles, CSF, and WML were segmented from MR images by an automated classification algorithm. Volume differences between 99 DM2 patients and 46 control participants were analyzed while correcting for differences in age, gender, level of education and intracranial volume. This showed a significant decrease in gray matter volume and significant increases in lateral ventricle and WML volumes in DM2 patients. This means that DM2 patients have more brain atrophy and also more severe white matter damage. Repeating the analysis for men and women separately, revealed a remarkable gender difference.

Female DM2 patients showed a decrease in gray matter volume and increases in lateral ventricle and CSF volumes, whereas in men no significant effects of DM2 were detected. It is not clear what causes these differences. In DM2 research, gender differences have received little attention. However, these findings clearly indicate that future research should include separate analyses for men and women.

Construction and evaluation of a reference lateral ventricle for WML mapping

Periventricular WMLs, i.e. lesions in the white matter surrounding the lateral ventricles, have been associated with DM2 more often than subcortical WMLs. To examine periventricular WML maps, these lesions should be accurately mapped to the same reference space. This is done by mapping the lateral ventricles of 61 DM2 patients and 26 controls to a reference and applying this deformation to the WMLs. Therefore, a reference lateral ventricle image is needed. First, the average size and position are determined and then a reference lateral ventricles image is constructed using a coarse non-rigid registration to correct for global shape differences. Registration of new images to the reference lateral ventricles requires fine scale non-rigid deformations to correct for the individual variation in shape and size. Evaluation shows that a good overlap with the reference ventricles is achieved. Although registration accuracy decreases at greater distances from the lateral ventricles, the evaluations have shown that within the periventricular area the registrations are accurate within a milimeter.

White matter lesion maps in DM2

To see if some periventricular areas in DM2 patients are particularly prone to lesion development, WML density maps were made. These showed that frontal capping of the lateral ventricles is very frequent in both control participants and DM2 patients. Analysis revealed that DM2 patients more frequently have frontal and occipital capping and lining of the ventricles. Analysis of the WML maps of men and women separately showed significant differences in the same areas for women, but no differences between male controls and DM2 patients. This agrees with the results of the volume analyses, which neither found effects of DM2 on WMLs in men. Thus, accurate mapping of WMLs has shown subtle differences in the pattern of WML occurrence in female DM2 patients.

Conclusion

Brain infarct maps for the study of internal carotid artery (ICA) related infarcts were created using an average CT brain image. These showed that the middle cerebral artery territory is more often involved in infarcts in patients with ICA occlusion, but no differences between infarcts in mild and severe stenosis were found.
Diabetes mellitus type 2 has serious consequences for the volume of the brain. Gray matter is reduced and lateral ventricular volume is increased. White matter lesions are more severe and more frequent capping and lining of the lateral ventricles occurs. Remarkably the effects of DM2 are more pronounced in women. These findings stress the need for more research into gender differences in the impact of DM2 on the brain.

Samenvatting

In het eerste gedeelte van dit proefschrift wordt de locatie van herseninfarcten bij mensen met een vernauwing van de halsslagader (arteria carotis interna) bekeken. Patiënten met een herseninfarct werden gegroepeerd afhankelijk van de vernauwing van hun halsslagader. Voor elke groep werd een beeld van de infarctdistributie gemaakt. De distributies werden vergeleken om gebieden in de hersenen te vinden die vaker door een infarct getroffen worden bij een vernauwde halsslagader.
Het tweede gedeelte van dit proefschrift is gericht op de effecten van diabetes mellitus type 2 op de hersenen. Hiervoor zijn de volumes van de grijze en witte stof, van de hersenkamers ofwel ventrikels, van het hersenvocht (liquor cerebrospinalis) en van afwijkingen in de witte stof bepaald. Van de witte stof afwijkingen zijn projecties gemaakt die de distributie weergeven. De volumes van de hersenweefsels en de distributies van de witte stof afwijkingen in diabetespatiënten zijn vergeleken met die in een controlegroep.

Arteria carotis interna stenose en herseninfarcten

Stenose ofwel vernauwing van de arteria carotis interna (halsslagader) kan de oorzaak zijn van een herseninfarct ofwel beroerte. Het operatief verwijderen van de vernauwing heeft een relatief hoog risico op overlijden. Daarom is het erg belangrijk om goed te kunnen bepalen wie baat heeft bij een operatie. Onderzoek naar de kenmerken van infarcten die gerelateerd zijn aan halsslagadervernauwing levert informatie op die gebruikt kan worden bij de selectie van patiënten voor de operatie. Bovendien wordt hiermee onze kennis over het ontstaansmechanisme van infarcten vergroot. Het onderzoek in dit proefschrift richt zich op het vinden van locaties in de hersenen die als gevolg van een vernauwde halsslagader door een infarct worden getroffen. Hiertoe worden projecties van de infarctdistributie gemaakt.

Constructie en evaluatie van een gemiddeld CT beeld van de hersenen

Om projecties van de infarctdistributie te maken is het noodzakelijk om de hersenen van individuele patiënten naar een referentiebeeld te transformeren. Hiervoor is een gemiddeld CT beeld van de hersenen gebruikt. De constructie van dit gemiddelde beeld verliep in twee stappen. Eerst werd een tijdelijk gemiddelde gemaakt van een beperkt aantal beelden. Dit tijdelijke gemiddelde diende als referentiebeeld voor de constructie van het echte gemiddelde CT beeld van de hersenen. Het tijdelijke gemiddelde is een beter uitgangspunt dan een enkel beeld. Drie verschillende gemiddelde beelden gebaseerd op dezelfde data zijn gemaakt voor de evaluatie van de

registratieconsistentie tijdens de constructie en voor de registratie van nieuwe beelden naar het gemiddelde beeld.

Herseninfarctdistributie bij vernauwing van de arteria carotis interna

Vernauwing van de arteria carotis interna, de halsslagader, werd gecategoriseerd als matig (0-49 % vernauwing), ernstig (50-99% vernauwing) of occlusie (100% oftewel volledige vernauwing). In totaal hadden 80 patiënten een matige vernauwing, 33 een ernstige vernauwing en 29 een occlusie van de halsslagader. Voor elke categorie zijn beelden van de infarctdistributie gemaakt door het CT beeld van iedere patiënt naar het gemiddelde beeld te registreren en de gevonden transformatie toe te passen op handmatig gesegmenteerde infarcten. Bij patiënten met een matige of ernstige vernauwing was de infarctfrequentie redelijk gelijkmatig verdeeld, maar bij patiënten met een occlusie was het hersengebied dat voorzien wordt door de middelste hersenslagader vaker getroffen door een infarct. Met behulp van een niet-parametrische randomisatietechniek zijn verschillen in infarctdistributie geanalyseerd. Dit toonde kleine verschillen aan tussen patiënten met een matige of ernstige vernauwing en patiënten met een occlusie. De verschillen lagen in het stroomgebied van de middelste hersenslagader. Ook hadden patiënten met een occlusie gemiddeld een groter infarct dan patiënten met een matige of ernstige vernauwing, welke niet verschilden qua infarctvolume. De standaard benadering om infarctdistributie te analyseren is door infarcten in te delen in categorieën. Dit leverde geen verschillen in infarct verdeling op tussen de verschillende stenosecategorieën. Hieruit blijkt dat het vergelijken van de infarctdistributie gevoeliger is.

Diabetes mellitus type 2 en de hersenen

Diabetes mellitus is een aandoening van de bloedsuikerregulatie. Diabetes mellitus type 2 (DM2) komt vaak voor bij ouderen en wordt ook wel ouderdomsdiabetes genoemd. DM2 is geassocieerd met een verslechterde cognitie en met dementie. Het is nog niet geheel duidelijk welke veranderingen DM2 in de hersenen veroorzaakt. In de meeste studies wordt een relatie tussen DM2 en hersenatrofie, het kleiner worden van de hersenen, en met herseninfarcten gevonden. Afwijkingen in de witte stof komen veelvuldig voor bij zowel gezonde ouderen als DM2 patiënten. Het is echter niet geheel duidelijk of DM2 invloed heeft op het ontstaan ervan. Dit wordt deels veroorzaakt door beperkingen in de methodes die vaak gebruikt worden om de ernst van de witte stof afwijkingen te bepalen. MR beelden van DM2 patiënten en van controles zijn verzameld als onderdeel van de Utrecht Diabetic Encephalopathy Study (UDES) naar cognitie bij patiënten met diabetes mellitus. Het onderzoek in dit proefschrift is gericht op het bepalen van veranderingen in het hersenvolume en de aanwezigheid en verdeling van witte stof afwijkingen bij patiënten met diabetes mellitus type 2.

Hersenvolume en het volume van witte stof afwijkingen bij patiënten met DM2

Door middel van een geautomatiseerde classificatietechniek zijn MR beelden verdeeld in grijze stof, witte stof, laterale ventrikels, hersenvocht en witte stof afwijkingen. Volume verschillen tussen 99 DM2 patiënten en 46 controles zijn geanalyseerd met correctie voor leeftijd, geslacht, opleidingsniveau en schedelinhoud. Dit liet een significante afname van het grijze stof volume en een significante toename van het volume van de laterale ventrikels en witte stof afwijkingen zien. Dit betekent dat DM2 patiënten meer atrofie van de hersenen en ook ernstigere witte stof afwijkingen hebben dan controles. Herhaling van de analyse voor mannen en vrouwen apart onthulde een opmerkelijk verschil. Vrouwelijke DM2 patiënten hadden een afname van het grijze stof volume en toename van het laterale ventrikel en hersenvocht volume, terwijl bij mannen geen significante effecten van DM2 gevonden konden worden. Het is niet duidelijk wat de oorzaak van deze verschillen is. Geslachtsverschillen hebben tot nu toe weinig aandacht gekregen in onderzoek naar de effecten van diabetes op de hersenen. Deze bevindingen tonen echter aan dat in toekomstig onderzoek ook analyses voor mannen en vrouwen apart nodig zijn.

Constructie en evaluatie van refentie laterale ventrikels

Periventriculaire witte stof afwijkingen, afwijkingen in de witte stof rond de laterale ventrikels, zijn geassocieerd met DM2. Om de distributie van periventriculaire witte stof afwijkingen te onderzoeken moeten deze afwijkingen nauwkeurig naar een referentie getransformeerd worden. Dit wordt gedaan door voor 61 patiënten en 26 controles de laterale ventrikels naar een referentiebeeld te registreren en deze transformatie op de witte stof afwijkingen toe te passen. Hiervoor is een refentie beeld van de laterale ventrikelsnodig. Voor de constructie van de referentie worden eerst de gemiddelde grootte en positie van de laterale ventrikels bepaald in 24 individuen en dan wordt een grove niet-rigide registratie toegepast om te corrigeren voor globale verschillen in vorm. Registratie van nieuwe beelden naar dit referentie beeld vereist een fijne, niet-rigide registratie om voor de individuele verschillen in vorm en grootte van de ventrikels te corrigeren. Evaluaties hebben aangetoond dat een goede overlap met het gemiddelde behaald wordt en hoewel de nauwkeurigheid van de registraties afneemt naarmate de afstand tot het ventrikel groter wordt, blijft de gemiddelde afwijking in het periventriculaire gebied binnen een milimeter.

Distributie van witte stof afwijkingen bij DM2

Distributies van witte stof afwijkingen zijn gemaakt voor controles en DM2 patiënten om te zien of er periventriculaire gebieden zijn die gevoeliger zijn voor het ontstaan van afwijkingen in DM2 patiënten. De verkregen distributies laten zien dat in zowel DM2 patiënten als in controles bedekking van de frontale hoorns (zogenaamde

capping) van de ventrikels met afwijkingen veel voorkomt. Analyse van de distributies toonde aan dat bij DM2 patiënten vaker bedekking met afwijkingen voorkomt, zowel frontaal als langs het hele laterale ventrikel. Aparte analyse voor mannen en vrouwen toonde significante verschillen aan in dezelfde gebieden voor vrouwen, maar er werden geen verschillen gevonden tussen mannelijke controles en DM2 patiënten. Dit komt overeen met de resultaten van de volumeanalyse, waarbij ook geen effecten van DM2 bij mannen werd gevonden. Door het nauwkeurig transformeren van de witte stof afwijkingen zijn subtiele veranderingen in de distributie ontdekt, met name bij vrouwelijke DM2 patiënten.

Conclusie

Herseninfarctdistributies, gemaakt met behulp van een gemiddeld hersen CT beeld, tonen aan dat het stroomgebied van de middelste hersenslagader vaker betrokken is bij herseninfarcten in patiënten met een occlusie van de halsslagader (arteria carotis interna) dan in patiënten met een matige of ernstige vernauwing. Patiënten met een occlusie hadden ook een gemiddeld groter infarctvolume dan patiënten met een matige of ernstige vernauwing.
Diabetes mellitus type 2 heeft ernstige consequenties voor de hersenen. Het vermindert het grijze stof volume en vergroot het lateraal ventrikel volume. Witte stof afwijkingen zijn erger in DM2 patiënten en bedekking van de laterale ventrikels met afwijkingen is frequenter. Opmerkelijk genoeg is het effect van DM2 sterker in vrouwen. Deze bevindingen benadrukken de noodzaak voor meer onderzoek naar de invloed van geslacht op het effect van DM2 op de hersenen.

List of publications

International Journals

Construction and evaluation of an average CT brain image for inter-subject registration
C. Jongen, J.P.W. Pluim, P.J. Nederkoorn, M.A. Viergever, W.J. Niessen
Computers in Biology and Medicine, 2004, 34(8):647-662

Atlas-based analysis of cerebral infarction pattern in CT images of patients with Internal Carotid Artery stenosis
C. Jongen, P.J. Nederkoorn, W.J. Niessen, J.P.W. Pluim
Investigative Radiology, 2004, 39(8):462-469

Brain tissue and white matter lesion volume analysis in diabetes mellitus type 2
C. Jongen, J. van der Grond, L.J. Kappelle, G.J. Biessels, M.A. Viergever, J.P.W. Pluim
Submitted

Periventricular white matter lesion patterns in diabetes mellitus type 2 patients
C. Jongen, J. van der Grond, G.J. Biessels, J.P.W. Pluim
Submitted

Conference Proceedings

Construction of an average CT brain image for brain infarct pattern comparison
C. Jongen, J.P.W. Pluim, M.A. Viergever, W.J. Niessen
Computer Assisted Radiology and Surgery, 2002, 425-429

Ventricle registration for inter-subject white matter lesion analysis
C. Jongen, J. van der Grond, J.P.W. Pluim
Medical Image Computing and Computer-Assisted Intervention, 2004
Lecture Notes in Computer Science, 3216:712-719

A voxel based analysis of white matter lesions in diabetic subjects
C. Jongen, J. van der Grond, J.P.W. Pluim
Neuroimage, 2005 vol. 26(Suppl. 1)

Other

Commentary: Analyzing group differences in stroke pattern
C. Jongen and J.P.W. Pluim
Neuroscience Imaging
In Press

Acknowledgements

The author would like to thank the Laboratory for Medical Imaging Research in Leuven for kindly supplying them with their software for mutual information-based registration.

The author would also like to thank Dr. P. Anbeek for kindly supplying them with the software for K-Nearest-Neighbor classification of brain MR images.

The Utrecht Diabetic Encephalopathy Study Group are:
(All part of the University Medical Center, Utrecht, The Netherlands)

Department of Clinical Neurophysiology: A.C. van Huffelen
Department of Internal Medicine: H.W. de Valk
Julius Center for Health Sciences and Primary Care: A. Algra, G.E.H.M. Rutten
Department of Medical Pharmacology: W.H. Gispen
Department of Neurology: A. Algra, G.J. Biessels, J. van Gijn L.J., Kappelle, S.M. Manschot
Department of Neuropsychology and Helmholtz Research Institute: A.M.A. Brands (currently: Zuwe Hofpoort Regionaal Psychiatrisch Centrum, Woerden, The Netherlands), E.H.F. de Haan, R.P.C. Kessels, E. van den Berg
Department of Radiology: J. van der Grond (currently: Leiden University Medical Center, Leiden, The Netherlands), C. Jongen, J.P.W. Pluim

Dankwoord

Het zit er bijna op. Het boekje is af en de promotiedatum nadert. De tijd is omgevlogen. En dat is een goed teken. Het doen van promotieonderzoek aan het ISI was een leuke en leerzame ervaring. Er zijn veel mensen die hieraan hebben bijgedragen en die wil ik daarvoor graag bedanken.

Allereerst dank aan degene die het mogelijk maakte dat ik mijn afstudeeronderzoek kon voortzetten en uitbreiden tot een promotieonderzoek, mijn promotor Max Viergever. Beste Max, jij hebt ervoor gezorgd dat het op het ISI goed toeven is. Er werken gezellige en kundige mensen en er is niet alleen aandacht voor wetenschappelijke activiteiten, maar ook voor sociale.
Josien Pluim, co-promotor en dagelijks begeleider, jij verdient zeker dank voor je bijdragen aan de totstandkoming van dit proefschrift. Niet alleen de bonbons voor het eerste artikel en het boekje “Pluim en stekeltje maken lawaai”, maar ook de discussies tijdens het werkoverleg en je nuttige commentaar op mijn artikelen heb ik erg gewaardeerd.
Beste Wiro Niessen, jij bent slechts korte tijd dagelijks begeleider bij mijn promotieonderzoek geweest, maar je was daarvoor al ruimschoots bij mijn onderzoek betrokken als begeleider tijdens mijn afstuderen. Bedankt voor je goede ideeën. Jouw enthousiasme heeft destijds zeker bijgedragen aan mijn keuze om promotieonderzoek te gaan doen.

Beste Paul Nederkoorn, hartelijk dank voor de vele uren handmatig herseninfarcten segmenteren. Het was gezellig om met je samen te werken.
Beste Jeroen van der Grond, jouw enthousiasme werkt aanstekelijk. Ik heb veel geleerd van je kritische blik op het schrijven van artikelen. Hartelijk dank voor alle bijdragen die je aan dit proefschrift hebt geleverd.
Verder wil ik alle leden van de Utrecht Diabetic Encephalopathy Study hartelijk bedanken voor het gebruik van de data. Geert-Jan Biessels, bedankt voor de discussies en voor de revisies van de artikelen.

Dan zijn er natuurlijk al die andere mensen die onmisbaar waren bij het totstandkomen van mijn proefschrift. Gerard van Hoorn, de stille kracht achter het tevreden zoemen van alle computers. En natuurlijk Koen Vincken, bedankt voor alle scriptjes. Jacqueline, Marjan en Renée voor de secretariële en Sandra voor de financiële zaken.

Nelly, kamergenoot tijdens bijna heel mijn promotieonderzoek. Het leek er soms op dat we probeerden elkaar zoveel mogelijk te ontlopen door een tactische planning van deeltijddagen, ouderschapsverlof en werkbesprekingen. Gelukkig was dat maar schijn en hebben we een gezellige tijd gehad en inderdaad zijn de verzorging van cavia's en kinderen uitgebreid besproken. Bedankt voor alle gezelligheid en ook heel erg bedankt dat ik gebruik kon maken van je segmentatie software.
Marleen, oud-kamergenoot, het is alweer even geleden dat je aan het ISI werkzaam was, maar toch nog hartelijk dank voor de leuke tijd.
Krista, ook jij bent alweer een tijd weg. Ik heb veel plezier beleefd aan onze squash partijtjes en gezellige gesprekken.
En natuurlijk Adriënne, we delen pas een paar maanden een kamer, maar ik heb je interesse en opgewektheid tijdens de laatste loodjes van het schrijven erg gewaardeerd.
En ook dank aan alle kamergenoten uit het vroegere R-lab. Ik denk nog steeds met plezier terug aan de goede sfeer en de grote kerstboom met het treintje.

Verder wil ik ook Marius, Martijn, Michiel, Niels, Peter, Rashindra, Sandra, Sara, en Stefan bijzonder bedanken voor de vele koffie-calls. Ik heb erg genoten van de gezellige pauzes met meer of minder diepgaande gesprekken.
Ingrid, bedankt voor de vele partijtjes sqaush, je liet me in ieder geval wel rennen.
En natuurlijk wil ik alle ISI-ers bedanken voor de goede sfeer, gezellige lunches en de leuke dingen die we met z'n allen gedaan hebben zoals Sinterklaas vieren, zeilen en de Ardennenweekenden.

Jorieke en Myrra, oud-huisgenoten en nog steeds goede vriendinnen. Bedankt voor jullie interesse en natuurlijk voor de leuke en gezellige afspraken. En Myrra, sinds jij verhuisd bent naar Zeist, is 's avonds in het donker terug naar huis fietsen een stuk gezelliger geworden.

En dan tot slot mijn familie. Papa en mama, heel erg bedankt voor alle steun en betrokkenheid die ik altijd van jullie gekregen heb. En zonder jullie als oppas opa en oma was dit boekje vast nog niet af geweest.
Marc en Evelyn, wat een geweldige broer en zus heb ik! Ik ben erg blij dat jullie mijn paranimfen willen zijn.
Lieve, vrolijke Tim, jij maakt het leven tot een feest. Ik geniet met volle teugen van je. En ik denk met veel plezier aan de "wetenschappelijke" activiteiten die we samen ondernomen hebben zoals het bezoeken van promotierecepties en de MICCAI 2004 conferentie in St. Malo, waarbij de pauzes in het teken van borstvoeding stonden.
Lieve Jiri, jij bent mijn beste maatje en meer. We hebben samen al veel gedaan en meegemaakt. Ik wil je heel erg bedanken voor al je liefde, interesse en steun en voor alle boterhammetjes die je voor me gesmeerd hebt.

Curriculum Vitae

Geboren 11 februari 1977

Crèche de Rakkertjes, Gouderak
‘t Hummeltje, Swalmen

Kleuterschool de Mortel, Swalmen

Basisschool de Mortel, Swalmen

de Schattenberg, Landgraaf
Biesendael, Goirle

Gymnasium R.S.G. Koning Willem II, Tilburg
(Cum Laude)

Grotius College, Heerlen

Studie Medische biologie, Universiteit Utrecht
(Cum Laude)

Stage *“Anticipatory behaviour in rats”* (9 mnd)
Gedrags farmacologie, Rudolf Magnus Instituut voor Neurowetenschappen
Extracurriculaire stage *“Stress and dominance in bank voles”* (6mnd)
Department of Animal Behavior, Copenhagen University, Denmark
Stage *“Internal carotid artery stenosis and infarct location”* (6 mnd)
Image Sciences Institute, Universitair Medisch Centrum Utrecht

Promotie onderzoek *Interpatient registration and analysis in clinical neuroimaging*
Image Sciences Institute
Universitair Medisch Centrum Utrecht

Verdediging 16 maart 2006